



**HAL**  
open science

# Study on Prediction and Verification of Electromagnetic and Mechanical Performances of Variable Frequency Stealth Radome

Daesung Son

► **To cite this version:**

Daesung Son. Study on Prediction and Verification of Electromagnetic and Mechanical Performances of Variable Frequency Stealth Radome. Materials and structures in mechanics [physics.class-ph]. Ecole nationale supérieure Mines-Télécom Lille Douai; Korea advanced institute of science and technology (Taejon, Corée du Sud), 2021. English. NNT : 2021MTLD0002 . tel-03352470

**HAL Id: tel-03352470**

**<https://theses.hal.science/tel-03352470>**

Submitted on 23 Sep 2021

**HAL** is a multi-disciplinary open access archive for the deposit and dissemination of scientific research documents, whether they are published or not. The documents may come from teaching and research institutions in France or abroad, or from public or private research centers.

L'archive ouverte pluridisciplinaire **HAL**, est destinée au dépôt et à la diffusion de documents scientifiques de niveau recherche, publiés ou non, émanant des établissements d'enseignement et de recherche français ou étrangers, des laboratoires publics ou privés.

# THÈSE

présentée en vue d'obtenir le grade de

## DOCTEUR

en

Mécanique des solides, des matériaux, des structures et des surfaces

par

**DAESUNG SON**

DOCTORAT DE L'UNIVERSITÉ DE LILLE DELIVRÉ PAR IMT LILLE DOUAI

**Study on Prediction and Verification of Electromagnetic and Mechanical Performances of Variable Frequency Stealth Radome**

Soutenance le 13 juillet 2021 devant le jury d'examen

Président	<b>OLIVIER Philippe, Professeur</b>	Université de Toulouse
Rapportrice	<b>DAGHIA Federica, Maître de conférences HDR</b>	ENS Paris Saclay
Rapporteur	<b>PARK Gyuhae, Professeur</b>	Chonnam National University
Examineur	<b>KIM Chun-Gon, Professeur</b>	KAIST
Membre invité	<b>LEPETIT Thomas, Ingénieur de recherche</b>	ONERA
Directeur	<b>PARK Chung-Hae, Professeur</b>	IMT LILLE DOUAI
Co-directeur	<b>Lee Jung-Ryul, Professeur</b>	KAIST
Co-encadrant	<b>CHAKI Salim, Maître assistant HDR</b>	IMT LILLE DOUAI

Laboratoire d'accueil

Centre d'Enseignement, de Recherche et d'Innovation (CERI) Matériaux et Procédés de IMT Lille Douai

Ecole Doctorale SMRE 104 (U. Lille, U. Artois, ULCO, UPHF, Centrale Lille, Chimie Lille, IMT Lille Douai)



# ACKNOWLEDGEMENTS

I would like to express my sincere gratitude to Professor Jung-Ryul LEE for giving me the opportunity to study in France and Korea. Thank you for giving me the direction of my research and helping me a lot whenever I have a difficult task. I would like to thank Professor Chung-Hae Park for helping not only with research advice but also with life issues when conducting research in France. Also, I am grateful to Dr. Salim CHAKI for helping with the administrative process as well as research advice in France.

Thanks to all of the KAIST lab colleagues who have been with me during my Ph.D. course. In particular, I would like to express my special thanks to Jong-Min HYUN who has been doing research together for a long time and always helping me a lot. And I would like to thank Young-Jun LEE, Jae-Yeong JANG, Seung-Chan HONG, Yun-Sil CHOI, Jin-Woo PARK, Yong-ho KIM, and Kyung-Hwan KIM who helped me in difficult times. Also, I sincerely appreciate all the other lab colleagues with me.

I sincerely thank all of the lab colleagues at IMT-Lille-Douai who have helped me so much while in France. Thanks keerthi-krishna PARVATHANENI and Anurag PISUPATI for your great help in my French life. I'm also grateful to other lab colleagues, Dr. Masoud BODAGHI, Anh-Duc LE, Anh-Duc LE, Xiao MA, etc.

Lastly, I would like to express my gratitude to my parents who helped me greatly whenever I was having a hard time. Other than that, I would like to thank those who have helped me a lot while conducting research. I was able to do it because of the help of many people. Thank you.

# Table of content

1	General Introduction .....	5
1.1	Research background .....	5
1.2	Previous research on frequency selective surface.....	10
1.3	Objectives .....	18
2	Electromagnetic Performance of Variable Frequency Stealth Radome .....	20
2.1	Analysis of electromagnetic characteristic of frequency selective surface .....	20
2.2	Active frequency selective surface design method .....	22
2.3	Electromagnetic design and performance measurement of variable frequency stealth radome.....	25
3	Prediction of Electromagnetic Performance of Curved Variable Frequency Stealth Radome .....	30
3.1	Electromagnetic performance prediction process of curved structure.....	30
3.2	Theoretical approach to electromagnetic performance in curved plates .....	32
3.3	Electromagnetic performance prediction using equivalent circuit model .....	34
3.4	Verification of prediction method using ray tracing method.....	42
4	Mechanical Performance Prediction of Variable Frequency Stealth Radome.....	51
4.1	Properties mapping technique of frequency selective surface .....	51
4.2	Structure analysis of Variable frequency stealth radome .....	56
4.3	Verification of structure analysis using properties mapping technique .....	63
5	Conclusion.....	67
6	Bibliography .....	70

# 1 General Introduction

## 1.1 Research background

Stealth technology is technology that prevents a friendly weapon system from being detected by enemy detection systems. Stealth technologies include radar stealth, infrared stealth, and acoustic stealth, and it is a system that includes various technologies.

When it comes to stealth technology, the first thing to consider is radar stealth technology. Radar technology is a technology that detects the reflection of strong electromagnetic waves transmitted from the radar to the target, and is widely used in detection systems because it can obtain highly accurate information on various target variables such as azimuth, altitude, distance, and target vector. In order not to be detected by such a radar, radar stealth technology is a technology that absorbs or scatters electromagnetic waves and minimizes the reflected electromagnetic waves.

The infrared detector is a technology that detects a target by using the temperature difference between the surrounding background and the target, and can accurately measure the azimuth and altitude. However, it is highly influenced by atmospheric conditions, i.e. the weather, and to measure distances it must be combined with other methods such as lasers. Therefore, it is mainly used for infrared-guided missiles rather than detecting enemies. Infrared stealth technology is a technology that makes it have a temperature similar to the outside temperature, such as reducing exhaust heat so that it is not detected by enemy infrared detectors.

SONAR (SOund Navigation And Ranging) is a system that detects the location of a target by measuring acoustic generated by the target. Since the acoustic generated in the water becomes a wave as it is, it is mainly used in submarines and surface ships, and in aircraft, it is used to detect jet engine noise caused by high-speed movement of high pressure air. Thus, acoustic stealth refers to all the techniques needed to minimize noise. Among these various detection technologies, radar stealth, which is the most used and prevents it from being detected by a precisely detectable radar, is the technology that prioritizes.

Radar stealth performance is superior to the smaller RCS (Radar Cross Section) detected on radar. RCS is an equivalent area of how large an object appears on the radar. It is composed of functions such as polarization of incident wave, incident angle, observation angle, target geometry (size, shape, etc.), surface condition, electrical characteristics, operating frequency, etc. To improve radar stealth performance, various studies [1-3] are being conducted to reduce RCS, and the following methods are used to reduce the RCS of fighter.

- Optimize the shape of the object
- RAM (Radar absorbing material)
- RAS (Radar absorbing structures)
- Stealth radome using FSS (Frequency selective surface)

First, there is a way to reduce the RCS by optimizing the shape. The simplest and most effective method is to reflect the transmitted electromagnetic waves in different directions using an inclined surface to prevent them from returning to the receiving antenna. The best application of this technique is the F-117. Almost all surfaces consist of inclined surface with no vertical surfaces and curved surfaces. However, in this case, the aerodynamic characteristics of the aircraft are significantly deteriorated.

Recently, in order to solve this problem, spike alignment technique that aligns the shape of the entire aircraft at a specific angle has been applied. Since the reflected electromagnetic wave can be concentrated in a specific direction, RCS is small in the azimuth angle except for the concentrated direction. Fighters with this technology are the F-22 and F-35. In addition, by using a surface such as a saw blade to scatter the reflected wave, it is possible to obtain the effect of reducing the RCS overall.

However, the biggest cause of the increase of RCS in aircrafts is the aircraft engine. To reduce the RCS of the engine part, the shape of the duct is designed in S-shape so that the reflected wave may be reflected in a different direction when it exits the intake port.



Figure 1.1: Stealth fighters [4]

Second, RCS can be reduced by using RAM. Materials that absorb electromagnetic waves can be classified into dielectrics, conductors, and magnetic materials depending on the material. The dielectric material uses a material with a high dielectric loss factor, but it is not very large in the high frequency range, so it is not well used for stealth technology. In the case of a conductor, it absorbs electromagnetic waves using the principle that the current induced by electromagnetic waves is converted into thermal energy due to resistance. RAM using a conductor is mainly made of carbon black or carbon fiber, and its absorption performance is degraded due to high conductivity at low frequencies, but it is importantly used as an electromagnetic wave absorbing material at high frequencies. In the case of magnetic materials, metal magnetic materials and oxide magnetic materials, which are materials that cause magnetic loss, are used. Among them, oxide magnetic materials are widely used for RAM, and as ferrite, which has excellent absorption capacity even at high frequencies, has been developed, it is most often used as an absorber material. Since such a radar absorbing material is applied to the outside of the aircraft, it must be able to withstand in the flight environment by satisfying wear resistance and strength. In

addition, since it is very important to accurately maintain the coating thickness, a robot system that can accurately apply is in operation.

To reduce RCS, the shape of the target object is optimized or RAM is used, but these methods have limitations. To reduce RCS, it must have the characteristics of PMC (Perfect Magnetic Conductor), but there is no material with such characteristics. Therefore, research on RAS using structural characteristics is actively underway.

RAS is a technology that absorbs electromagnetic waves due to structural characteristics as well as material properties. A typical RAS uses a multi-layered structure in which PEC (Perfect Electric Conductor) is located in the last layer as shown in Figure 1.2. When RAS is designed in multiple layers, it can absorb electromagnetic waves of a wide frequency bandwidth.

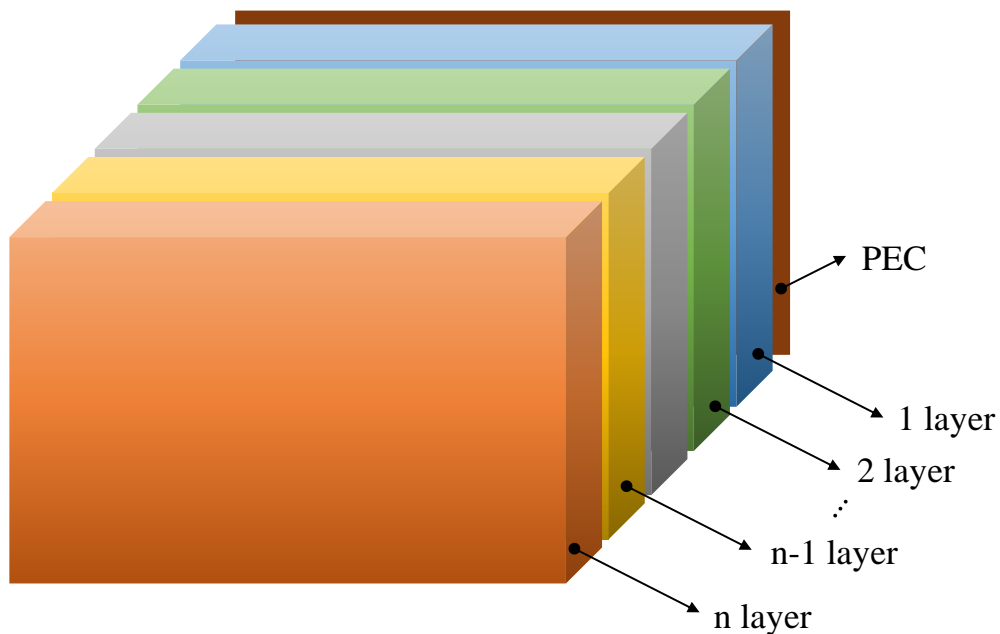


Figure 1.2: Multi-layered RAS [5]

Rather than absorbing electromagnetic waves of a wide frequency bandwidth, RAS used in fighters is designed according to the x-band and ku-band, which are the frequency bandwidths of various radars. To absorb a specific frequency bandwidth, a two-layer structure with PEC, insulator, conductor or magnetic material is mainly used as shown in Figure 1.3. It is a structure that absorbs electromagnetic waves by canceling the incident electromagnetic waves and the electromagnetic waves reflected by the PEC, and the absorbed frequency band varies depending on the material and thickness.

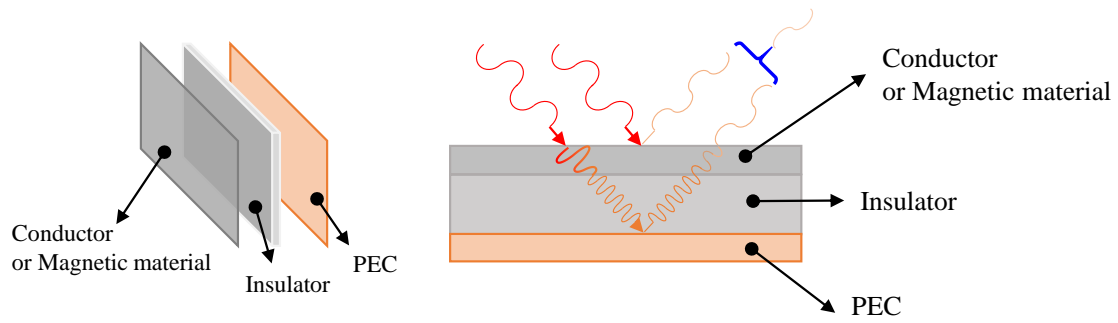


Figure 1.3: Schematic diagram of a two-story RAS [5]

In addition to this structure, RAS is designed by fabricating a conductor with a specific pattern as shown in Figure 1.4. FSS (Frequency Selective Surface) is manufactured with a specific pattern of conductors, and the frequency of transmission and reflection varies depending on the pattern. In RAS, since the absorbed frequency band varies according to the electromagnetic characteristics of the frequency selective surface, it is most important to analyze the electromagnetic characteristics of the frequency selective surface.

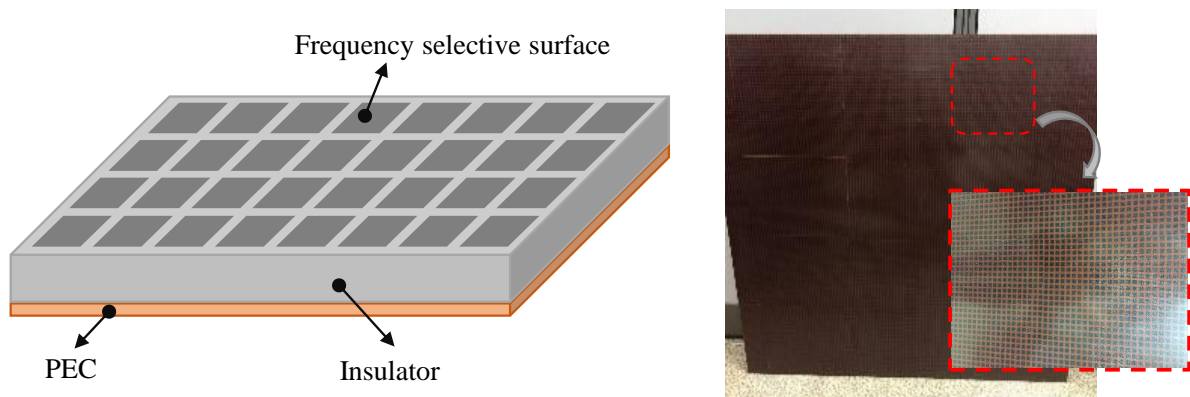


Figure 1.4: RAS with frequency selective surface [6]

In order for RAS with the ability to absorb electromagnetic waves to be applied to fighters, Mechanical performance must be satisfied to withstand the operating environment. Therefore, when designing RAS, many composite materials with excellent mechanical properties are used, and RAS design technology capable of satisfying electromagnetic and mechanical performances at the same time is required.

While the stealth technology introduced earlier was aimed at scattering or absorbing electromagnetic waves, the stealth radome requires another electromagnetic performance. The stealth radome has an internal antenna,

so if it blocks all electromagnetic waves, the antenna cannot function properly. Therefore, the stealth radome must have an electromagnetic characteristic that transmits only the communication frequency of the internal antenna and absorbs or reflects other frequencies as shown in Figure 1.5. It is the frequency selective surface that makes this characteristic possible. It is also used in RAS as shown in Figure 1.4, but it is a key technology in stealth radome.

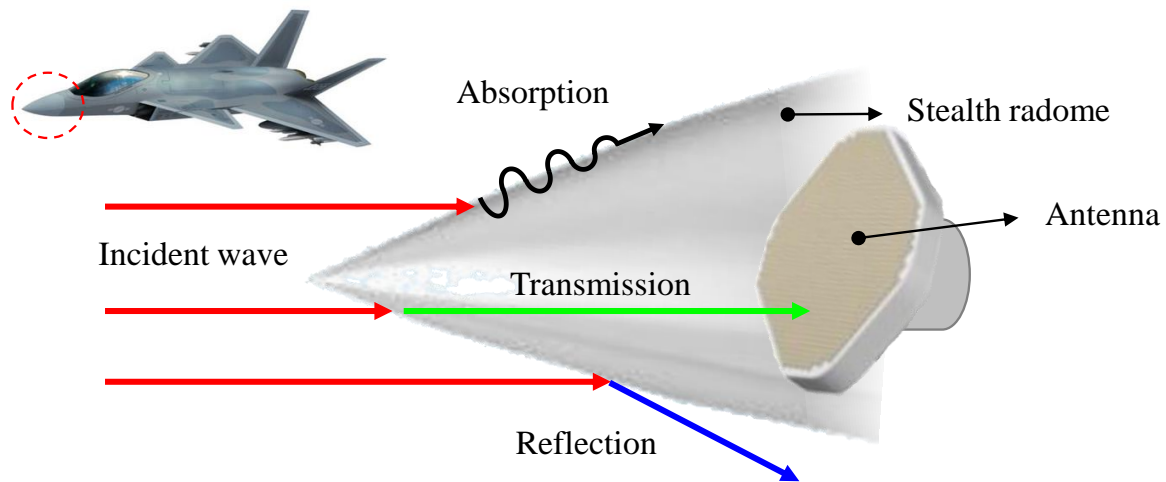


Figure 1.5: Electromagnetic characteristics of stealth radome [7]

Stealth radome must satisfy these electromagnetic characteristics as well as mechanical performance because it must withstand the loads generated in the flight environment. Therefore, when designing a stealth radome, it must be designed in consideration of not only electromagnetic characteristics but also mechanical performance. To satisfy the mechanical performance, the stealth radome is designed with a structure in which a frequency selective surface is inserted inside a sandwich structure applied with a composite material.

As stealth technology develops, research on anti-stealth technology is also actively progressing. Russia claims that the S-400 air defense system is capable of detecting and intercepting stealth fighter, and China claims that their destroyer radar detected an F-35A fighter from a distance of 350 km in 2014. In addition, a German radar manufacturer claims to have successfully tracked two F-35s returning to the United States after the 2018 Berlin Air Show for 100 miles. As such, research on anti-stealth technology is actively underway in various countries, and the need for anti-stealth technology will further increase.

One of the most widely known anti-stealth technologies is the multi-static radar system shown in Figure 1.6. In general, Since the general antenna is a mono-static radar in which the transmitting and receiving antennas are in the same position, the RCS is lowered by concentrating the radar reflected signal in a specific direction using

the spike alignment technique. However, in the case of using a multi-static antenna system, since the locations of the transmitting and receiving antennas are different, it is possible to detect a reflected signal concentrated in a specific direction.

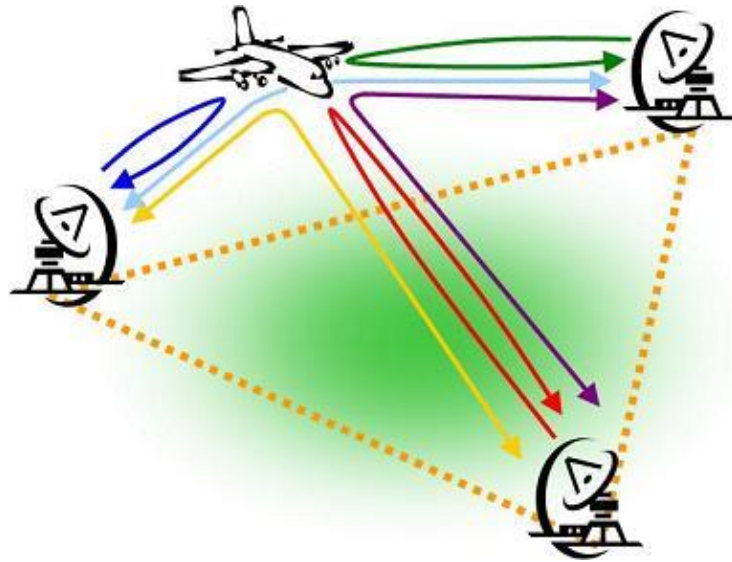


Figure 1.6: Multi-static radar system [8]

In addition, one of the other anti-stealth technologies is a method using the transmission frequency of the stealth radome. Stealth radome is characterized by transmitting a specific frequency to use an internal antenna. When a fighter is detected with the transmission frequency of the stealth radome using this feature, the antenna inside the stealth radome is exposed as it is. Therefore, RCS of the fighter increases, which increases the likelihood of being detected by radar. For this reason, the transmission frequency of the stealth radome is managed so that it is not exposed to the enemy as a confidential matter. Since the transmission frequency of the stealth radome is determined by the pattern of the frequency selective surface inserted inside, the stealth radome itself must be changed to change the transmission frequency. Therefore, it is necessary to develop a stealth radome that can change the transmission frequency as a stealth technology to cope with the anti-stealth technology.

## **1.2 Previous research on frequency selective surface**

The most important thing in stealth radome is the design of the frequency selective surface. The frequency selective surface has been studied for various purposes as a kind of spatial filter that transmits or reflects only required electromagnetic waves. The frequency selective surface having these characteristics has made significant advances in analysis technology and manufacturing technology for use in various fields.

Since the mid-1960s, intensive research has continued due to the potential for military use of frequency selective surface. The oldest patent on record was held by well-known Marconi and Franklin in 1919. Early frequency selective surface research focused on developing cassegrain sub-reflectors for use in parabolic antennas. As stealth technology has been developed over time, the importance of frequency selective surface technology has increased, and it is used for various purposes such as electromagnetic wave absorption, RCS reduction, and stealth radome.

In the frequency selective surface, conductors with a specific pattern are arranged with a certain periodicity as shown in Figure 1.7. Due to this pattern, the electromagnetic characteristics are changed, and it operates as a low-pass filter, a high-pass filter, a stop-band filter, and a pass-band filter like a microwave circuit filter. To understand the characteristics as a filter, it is necessary to understand the electromagnetic characteristics that vary depending on the pattern.

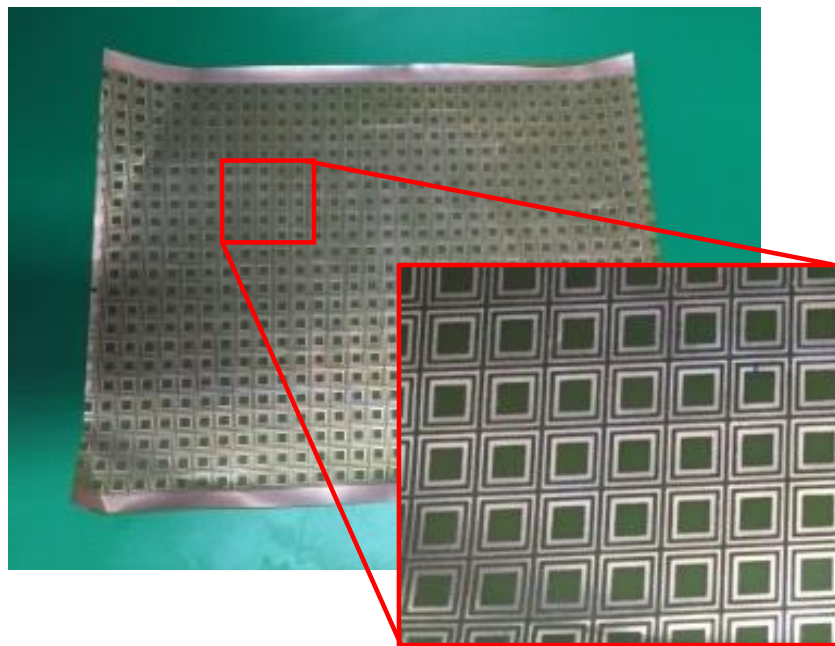


Figure 1.7: Specimen of the frequency selective surface [9]

An induced current flows on the surface by incident electromagnetic waves on the frequency selective surface. Since the surface has characteristics such as capacitors and inductances according to the shape of the pattern, the frequency selective surface has characteristics similar to those of a circuit. The circuit characteristics are determined according to the shape design of the pattern, and by configuring the characteristics of the circuit to be the same as the filter, it performs the same function as the filter. Therefore, the proper selection of frequency selective surface array elements, shapes, dimensions and materials is the most important part of the design

process.

Frequency selective surface can be classified according to array element, structure, and application as shown in Figure 1.8 [10]. Array element can be classified into three types: basic element type, convolution or meander type and fractal type. First of all, the basic element type can be divided into 4 groups as shown in Figure 1.9. Group 1 contains a pattern consisting of a dipole, a triple pole, a square helix, a Jerusalem cross-connected or N pole. Group 2 includes patterns in which circular, square, and hexagonal loops are arranged repeatedly. Group 3 contains patches of various shapes that are filled inside. Group 4 includes patterns combined in various configurations. The frequency selective surface designer selects an array element from one of these groups or uses a combination of these, depending on the application target.

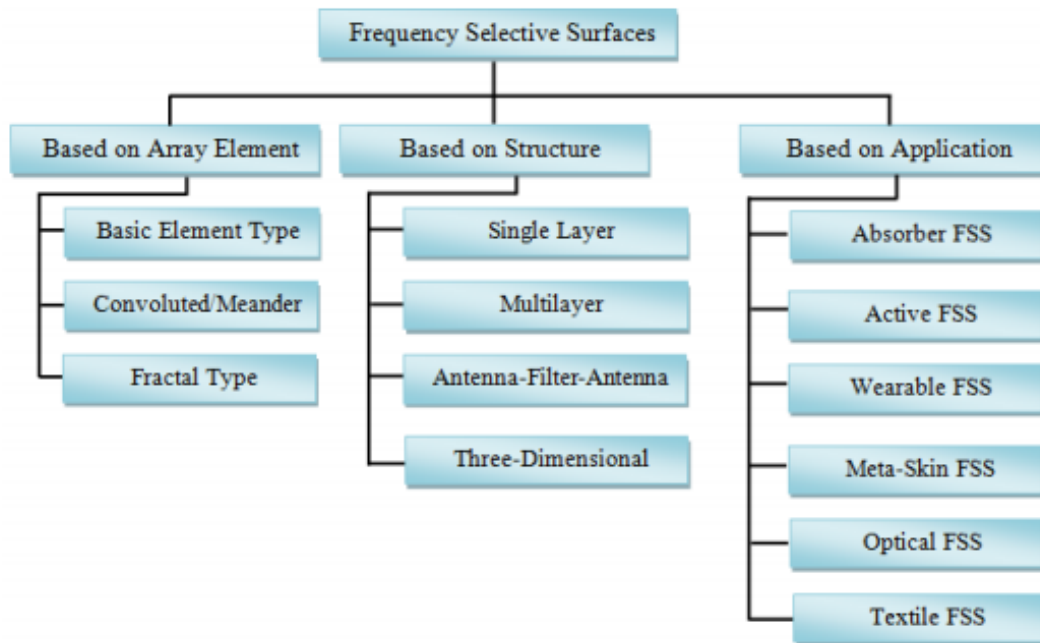


Figure 1.8: Classification of the frequency selective films by pattern and function [10]

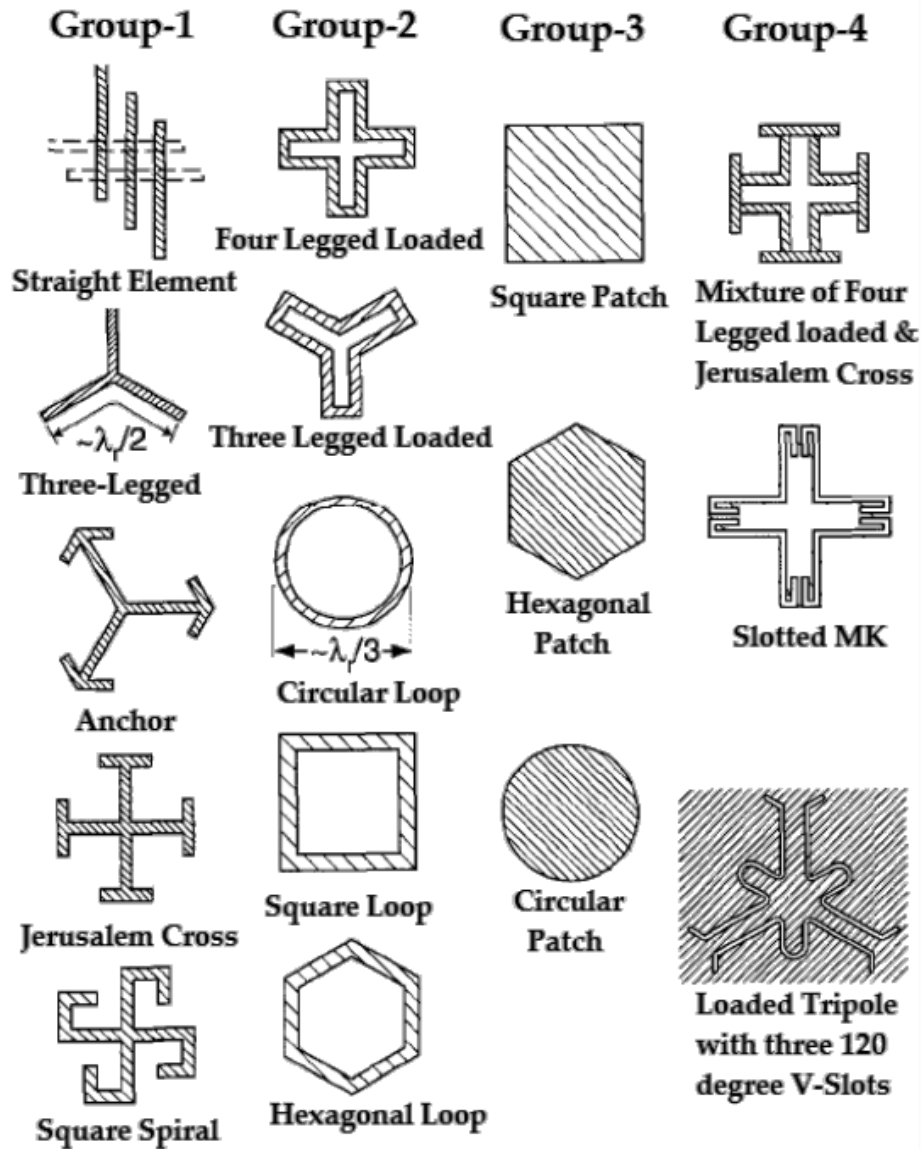


Figure 1.9: Classification of the frequency selective films according to element arrangement [11]

If convolutional or meander arrays are used, the equivalent inductance and capacitance can be efficiently increased at the same time, so it can be designed to have a smaller unit cell size than the basic array. Fabrication in smaller unit cell sizes results in less distortion at the specified curvature and improved angular stability.

A small frequency selective surface with convolutional square loop array elements was proposed by Parker [12]. Nauman [13] designed a convolutional square loop arrangement as shown in Figure 1.10a. This frequency selective surface provides effective shielding in the x-band with a 3dB FBW (Fractional Band Width) of about 48% sufficient to cover this band. Yan [14] conducted a study on a similar meander arrangement as shown in Figure 1.10b. The concept of such an array element not only reduces the unit cell size, but also obtains a stable stopband

frequency response for a higher incident angle.

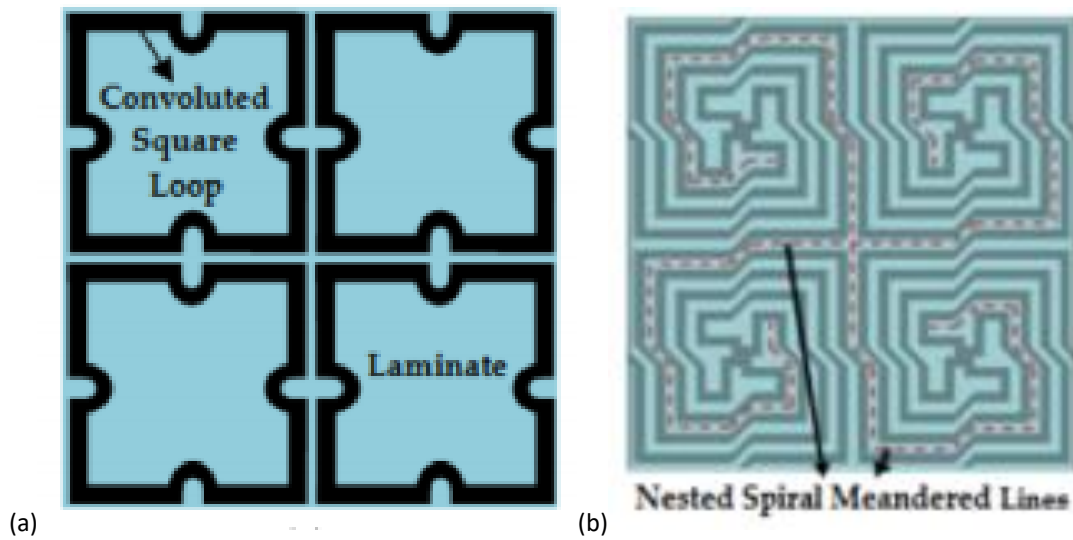


Figure 1.10: (a) convoluted arrangement [13] (b) meander arrangement [14]

Recently, research on a new type of frequency selective surface design technology based on fractal geometry theory is being conducted [15]. The biggest advantage of fractals is that you can get arbitrarily longer curvatures confined to a given area or volume. This characteristic is effectively utilized to reduce the spacing between elements between the resonance shapes of the frequency selective surface. In addition, the function of "self-similarity" helps to realize multi-band performance. Therefore, if a fractal arrangement is used as shown in Figure 1.11, it can have the advantage of reducing the element size and operating in multiple bands.

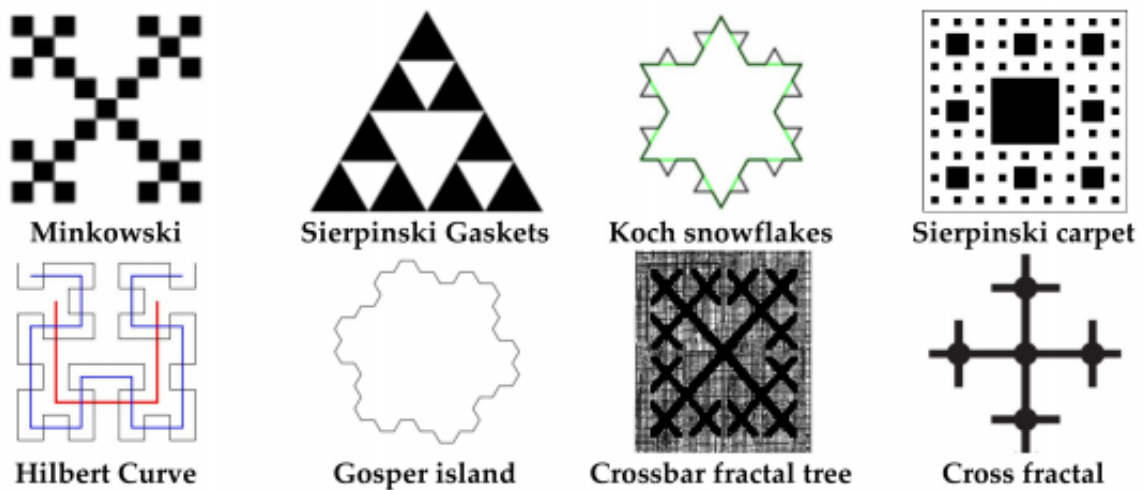


Figure 1.11: Frequency selective surface pattern applied with fractal theory [10]

The classification of the frequency selective surface above can be classified not only according to array element but also according to the structure. If classified according to the structure, it is possible to classify into a structure using only a single layer, a structure using multiple layers, an antenna-filter-antenna structure, and a three-dimensional structure. As for the structure using a single layer, the electromagnetic performance varies greatly depending on how the element arrangement is designed, as in previous studies introduced above. However, the use of a single layer limits the operating bandwidth. Therefore, multi-band response and overall bandwidth can be improved by fabricating the frequency selective surface in a multilayer structure as shown in Figure 1.12a [16]. The antenna-filter-antenna is composed of a receiving antenna, a non-radiative resonant structure, and a transmitting antenna as shown in Figure 1.12b, and is used as impedance response surface and a waveguide band-pass filter [17].

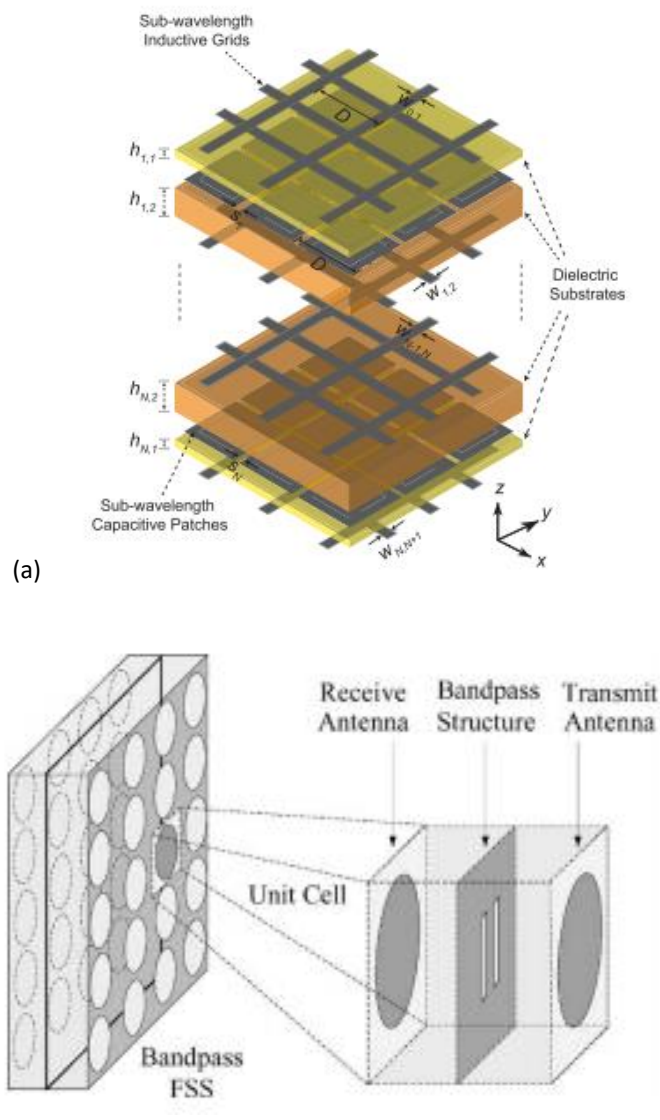


Figure 1.12: (a) Multilayer frequency selective surface [16], (b) Antenna-filter-antenna array [17]

Frequency selective surface with a three-dimensional structure have recently been studied due to strict requirements. Significant improvements in frequency selective surface analysis methods, computational capabilities, and manufacturing techniques have made this research possible. Based on this, a lot of interesting designs have recently been reported with a three-dimensional frequency selective structure [18,19] that is fundamentally different from the existing frequency selective surface as shown in Figure 1.13.

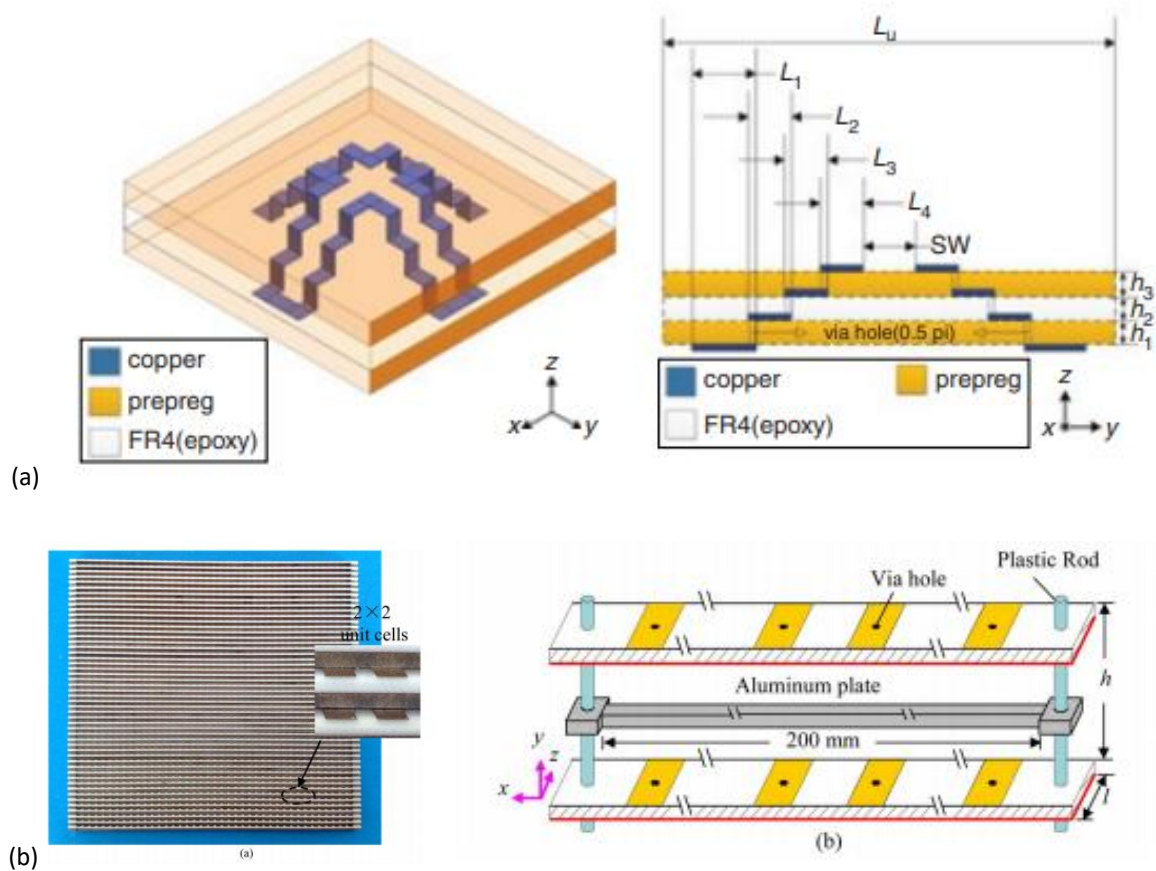


Figure 1.13: (a) 3D frequency selective structures for stable angle of incidence [18] (b) 3D bandpass frequency selective structures with multiple transmission zeros [19]

Finally, since the frequency selective surface is applied in various fields and it is very difficult to classify according to the application, only a few major applications were investigated. First of all, the frequency selective surface can be used as an absorber by being applied to RAS among stealth technologies as shown in Figure 1.4. Absorbers with frequency selective surface are used as high-efficiency broadband absorbers to reduce detection potential in applications such as helicopters, airplanes, gliders and missiles.

In addition, active frequency selective surface has been developed and used to change the frequency response in specific applications. The electromagnetic performance of a typical frequency selective surface is determined once it is fabricated, but an active frequency selective surface can change its electromagnetic characteristics even during operation by adding an active element. Mainly used active devices include PIN diodes, varactor diodes, varicaps, and Schottky diodes.

Active frequency selective surface can be classified into two types. The first type is a method of changing the transmission and reflection characteristics like a switch using a PIN diode. The second type is a method of moving the resonant frequency in a specific frequency band by using a varactor diode. The two types are classified according to which active element is used, so it is selected according to the required electromagnetic characteristics.

In the active frequency selective surface, a voltage feed line is generally added to control the impedance of an active element. However, since the added voltage feed line can have a great influence on the electromagnetic performance of the active frequency selective surface, it is necessary to design the voltage feed line effectively. In addition, when active elements are connected in series, a high driving voltage is required as the size of the active frequency selective surface increases. Therefore, in order to lower the driving voltage, an active frequency selective surface that connects active elements in parallel has been developed.

Table 1.1 summarizes the active frequency selective surface studied so far by function. Most of the preceding studies used active elements in parallel, but most of them were connected in parallel using via holes. Even if parallel connection was made without via holes, there was a problem that polarization stability was deteriorated.

Table 1.1: Classification of the previous researches on active frequency selective surface

AFSS design	Diode	Feed pattern	Number of layers	Polarization insensitivity
[20]	Varactor	Parallel	1	No
[21]	Varactor	Parallel with vias	2	Yes
[22]	PIN	Series	1	Yes
[23]	Varactor & PIN	Parallel & Series	2	No
[24]	PIN	Series	2	Yes
[25]	Varactor & PIN	Parallel	2	Yes
[26]	PIN	Series	1	Yes
[27]	PIN	Parallel with vias	2	No
[28]	PIN	Parallel with vias	2	Yes

[29]	PIN	Series	1	Yes
[30]	PIN	Parallel with vias	3	No
[31]	PIN	Parallel with vias	2	No
[32]	Varactor	Parallel	1	No
[33]	Varactor	Parallel & Parallel with vias	1 & 2	No
[34]	Varactor	Parallel with vias	2	No
[35]	Varactor	Parallel with vias	2	Yes
[36]	PIN	Series	1	Yes
[37]	Varactor & PIN	Parallel	1	No
[38]	Varactor	Parallel	1	No

### 1.3 Objectives

The purpose of this study is to predict and verify the electromagnetic and mechanical performances of a variable frequency stealth radome. The variable frequency stealth radome is a radome that has the function of shifting the transmission frequency of the stealth radome by applying an active frequency selective surface to the stealth radome. If the structure of the variable frequency selective surface is complex, it is very difficult to verify the mechanical performance, so it should be designed to have the simplest shape as possible. In addition, when an active frequency selective surface having a small unit cell is applied to a large stealth radome, many unit cells are applied. At this time, if the active element supplies voltage in series, a high driving voltage is required. Therefore, active elements must be connected in parallel to be designed to operate at low voltages. The objective of this study is to design an active frequency selective surface that satisfies these conditions and verify its applicability to stealth radomes.

To predict the electromagnetic performance of a variable frequency stealth radome, a study is conducted on an electromagnetic performance prediction technique that varies depending on the curvature and incident angle. In general, in order to measure the electromagnetic performance of a stealth structure, a flat specimen is manufactured and measured using free space measurement. However, since the stealth radome is composed of curvature to form the aerodynamic surface, the electromagnetic performance is distorted. To accurately predict such distortion, the electromagnetic performance according to the curvature is accurately predicted by using a theoretical approach to the curvature structure, an equivalent circuit model, and ray tracing method.

In addition, the stealth radome must have mechanical performance that can withstand the aircraft operating environment. General stealth radomes are manufactured using a structure in which a frequency selective surface is inserted inside a sandwich structure applied with a composite material. However, since an active frequency

selection surface with an active element mounted on the surface is applied to the variable frequency stealth radome, if inserted inside, a large load is applied to the diode, causing damage. Therefore, it must be manufactured in a structure in which an active frequency selective surface is attached inside a radome applied with a sandwich structure as shown in Figure 14. As a result, design constraints arise in that the active frequency selective surface must be mounted on only one-side surface. While satisfying these design constraints, the active frequency selective surface must be designed to function properly.

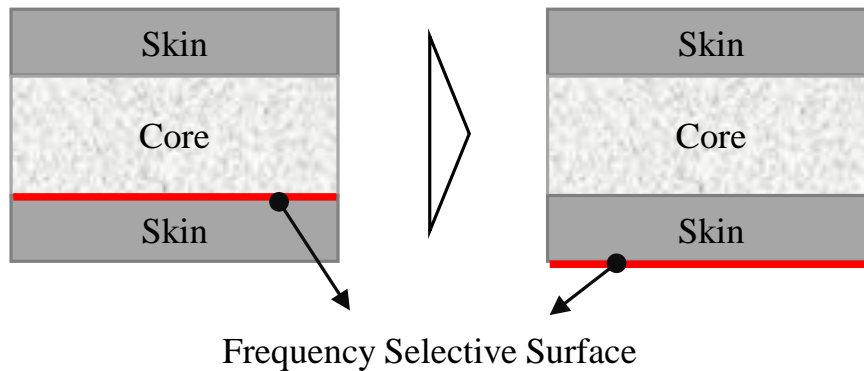


Figure 1.14: Cross section of the stealth radome

Since the active frequency selective surface has a specific pattern, mechanical performance should be predicted in consideration of this pattern. In general, since the pattern of the active frequency selective surface is smaller than the size of the stealth radome to be applied, a multi-scale technique must be applied. In this study, a study on a mapping technique that can directly apply the equivalent properties reflecting the pattern information of the active frequency selective surface to the analysis model without using such a multi-scale technique is conducted. By not using the multi-scale technique, the analysis cost is reduced and the structural analysis of the variable frequency stealth radome having a complex pattern is possible.

## 2 Electromagnetic Performance of Variable Frequency Stealth Radome

### 2.1 Analysis of electromagnetic characteristic of frequency selective surface

Frequency selective surface manufactured from conductors with specific patterns has a characteristic of transmission and reflection at a specific frequency. To design a frequency selective surface, it is necessary to analyze how the frequency selective surface operates on the principle and what characteristics it has.

The principle of operation of the frequency selective surface is as follows. First, an induced current flows on the surface of the frequency selective surface by incident electromagnetic waves on the frequency selective surface. The induced current flows on the surface in the opposite direction as the electric field. If there is a thin conductor on the surface of the frequency selective surface, it has the same effect as inductance, and if the conductor is separated by a small gap, it acts like a capacitor. Therefore, if the patterns functioning as an inductance and a capacitor are adjacent to each other, the frequency selection surface will generate resonance in the same principle as the LC circuit. As a result, it has an electromagnetic characteristic that transmits or reflects an electromagnetic wave at a resonant frequency.

Since the frequency selective surface has the same characteristics as the circuit, it can be converted into an equivalent circuit model. Using such an equivalent circuit model, it is possible to easily analyze the electromagnetic characteristics of the frequency selective surface. As shown in Figure 2.1, the equivalent circuit model can be constructed by separating capacitor and inductance in the cross-loop pattern. If the equivalent circuit model constructed in this way is applied to the transmission line theory, the electromagnetic characteristics can be easily predicted.

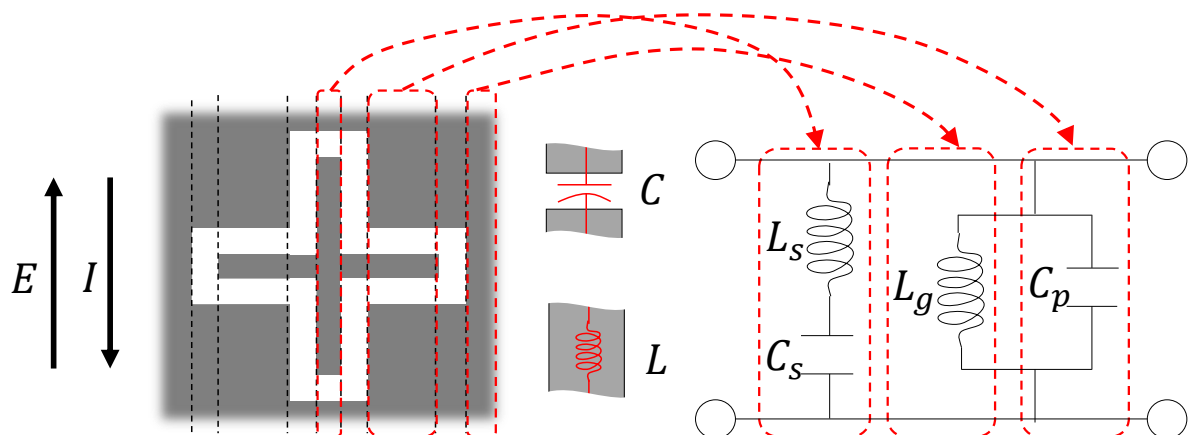


Figure 2.1: Example of converting the equivalent circuit model of a frequency selective surface

The frequency selective surface has various and complex shapes according to the required electromagnetic performance, but in this study, the basic pattern is classified into grids, square loops, and patches, which are easiest to construct an equivalent circuit model. The grid basically acts like an inductance due to a thin line. The patch shape acts like a capacitor due to the narrow spacing between the patches. Square loops have the same characteristics as circuits in which capacitors and inductances are connected in series due to the thin line and the narrow spacing between the loops. By combining three basic pattern, a frequency selective surface having the required electromagnetic performance can be designed, and the combination is shown in Figure 2.2.

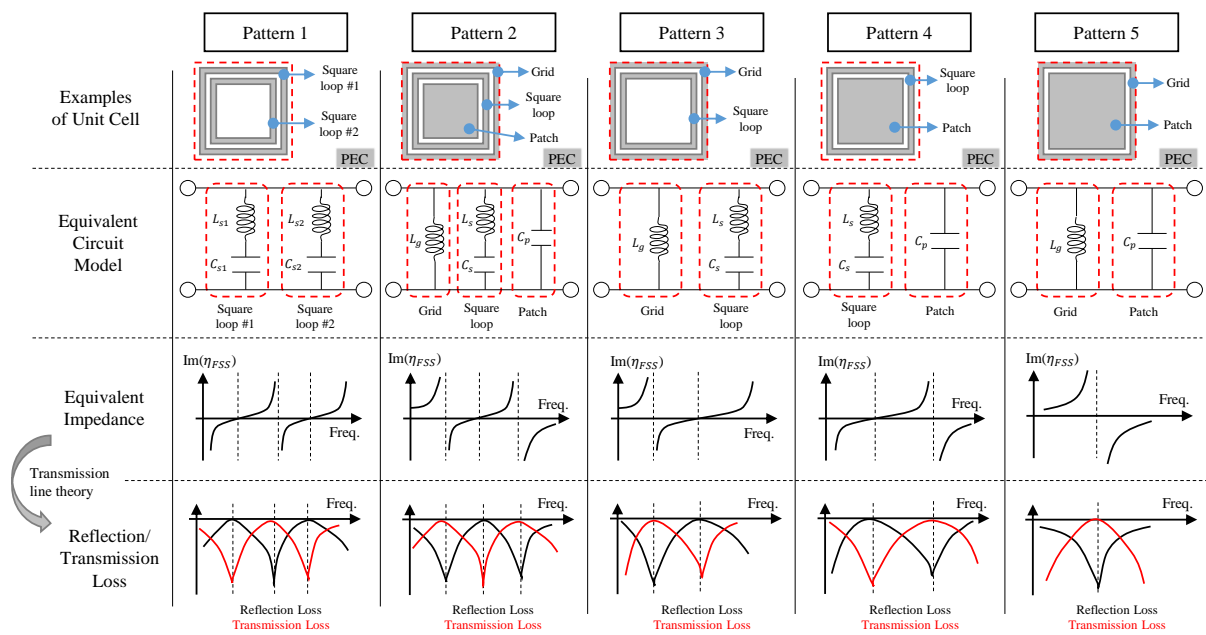


Figure 2.2: Classification of electromagnetic characteristic by combination of frequency selective surface

In the first pattern, two square loop shapes were applied. The square loop basically has one resonance frequency because it has the characteristic of a circuit in which inductance and a capacitor are connected in series. Combining two square loops having such characteristics results in two resonance frequencies, respectively. Each resonant frequency is determined according to the dimensions of each square loop, and by adjusting it, a desired resonant frequency can be obtained.

The second pattern is a combination of grid, square loop and patch shape. In the case of this pattern, it is a pattern that can be obtained by inverting the first pattern, and has the characteristic that the transmission and reflection characteristics are opposite to each other.

The third pattern is a combination of a grid and a square loop. When looking at the equivalent impedance, it can be confirmed that the transmission frequency is generated by the grid dissipating the impedance indefinitely at the low frequency.

The fourth pattern is a combination of square loops and patches. Unlike the third pattern, the fourth pattern is characterized by infinitely dissipating impedance in the high frequency region. By adding a grid and a patch through the third and fourth patterns, it was confirmed how the electromagnetic characteristics of the frequency selective surface changed.

Finally, it is a pattern that combines a grid and a patch. In the case of this pattern, it can be seen that the square loop is inverted and the transmission and reflection characteristics of the square loop are reversed. This information can serve as a guide for how to model the frequency selective surface in an initial design. In addition, if the equivalent circuit model is made and compared with Figure 2.2, it is possible to predict the tendency for transmission and reflection loss.

## ***2.2 Active frequency selective surface design method***

In general, stealth radomes have a sandwich structure applied with a composite material, and a frequency selective surface is inserted inside. However, since active elements are mounted on the surface of the active frequency selective surface, it is difficult to satisfy mechanical performance with conventional structure. This is because when an active frequency selective surface is placed inside a sandwich structure applied with composite material, small diodes are surrounded by the composite material, and many bonding interfaces are generated. In addition, when a load is applied to the stealth radome, a shear load occurs between the interfaces, thereby increasing the probability of damage to the diode. Therefore, if the active frequency selective surface is placed outside as shown in Figure 1.14, the shear load is hardly received and most of the load is supported by the sandwich structure, so the breakage of the active frequency selective surface can be prevented. To apply this structure, the active frequency selective surface should be designed to use only one-side surface so that it can be attached inside the stealth radome.

In the active frequency selection surface, an active element is mounted on the surface, and the resonance frequency can be shifted by controlling the impedance of the active elements. To control the impedance of the active elements, the same voltage must be applied to all active elements. There are two main ways to apply voltage to active elements.

The first is a method of supplying voltage by connecting active elements in series, and the second is a method of supplying voltage in parallel by adding a voltage feed line. When voltage is supplied by connecting active elements in series, the required voltage increases as the size of the active frequency selection surface increases. Therefore, since the size of the stealth radome is larger than the size of the unit cell of the active frequency selective surface, the method of supplying voltage in series to the active elements is not suitable. In the case of supplying voltage in parallel, it is a suitable method of use only when the size of the object to be applied is small.

In conclusion, the active frequency selective surface for application to stealth radomes should use a method of supplying voltage in parallel. In this case, a voltage feed line is indispensable. Therefore, the active frequency selective surface applicable to the stealth radome should use only one-side surface and can supply voltage to

the active elements in parallel.

To design an active frequency selective surface, it is necessary to understand what kind of electromagnetic characteristics it has when an active element is applied to the frequency selective surface. Therefore, the electromagnetic characteristics of the active element were analyzed using diode mainly used in active frequency selective surface.

The electromagnetic characteristics of the diode change according to the direction of the applied voltage and current. Figure 2.3 shows the diode applied to the basic shape of the frequency selective surface in consideration of the characteristics of diode. In the figure,  $R_f$  is the resistance when the diode is in the forward direction,  $R_r$  is the resistance when the diode is in the reverse direction, and  $C_d$  is the capacitor when the diode is in the reverse direction. In addition,  $L_g$ ,  $C_p$ ,  $L_s$ , and  $C_s$  are generated by the pattern of frequency selective surface.

A diode has characteristics of resistance when the current flows in the forward direction, and resistance and capacitor when the current flows in the reverse direction.

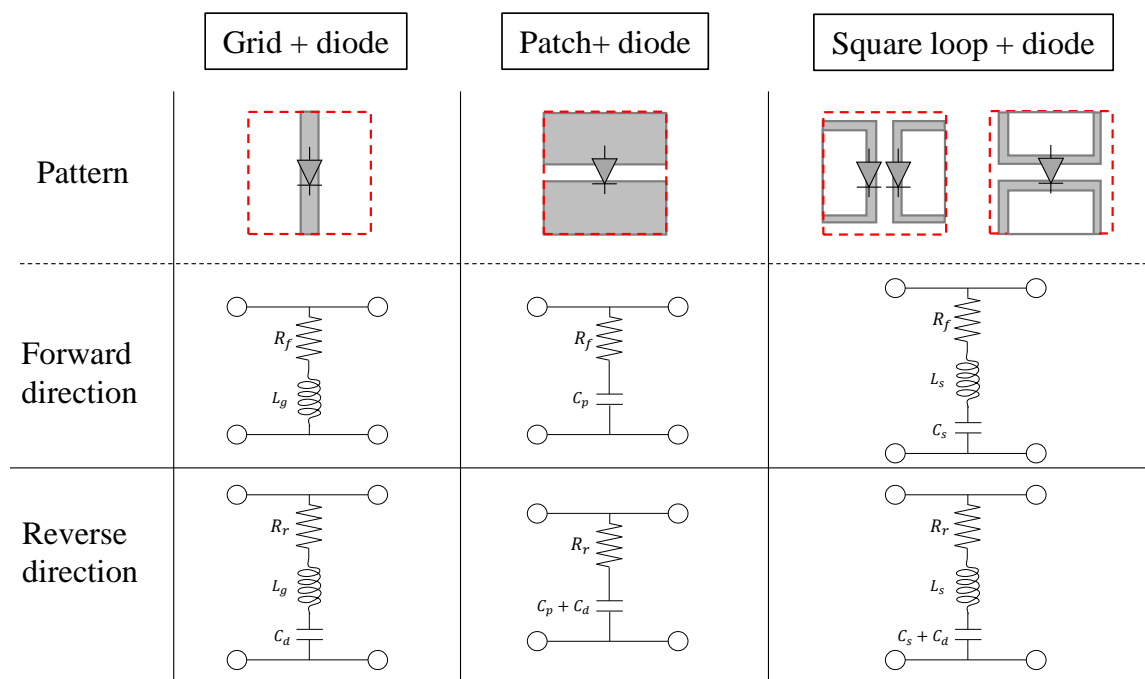


Figure 2.3: Combination of diode and basic pattern

In consideration of the characteristics of these diodes, an equivalent circuit model was constructed in each case. The forward equivalent circuit model of a pattern that combines a grid and a diode is simply a circuit that connects resistance and inductance. Therefore, since resonance does not occur, it is not suitable for a frequency selective surface. The reverse equivalent circuit model of the pattern combining the grid and the diode is the same as that of a typical RLC circuit, and it can be confirmed that the resonant frequency occurs.

In the pattern in which the patch and diode are combined, the forward and reverse equivalent circuit model is a circuit that connects a resistor and a capacitor, and does not generate a resonant frequency, so it is not suitable for a frequency selection surface.

The pattern in which the square loop and the diode are combined can be classified into two according to the position of the diode. It is a pattern in which a diode is mounted inside a square loop and a pattern that connects the square loop with a diode. Both patterns have the same equivalent circuit model, but in the case of the pattern connecting the square loop, the degree of freedom in dimension design is low due to the size of the diode. Therefore, it is easier to design the diode to be applied inside the square loop.

In the case of a pattern in which a square loop and a diode are combined, both forward and reverse equivalent circuit models are composed of RLC circuits and have a resonant frequency. However, in the case of the forward direction, the electromagnetic performance of the diode does not change depending on the voltage, so it is not suitable for an active frequency selective surface. Therefore, the pattern suitable for the active frequency selective surface is a pattern in which a grid and a diode are combined, a pattern in which a square loop and a diode are combined, and both patterns must supply voltage in the reverse direction.

General antennas mainly have polarization characteristics, so there is no problem in using both patterns. However, in order to improve the antenna performance of fighter, research on an antenna to which double polarization is applied is actively in progress. The pattern in which the grid and the diode are combined has poor polarization stability and is difficult to apply to a double polarization system. Therefore, in this study, in order to consider polarization stability, an active frequency selective surface was designed with a pattern in which a square loop and a diode are combined.

To design an active frequency selective surface suitable for stealth radome, voltage must be supplied to the active elements in parallel. Therefore, a voltage feed line has to be added. In the previous research, a new layer was added to add a voltage feed line and a voltage was supplied through the via hole.

In some studies, there is a study in which a voltage feed line is added using only one-side surface without adding a new layer, but there is a problem that the polarization stability is poor. To solve this problem, a study was also conducted to satisfy polarization stability by configuring an active frequency selective surface with poor polarization stability into two layers. However, if two active frequency selective surface are added to the stealth radome, mechanical stability is degraded because the active frequency selective surface must be inserted inside the sandwich structure as mentioned above.

In this study, the diode was connected in parallel using the method of adding a voltage feed line without creating an additional layer in the previously selected square loop and diode-coupled pattern. Figure 2.4 shows an active frequency selective surface designed. Only one-side surface was used, and diodes were connected in parallel to operate at a low voltage. To minimize the voltage feed line, positive and negative voltages were alternately arranged, and a pattern in which a square loop and a diode were combined was added between them. A square loop and a voltage feed line were connected to allow voltage to be applied to the diode, and the pattern

was designed to be as symmetrical as possible. As a result, as the voltage feed line was added, it was designed in a pattern similar to the pattern in which the square loop and the grid are combined, and the electromagnetic characteristics are also considered to be similar to the pattern.

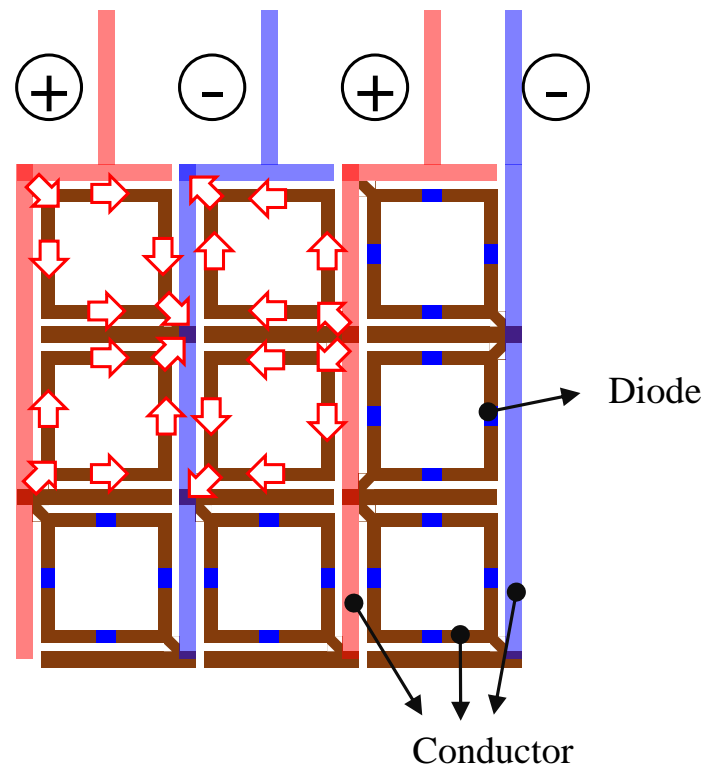


Figure 2.4: Voltage supply method of the active frequency selective surface

### ***2.3 Electromagnetic design and performance measurement of variable frequency stealth radome***

There are two types of diodes that can be used for the variable frequency selective surface. One is a PIN diode and the other is a varactor diode. PIN diodes are mainly used for ON/OFF, and varactor diodes are used to shift the resonant frequency.

It is more advantageous to improve the survivability of a fighter to shift the transmission frequency rather than turning the transmission frequency ON/OFF of the stealth radome. To improve the survivability of the fighter, the antenna communicates using various frequencies. The transmission frequency of the stealth radome for protecting such an antenna must also have various transmission frequencies to match the frequency of the antenna. Therefore, among the two diodes, an active frequency selective surface was designed using a varactor diode suitable for stealth radome.

The varactor diode used was MAVR-000120, and it was designed to apply an active frequency selective surface to a sandwich structure. The dimensions of the designed variable frequency stealth radome are shown in Figure 2.5. To fabricate the designed active frequency selective surface, a film coated with 64  $\mu\text{m}$  of copper on 25  $\mu\text{m}$  of polyimide was used. A copper pattern designed through a photoresist process was manufactured, and varactor diodes were mounted on it to manufacture active frequency selective surface specimen. GFRP used for sandwich structure is GEP-112 and fomex is used for PVC foam. GFRP and PVC foam were bonded using 3M AF-126, and when bonding, using an autoclave, vacuum and 3 bar pressure were applied and cured at 120 degrees for 1 hour. The sandwich structure and active frequency selective surface were attached using 3M Super-77, and the fabricated specimen is shown in Figure 2.6.

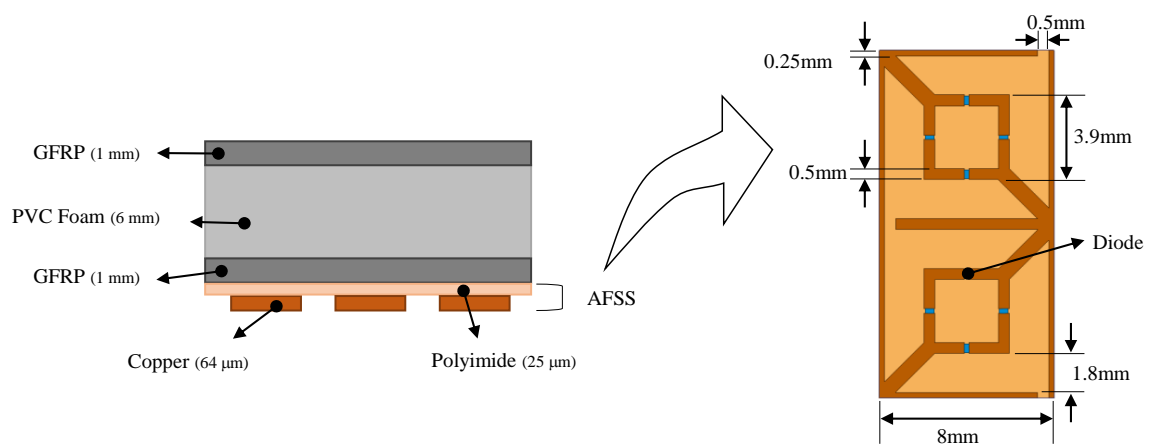


Figure 2.5: Designed variable frequency stealth radome (AFSS: Active frequency selective surface)

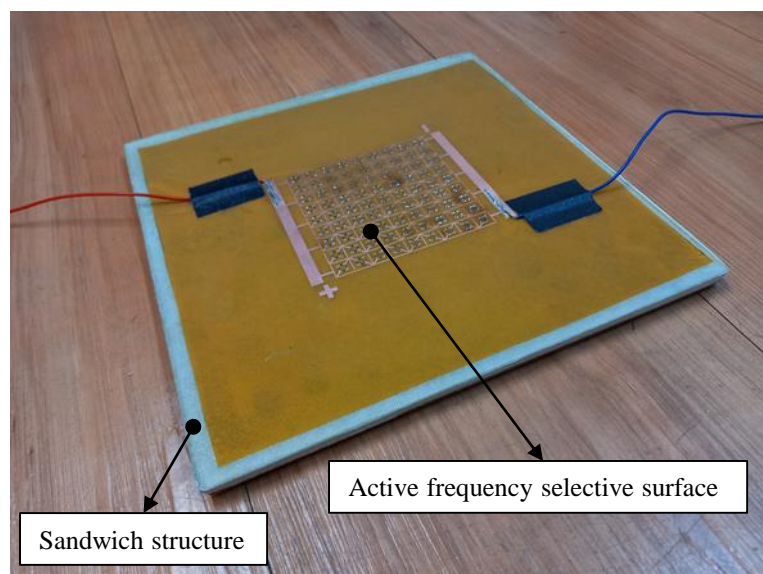


Figure 2.6: Flat variable frequency stealth radome specimen

To measure the electromagnetic performance of the active frequency selective surface, free space measurement with a focused horn antenna was used as shown in Figure 2.7. To measure the electromagnetic performance of a variable frequency stealth radome, the pattern of the active frequency selective surface must be considered. In the case of an active frequency selective surface, it is not a perfectly symmetrical structure because it has a pattern in which a voltage must be applied to the diode. Therefore, the electromagnetic performance varies depending on the direction of the electric field of the incident electromagnetic wave. Electromagnetic performance was measured by dividing the case where the direction of the electric field of the incident electromagnetic wave is perpendicular and parallel based on the direction in which the voltage is applied. The result is shown in Figure 2.8.

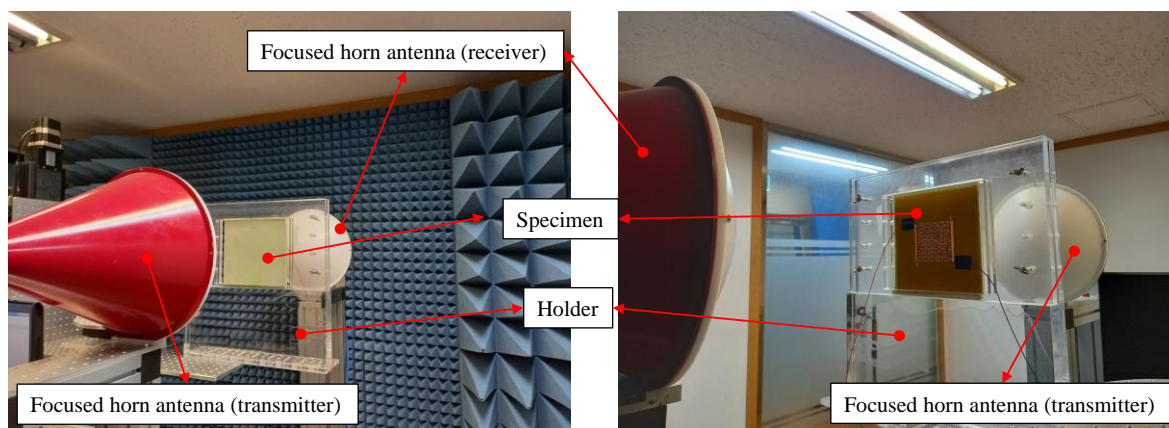
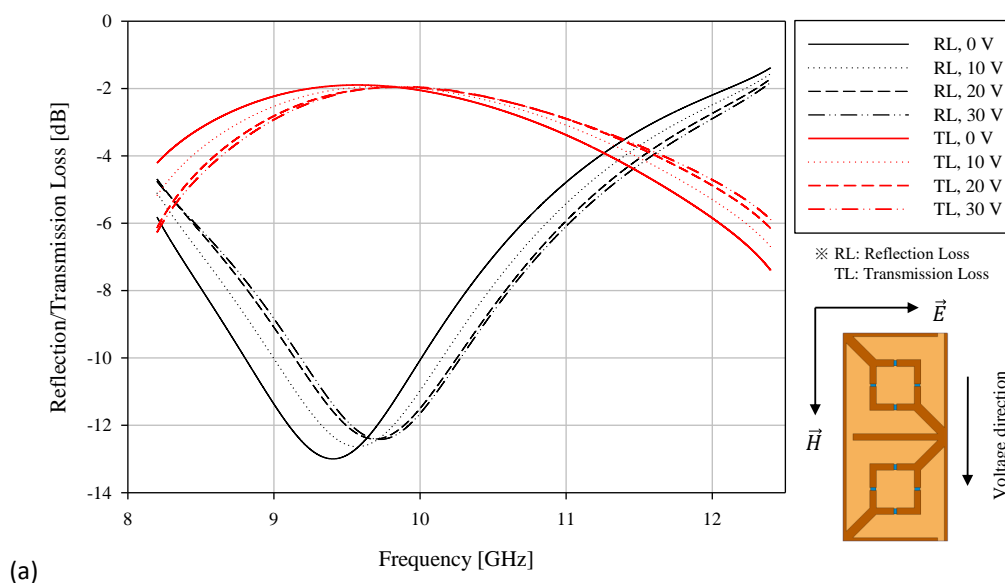


Figure 2.7: Electromagnetic performance measurement of variable frequency stealth radome specimen using a free space measurement system



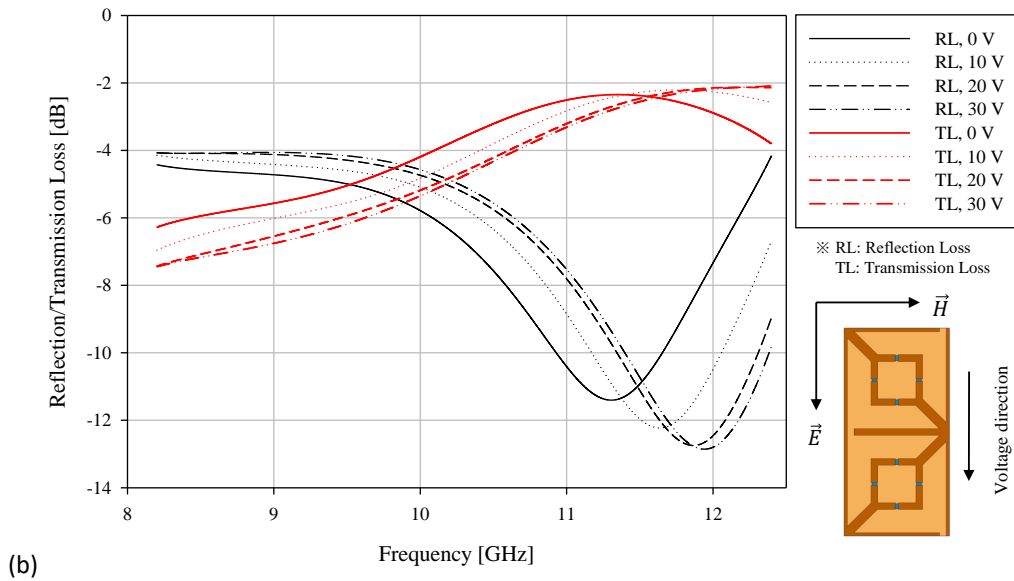


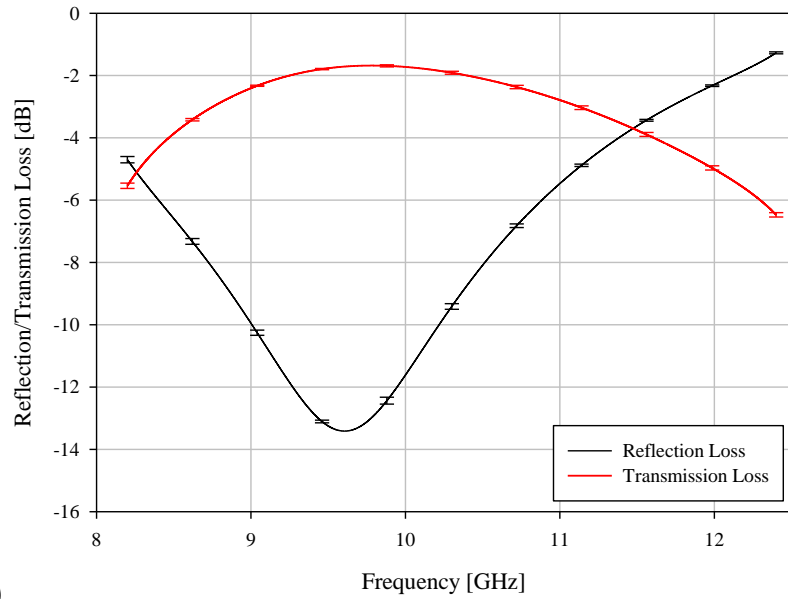
Figure 2.8: Measurement result of electromagnetic performance (a) perpendicular electric-voltage direction

(b) parallel electric-voltage direction

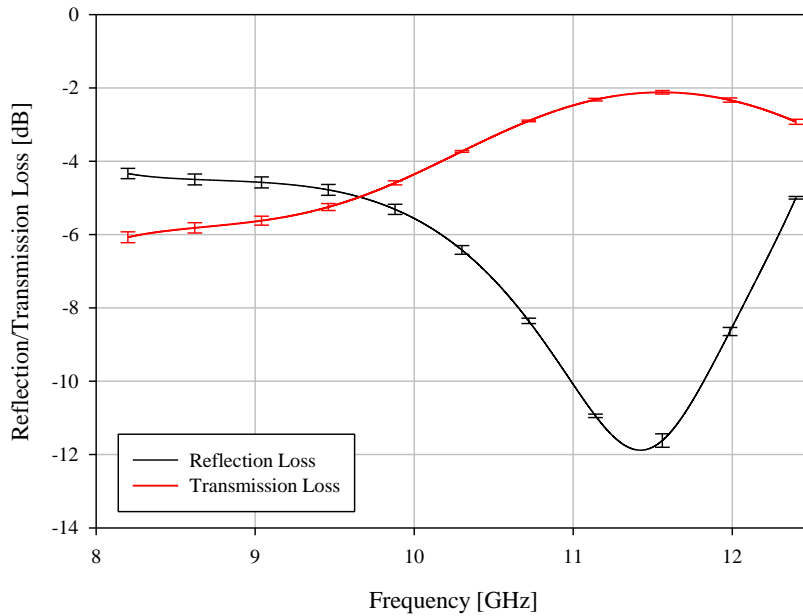
In the case of the perpendicular electric-voltage direction, it has a transmission frequency of 9.4 GHz when the voltage is 0 V, and 9.72 GHz when the voltage is 30 V. It was confirmed that the transmission loss at the transmission frequency was -1.89 dB at 0 V and -1.94 dB at 30 V. In the case of parallel electric-voltage direction, it has a transmission frequency of 11.35 GHz when the voltage is 0 V and 12.16 GHz when the voltage is 30 V. It was confirmed that the transmission loss at the transmission frequency was -2.34 dB at 0 V and -2.08 dB at 30 V.

It was confirmed that the transmission frequency shifted in both directions in the X band, and the transmission frequency shifted 0.32 GHz in the Perpendicular electric-voltage direction and 0.81 GHz in the Parallel electric-voltage direction. Since the electromagnetic characteristics change according to the direction of the electric field of the incident electromagnetic wave, the direction of the unit cell must be determined in consideration of the polarization characteristics of the antenna inside the stealth radome.

Since the active frequency selective surface has a unit cell, it is necessary to confirm whether it has the same electromagnetic performance regardless of the size of the unit cell. The size of the electromagnetic wave generated from the focused horn antenna is 60 mm, and the unit cell size of the designed active frequency selective surface is 8 mm. Therefore, the specimen was moved up and down and left and right by 2 mm to measure the electromagnetic performance of a total of 9 points. It was measured without applying voltage, and the result is shown in Figure 2.9.



(a)



(b)

Figure 2.9: Electromagnetic performance measurement result of variable frequency stealth radome specimen measured at 2 mm intervals (a) perpendicular electric-voltage direction (b) parallel electric-voltage direction

As a result, it was confirmed that the average of the standard deviation values at each frequency was 0.055 dB in the perpendicular electric-voltage direction and 0.095 dB in the parallel electric-voltage direction. These levels can be seen to have almost the same results, and it can be confirmed that the electromagnetic performance does not differ significantly depending on the size and location of the unit cell.

## **3 Prediction of Electromagnetic Performance of Curved Variable Frequency Stealth Radome**

### ***3.1 Electromagnetic performance prediction process of curved structure***

The stealth radome is manufactured in a curved structure to form the aerodynamic surface of an aircraft. Therefore, a technique for predicting the electromagnetic performance of a curved structure is required, and many researches are being conducted to analyse more realistic aerospace structural shapes.

Philips [39] predicted the transmission loss in the curved structure using ray tracing method. Also, in study of sipus [40], the curved structure was approximated by overlapping the subarrays. In study of Ding [41], the curved structure was evaluated by applying a multilevel fast multipole algorithm (MLFMA) to the volume-surface integral equation (VSIE). Other previous researches predicted electromagnetic performance using electromagnetic analysis methods [42-46], and predicted electromagnetic performance of curved structures using various theoretical approaches [47,48].

In this study, since the size of the unit cell of the active frequency selective surface is very small compared to the size of the stealth radome, the method of predicting the electromagnetic performance by electromagnetic analysis is very inefficient.

To predict the electromagnetic performance of the structure applied to the frequency selective surface, a commercial electromagnetic analysis software is generally used. The electromagnetic performance is predicted by modeling only the unit cell without modeling the entire structure. This method can only be applied to a flat structure, and it is impossible to predict the electromagnetic performance of a curved structure. By combining the unit cell analysis method with other methods, the electromagnetic performance in the curved structure can be predicted. In this study, an electromagnetic performance prediction process that combines unit cell analysis, equivalent circuit model, and ray tracing method is proposed, and this method is shown in Figure 3.1.

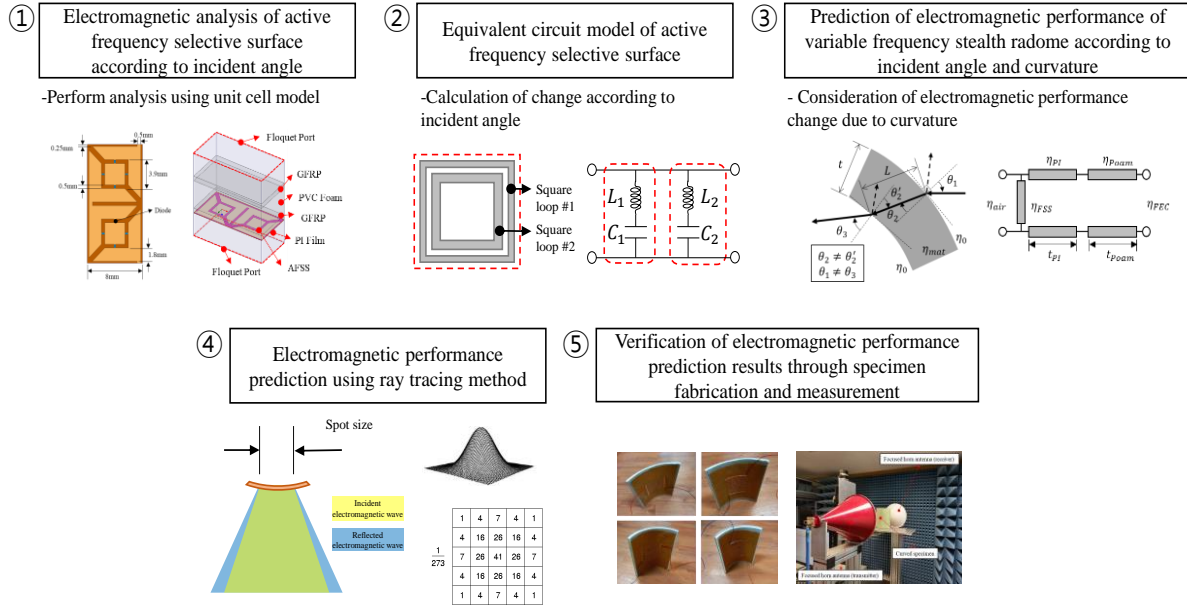


Figure 3.1: Electromagnetic performance prediction process of curved structure applied with frequency selective surface

First, electromagnetic analysis according to the incident angle of the structure to be predicted is performed. It performs electromagnetic analysis according to the incident angle by modeling the unit structure like predicting the electromagnetic performance of a plate.

Then, through the pattern of the frequency selective surface and the structure of the stealth radome, the equivalent circuit model of the frequency selective surface and the equivalent circuit model of the stealth radome are constructed. Using the electromagnetic analysis results, it is possible to obtain accurate values of each component of the equivalent circuit model. When the obtained equivalent circuit model of the frequency selective surface is applied to the equivalent circuit model considering the incident angle and curvature, the electromagnetic performance of the curved structure can be predicted. The equivalent circuit model considering the incident angle and curvature uses a theoretical approach that can predict the reflection and transmission loss in a curved plate proposed in the next chapter.

Finally, in order to verify the method of predicting the electromagnetic performance according to the curvature and the incident angle, the same electromagnetic wave as the measurement system is generated, and the ray tracing method is used to determine how the electromagnetic wave propagates. In this method, the electromagnetic performance of the curved structure applied with the frequency selective surface can be predicted. This method has the advantage of being able to predict the electromagnetic performance according to the incident angle and curvature using the result of the unit cell analysis. And by constructing only an equivalent circuit model, even large structures can easily predict electromagnetic performance without complex analysis. In the next section, the electromagnetic performance of curved variable frequency stealth radome is

predicted and verified using this prediction process.

### 3.2 Theoretical approach to electromagnetic performance in curved plates

To predict the electromagnetic performance of curved variable frequency stealth radome, a theoretical approach is proposed for the reflection and transmission loss of curved plates. When a plane wave is incident on a structure with a constant curvature, the path of the electromagnetic wave to predict the electromagnetic performance in a curved structure is shown in Figure 3.2.

The electromagnetic wave incident at  $\theta_1$  is transmitted to  $\theta_2$  at the first interface, but the incident angle changes to  $\theta'_2$  at the second interface due to the curvature. In the case of a flat plate,  $\theta_1$  and  $\theta_3$  will be the same, but due to the thickness of the curved structure, the angle of the electromagnetic wave incident on the curved structure and the angle of the transmitted electromagnetic wave are different. This difference increases as the thickness of the path of the electromagnetic wave increases and the curvature increases.

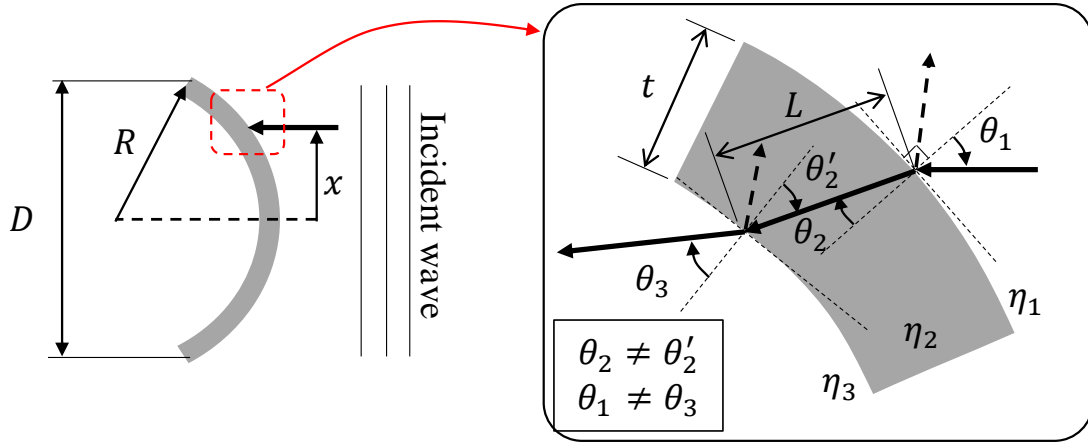


Figure 3.2: Schematic diagram of the electromagnetic wave path in a curved structure

To express the phenomenon due to the curvature by equations, first, the reflection coefficient at the second interface is calculated as shown in the following equations. Where  $\eta$  is the intrinsic impedance and  $\beta$  is the phase constant. Since it is incident on the interface at a specific angle, it is classified into TE and TM mode.

$$\Gamma_{23}^{TE} = \frac{\eta_3 \sec \theta_3 - \eta_2 \sec \theta'_2}{\eta_3 \sec \theta_3 + \eta_2 \sec \theta'_2} \quad (3.1)$$

$$\Gamma_{23}^{TM} = \frac{\eta_3 \cos \theta_3 - \eta_2 \cos \theta'_2}{\eta_3 \cos \theta_3 + \eta_2 \cos \theta'_2} \quad (3.2)$$

And if the impedance ( $\eta_w$ ) according to the thickness direction is defined inside the curved structure using Equations 3.1 and 3.2, it is as follows. Here,  $z$  is the coordinate in the thickness direction with the second interface as the origin.

$$\eta_w^{TE}(z) = \eta_2 \frac{e^{-j\beta_2 z \cos \theta_2} + \Gamma_{23}^{TE} e^{j\beta_2 z \cos \theta_2}}{e^{-j\beta_2 z \cos \theta_2} - \Gamma_{23}^{TE} e^{j\beta_2 z \cos \theta_2}} \quad (3.3)$$

$$\eta_w^{TM}(z) = \eta_2 \frac{e^{-j\beta_2 z \cos \theta_2} + \Gamma_{23}^{TM} e^{j\beta_2 z \cos \theta_2}}{e^{-j\beta_2 z \cos \theta_2} - \Gamma_{23}^{TM} e^{j\beta_2 z \cos \theta_2}} \quad (3.4)$$

Impedance at the first interface can be calculated by substituting  $L \cos \theta_2$ , which is the thickness direction distance between the second interface and the first interface, into  $z$ , and substituting Equations 3.1 and 3.2 into Equations 3.3 and 3.4. This can be simply summarized as the following equations.

$$\eta_w^{TE} = \eta_{2s} \frac{\eta_{3s} \cos(\beta_2 L \cos^2 \theta_2) + j\eta'_{2s} \sin(\beta_2 L \cos^2 \theta_2)}{\eta'_{2s} \cos(\beta_2 L \cos^2 \theta_2) + j\eta_{3s} \sin(\beta_2 L \cos^2 \theta_2)}$$

$$\left( \text{Where, } \eta_{1s} = \eta_1 \sec \theta_1, \quad \eta_{2s} = \eta_2 \sec \theta_2, \quad \eta'_{2s} = \eta_2 \sec \theta'_2, \quad \eta_{3s} = \eta_3 \sec \theta_3, \quad (3.5) \right.$$

$$\left. \beta = \frac{\omega}{c_0} \sqrt{\mu_r \epsilon_r}, \quad \frac{\beta_1}{\beta_2} = \frac{\sin \theta_2}{\sin \theta_1} \right)$$

$$\eta_w^{TM} = \eta_{2p} \frac{\eta_{3p} \cos(\beta_2 L \cos^2 \theta_2) + j\eta'_{2p} \sin(\beta_2 L \cos^2 \theta_2)}{\eta'_{2p} \cos(\beta_2 L \cos^2 \theta_2) + j\eta_{3p} \sin(\beta_2 L \cos^2 \theta_2)}$$

$$\left( \text{Where, } \eta_{1p} = \eta_1 \cos \theta_1, \quad \eta_{2p} = \eta_2 \cos \theta_2, \quad \eta'_{2p} = \eta_2 \cos \theta'_2, \quad \eta_{3p} = \eta_3 \cos \theta_3, \quad (3.6) \right.$$

$$\left. \beta = \frac{\omega}{c_0} \sqrt{\mu_r \epsilon_r}, \quad \frac{\beta_1}{\beta_2} = \frac{\sin \theta_2}{\sin \theta_1} \right)$$

By obtaining the impedance at the first interface, the reflection coefficient of the curved structure can be finally calculated, and the equations is as follows.

$$\Gamma_{TE} = \frac{\eta_{TE} - \eta_{1s}}{\eta_{TE} + \eta_{1s}} \quad (3.7)$$

$$\Gamma_{TM} = \frac{\eta_{TM} - \eta_{1p}}{\eta_{TM} + \eta_{1p}} \quad (3.8)$$

By calculating the reflection coefficient according to the TE and TM modes of the electromagnetic wave incident on the curved structure using the proposed equations, it is possible to understand the characteristics of the electromagnetic wave that are changed by the curvature and thickness of the structure. These equations are

then used to predict the electromagnetic properties of the curved structure.

### 3.3 Electromagnetic performance prediction using equivalent circuit model

To predict the electromagnetic performance of a curved variable frequency stealth radome, the electromagnetic analysis according to the incident angle must first be performed. When electromagnetic waves are incident on the curved structure, an incident angle must occur. Since the electromagnetic performance of the frequency selective surface varies depending on the incident angle, the electromagnetic performance must be predicted in consideration of this characteristic.

To create an equivalent circuit model, electromagnetic analysis was performed using ANSYS Electronics 2020 R1, a commercial electromagnetic analysis software. The variable frequency stealth radome designed in Chapter 2 was used as it is, and the analysis model is shown in Figure 3.3. A lumped RLC boundary was used to model diodes with capacitor characteristics when current flows in one direction. Referring to the data sheet of the diode (MAVR-000120) used in the design, 1 pF was applied when there was no voltage in the capacitor and 0.15 pF was applied when the voltage of 15 V was applied.

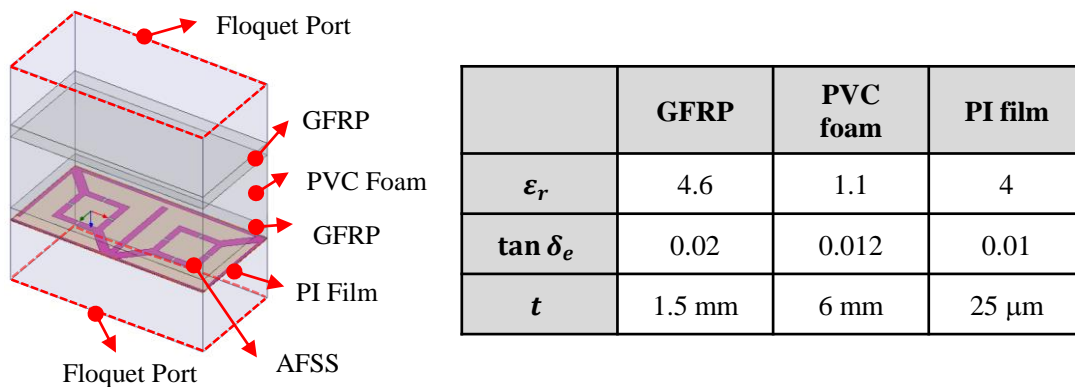


Figure 3.3: Unit cell analysis model of variable frequency stealth radome

To perform electromagnetic analysis according to the incident angle, the incidence angle analysis is generally divided into the TE and TM modes. The TE mode is a case where the electric field is perpendicular to the incident surface, and the TM mode is a case where the magnetic field is perpendicular to the incident surface. Since the designed active frequency selective surface is not perfectly symmetric, the direction of the voltage and the direction of the electric field must be considered as mentioned above. Therefore, in order to predict the electromagnetic performance according to the incident angle of the active frequency selective surface, all four cases must be considered as shown in Figure 3.4.

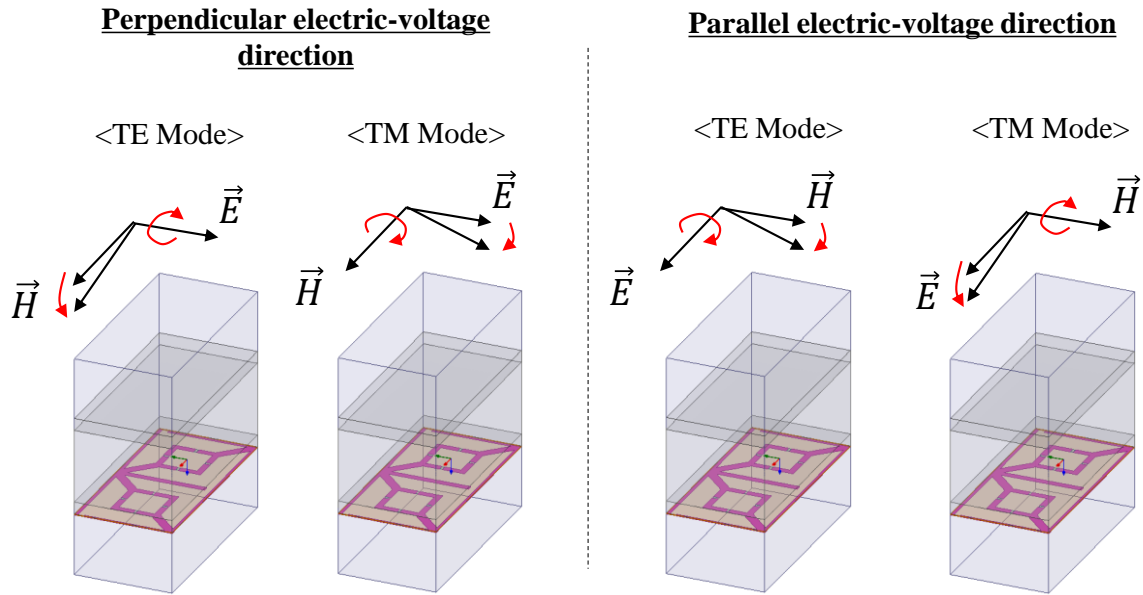


Figure 3.4: Incident angle cases considering active frequency selective surface pattern and TE and TM mode

The results of electromagnetic analysis according to the TE and TM mode are shown in Figures 3.5 and 3.6. First, when there is no voltage the transmission frequency and transmission loss decrease as the incident angle increases in TE mode of the perpendicular electric-voltage direction. In TM mode, as the incident angle increases, the transmission frequency is divided into two. This is because the incident electric field is not parallel to the surface. Due to this angle, the distribution of the electric field induced in the diode in the horizontal direction and the diode in the vertical direction is different, resulting in a phenomenon in which the transmission frequency is divided into two.

In the TE mode of parallel electric-voltage direction, the transmission frequency increases as the incident angle increases. This is the opposite of the TE mode of perpendicular electric-voltage direction. In the TM mode, as the incident angle increased, the peak of transmission loss gradually disappeared. This is because the incident electric field is not parallel to the surface, as the TM mode of the previous perpendicular electric-voltage direction, so the distribution of the electric field induced to the diode is different. The difference from the perpendicular electric-voltage direction is that it does not clearly divide into two transmission frequencies, and the result appears as if the peak value gradually disappears. As shown in Figure 3.6, the analysis result of applying a voltage of 30 V also has the same tendency as when there is no voltage, and since voltage is applied to the diode, the result of an increase in the transmission frequency as a whole can be obtained.

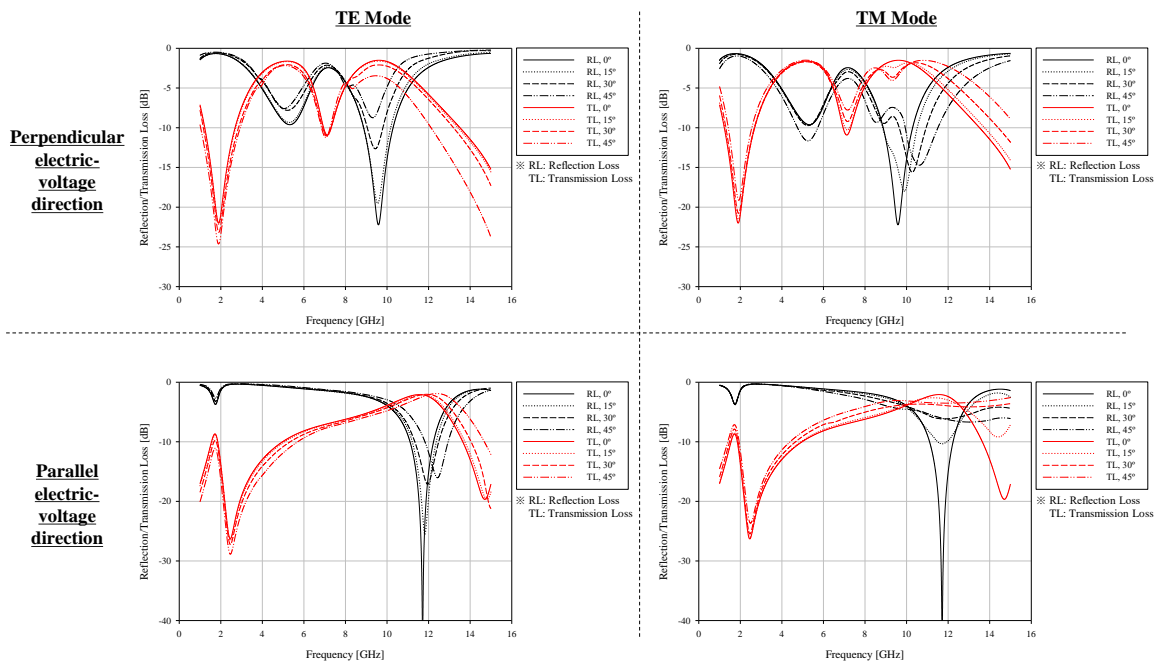


Figure 3.5: Electromagnetic analysis results of a variable frequency stealth radome according to the incident angle when there is no voltage

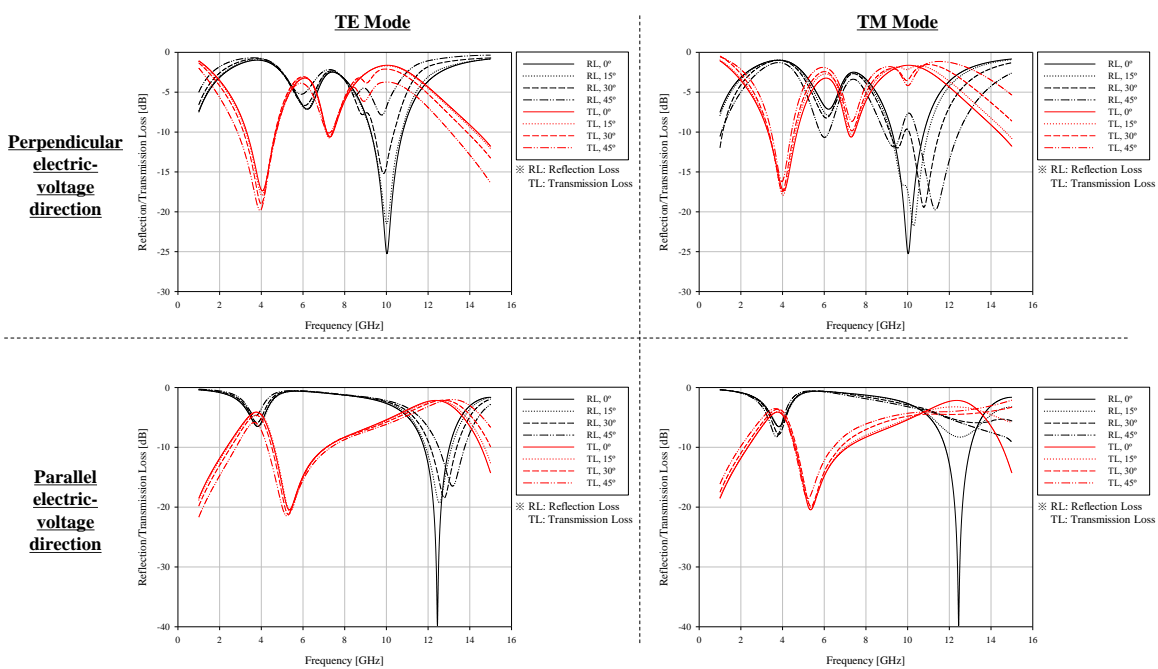


Figure 3.6: Electromagnetic analysis results of a variable frequency stealth radome according to the incident angle when the voltage is 30 V

To verify that the electromagnetic analysis according to the incident angle is the same as the actual

measurement result, the incident angle was given to the specimen to the free space measurement and the electromagnetic performance was measured. The reflected electromagnetic wave was not measured, and the result is shown in Figures 3.7 and 3.8. As a result of the measurement, the transmission frequency tended to decrease as the voltage increased in TE mode of Perpendicular electric-voltage direction as predicted in the analysis. In TM mode, as predicted by the analysis, the transmission frequency tends to be divided as the incident angle increases. Similarly, in the TE mode of the parallel electric-voltage direction, the transmission frequency tended to increase as the incident angle increased. As predicted in the TM mode analysis, it was confirmed that the peak value of the transmission loss gradually disappeared.

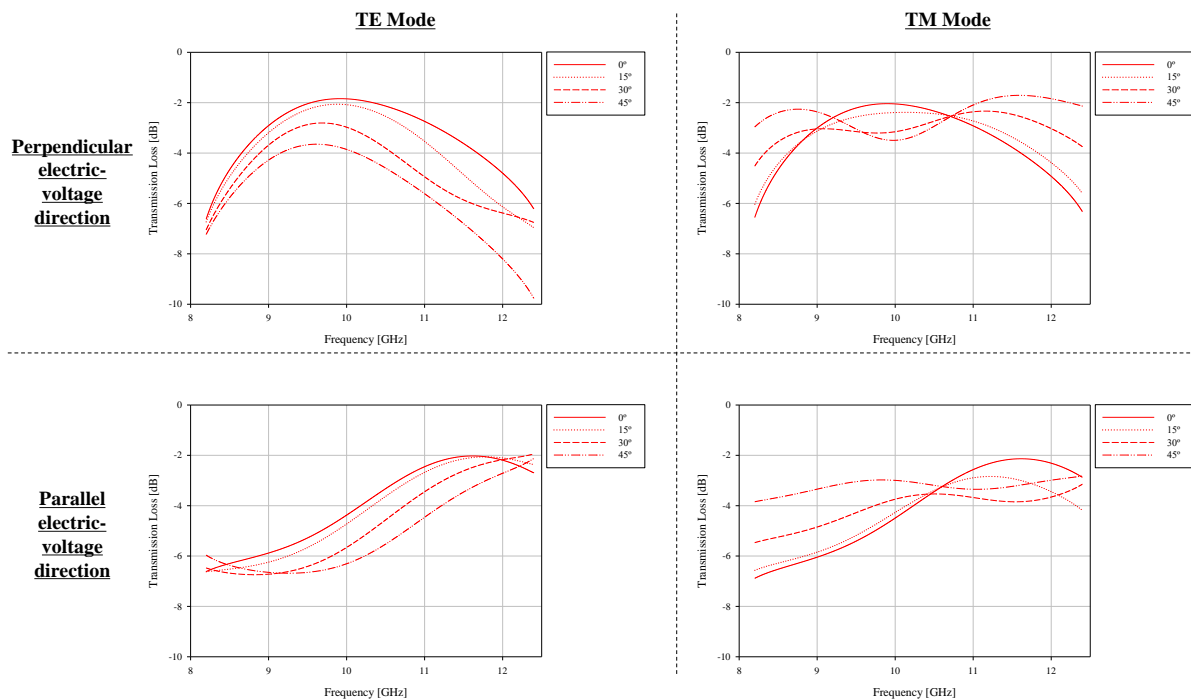


Figure 3.7: Transmission loss measurement results of a variable frequency stealth radome according to the incident angle when there is no voltage

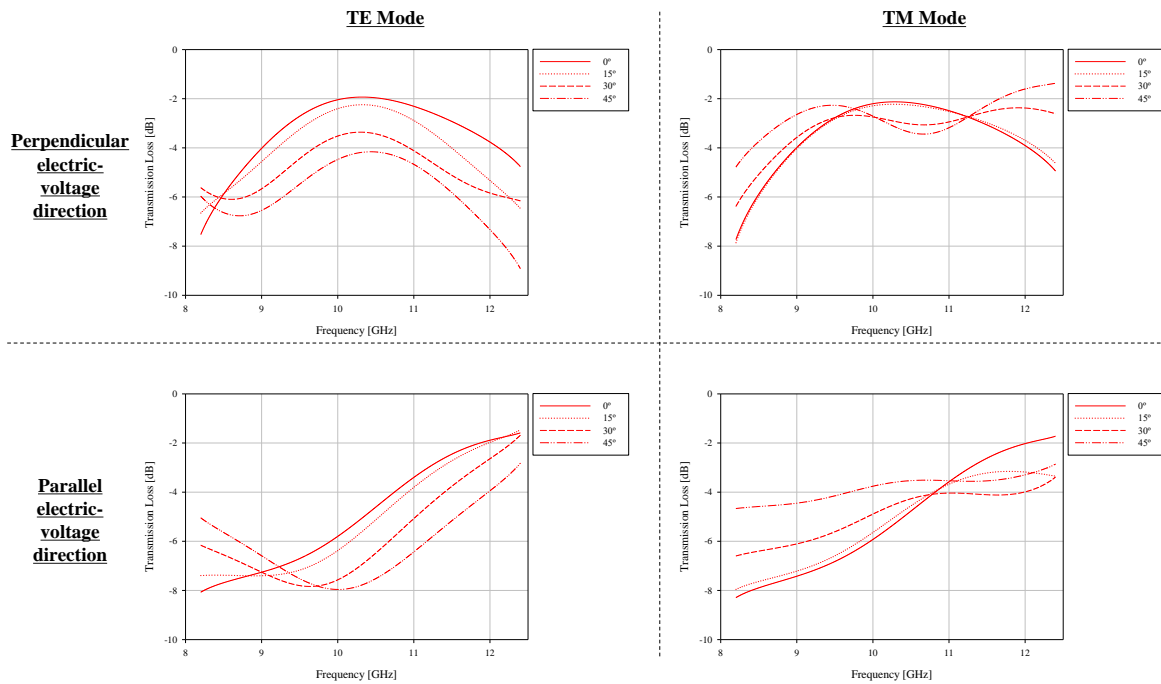


Figure 3.8: Transmission loss measurement results of a variable frequency stealth radome according to the incident angle when the voltage is 30 V

Figure 3.9 shows the equivalent circuit model of a variable frequency stealth radome to predict electromagnetic performance according to the incident angle. To construct an equivalent circuit model of an active frequency selective surface, it is necessary to construct a different equivalent circuit model according to the direction of the electric field and voltage as previously measured the electromagnetic performance of the variable frequency stealth radome specimen. This is because the pattern of the active frequency selective surface is not perfectly symmetric. The equivalent circuit model of the designed active frequency selective surface is shown in Figure 3.10.

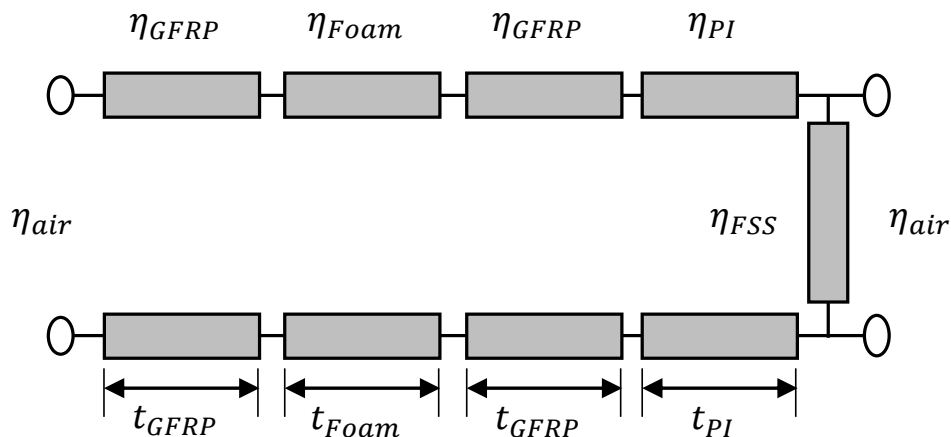


Figure 3.9: Equivalent circuit model of variable frequency stealth radome

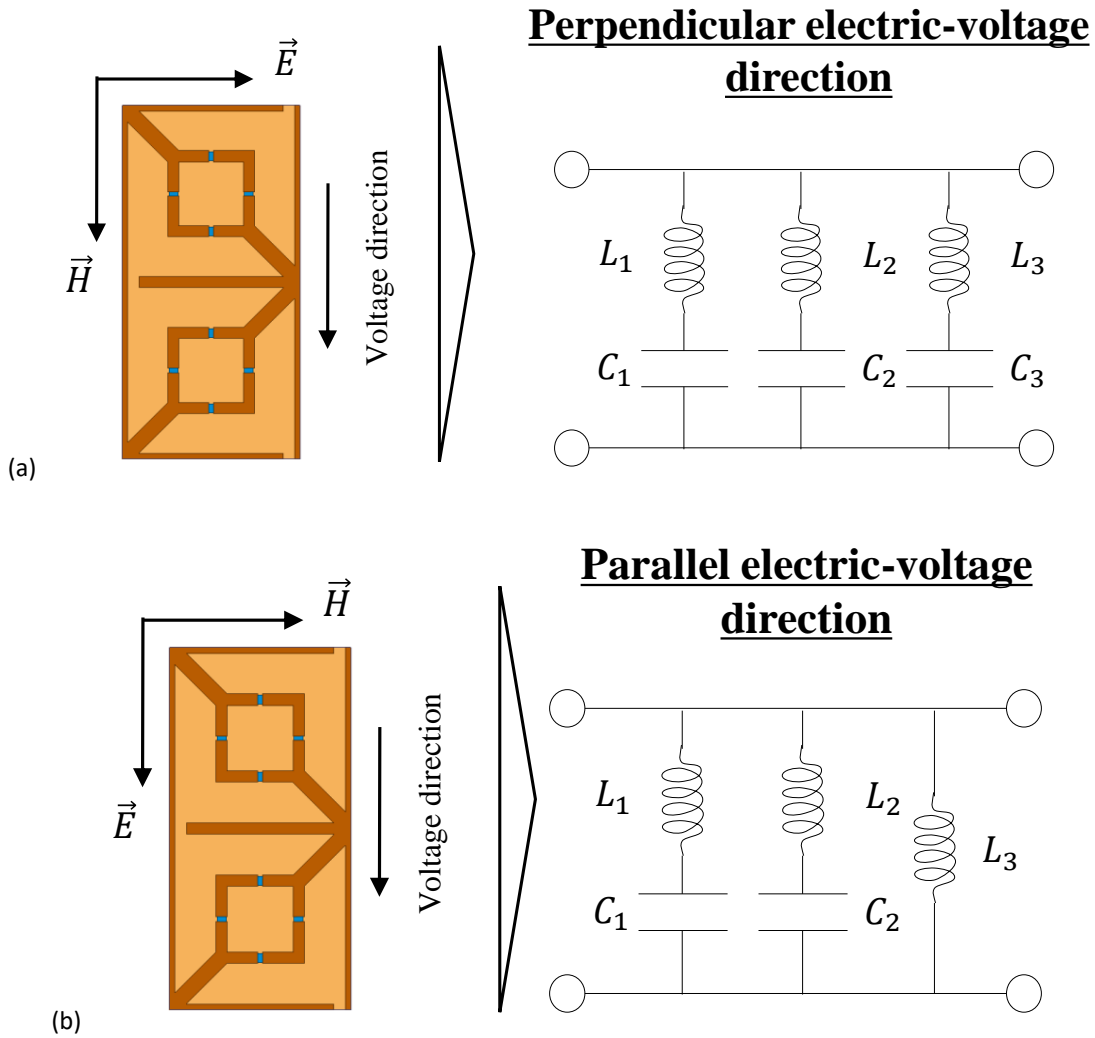


Figure 3.10: Equivalent circuit model of active frequency selective surface (a) Perpendicular electric-voltage direction (b) Parallel electric-voltage direction

When constructing the equivalent circuit model, the direction of the electric field must be considered. This is because an induced current is generated on the surface of the active frequency selective surface in the direction of the electric field. Therefore, the equivalent circuit model was constructed assuming that the current flows in the direction of the electric field.

The equivalent circuit model of perpendicular electric-voltage direction can be composed of an LC circuit by a square loop shape, an LC circuit by a diode, and an LC circuit by a gap between the grid and the grid. The equivalent circuit model of parallel electric-voltage direction was constructed in the same way. The equivalent circuit model of the parallel electric-voltage direction was composed of an LC circuit by a square loop shape, an LC circuit by a diode, and an inductance by a grid. Unlike the perpendicular electric-voltage direction, since there is no gap in the grid in the electric field direction, no additional capacitor is added.

The equivalent circuit model constructed in this way is applied to the transmission line theory to calculate the electromagnetic performance. First, the equivalent impedance in the equivalent circuit model of the perpendicular electric-voltage direction is as Equation 3.9, and the impedance in the equivalent circuit model of parallel electric-voltage direction is as Equation 3.10.

$$\eta_{FSS} = \frac{(1 - \omega^2 L_1 C_1)(1 - \omega^2 L_2 C_2)(1 - \omega^2 L_3 C_3)}{j\omega[C_1(1 - \omega^2 L_2 C_2)(1 - \omega^2 L_3 C_3) + C_2(1 - \omega^2 L_1 C_1)(1 - \omega^2 L_3 C_3) + C_3(1 - \omega^2 L_1 C_1)(1 - \omega^2 L_2 C_2)]} \quad (3.9)$$

$$\eta_{FSS} = \frac{j\omega L_3(1 - \omega^2 L_1 C_1)(1 - \omega^2 L_2 C_2)}{(1 - \omega^2 L_1 C_1)(1 - \omega^2 L_2 C_2) - \omega^2 L_3[C_1(1 - \omega^2 L_2 C_2) + C_2(1 - \omega^2 L_1 C_1)]} \quad (3.10)$$

The inductance and capacitor required to calculate the impedance of the active frequency selective surface varies depending on the incident angle, and can be calculated using the electromagnetic analysis result. By applying the calculated equivalent impedance of the active frequency selective surface to Equations 3.11 to 3.16, it is possible to calculate the electromagnetic performance of the variable frequency stealth radome.

$$\eta_a = \frac{\eta_{FSS}\eta_{air}}{\eta_{air} + \eta_{FSS}} \quad (3.11)$$

$$\eta_b = \eta_{PI} \frac{\eta_a \cos(\beta_{PI}t) + j\eta_{PI} \sin(\beta_{PI}t)}{\eta_{PI} \cos(\beta_{PI}t) + j\eta_a \sin(\beta_{PI}t)} \quad (3.12)$$

$$\eta_c = \eta_{GFRP} \frac{\eta_b \cos(\beta_{GFRP}t) + j\eta_{GFRP} \sin(\beta_{GFRP}t)}{\eta_{GFRP} \cos(\beta_{GFRP}t) + j\eta_b \sin(\beta_{GFRP}t)} \quad (3.13)$$

$$\eta_d = \eta_{Foam} \frac{\eta_c \cos(\beta_{Foam}t) + j\eta_{Foam} \sin(\beta_{Foam}t)}{\eta_{Foam} \cos(\beta_{PIFoam}t) + j\eta_c \sin(\beta_{Foam}t)} \quad (3.14)$$

$$\eta_e = \eta_{GFRP} \frac{\eta_d \cos(\beta_{GFRP}t) + j\eta_{GFRP} \sin(\beta_{GFRP}t)}{\eta_{GFRP} \cos(\beta_{GFRP}t) + j\eta_d \sin(\beta_{GFRP}t)} \quad (3.15)$$

$$\Gamma = \frac{\eta_e - \eta_{air}}{\eta_e + \eta_{air}} \quad (3.16)$$

The inductance and capacitor of the active frequency selective surface were calculated so that the result using the equation of the equivalent circuit model is the same as that of the electromagnetic analysis. Genetic Algorithm was used to calculate the equivalent circuit model inversely based on the electromagnetic analysis results. An objective function was defined that minimizes the difference between the electromagnetic analysis result and the equivalent circuit model result. If the objective function that minimizes the reflection coefficient obtained in Equation 3.16 is simply used, the most important transmission frequency in electromagnetic performance may not be correct, so the objective function was defined as the sum of the difference between the reflection coefficient and the difference between the resonance frequency. The weight ratio of the reflection coefficient was set to 1, and the weight ratio of the resonance frequency was set to 6. As conditions of Genetic

Algorithm, the number of individuals was 1000 and the number of generations was 100. In addition, the equivalent circuit model equation is easily converged to the local minimum value because of the large nonlinearity. To prevent convergence to this local minimum value, the mutation rate was set to be relatively large as 0.4. The results using the obtained equivalent circuit model are shown in Figures 3.11 and 3.12.

It can be confirmed that both the perpendicular electric-voltage direction and the parallel electric-voltage direction tend to be the same as the previously predicted and measured results. Applying the theoretical approach to the previously proposed curved plate to the defined equivalent circuit model makes it possible to predict the electromagnetic performance according to the curvature.

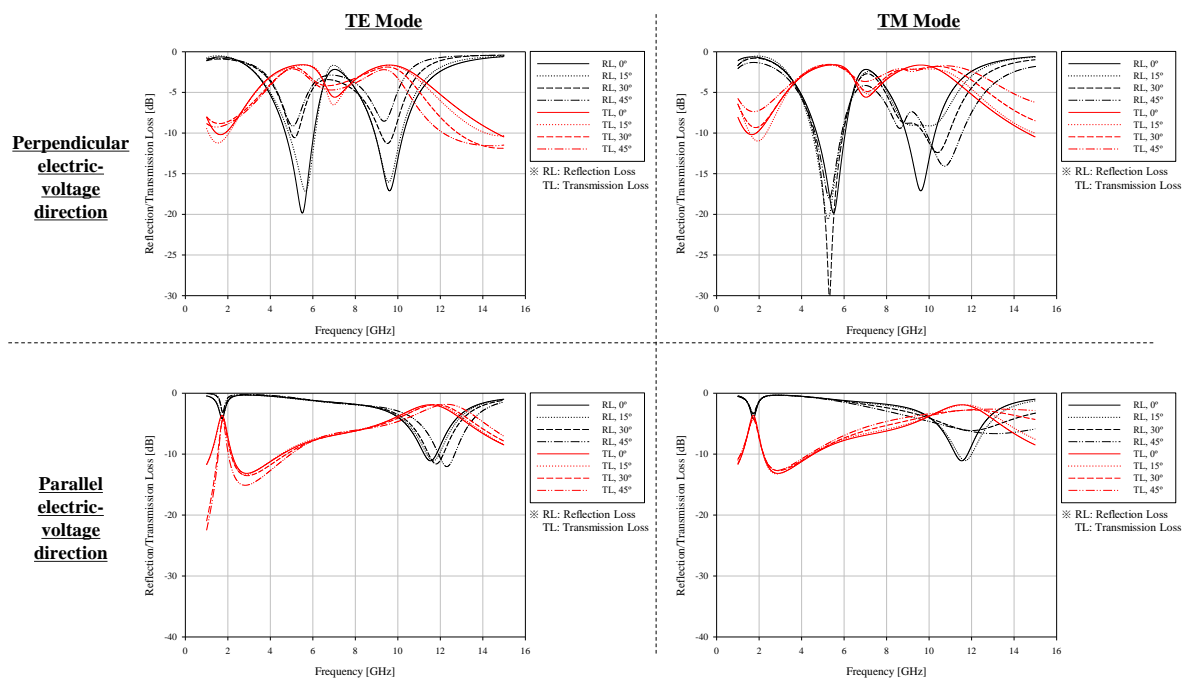


Figure 3.11: Results of the prediction by the equivalent circuit model of a variable frequency stealth radome according to the incident angle when there is no voltage

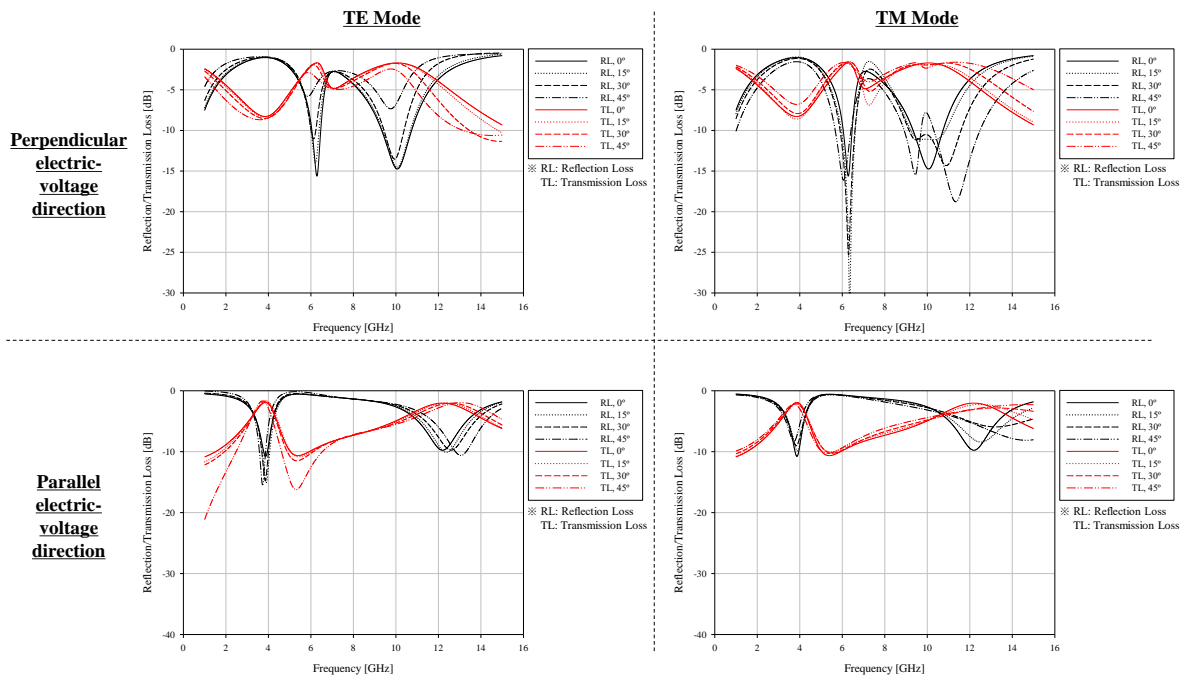


Figure 3.12: Results of the prediction by the equivalent circuit model of a variable frequency stealth radome according to the incident angle when the voltage is 30 V

### 3.4 Verification of prediction method using ray tracing method

The electromagnetic performance prediction method using the previously calculated equivalent circuit model is a method of predicting electromagnetic performance at a very small point. However, there is currently no equipment that can measure electromagnetic performance at such small points. Even if a focused horn antenna is used, the concentrated electromagnetic waves have a specific size of beam.

Therefore, as shown in Figure 3.13, the electromagnetic wave reflected by the curvature spreads more widely and the reflected electromagnetic wave to the antenna decreases. The transmitted electromagnetic waves are more concentrated by the curvature, and most of the electromagnetic waves reach the receiver antenna. To consider the propagation characteristics of such electromagnetic waves, the electromagnetic performance was predicted using the ray tracing method.

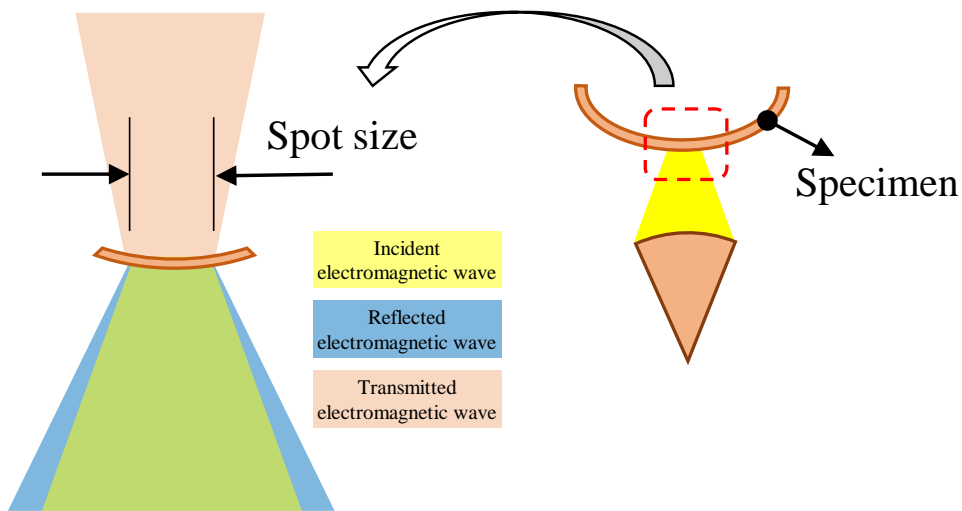


Figure 3.13: Propagation of the electromagnetic waves in using a focused horn antenna

In order to apply the transmitted electromagnetic waves from the focused horn antenna to the ray tracing method, the electromagnetic performance must be predicted by dividing the electromagnetic waves and applying each to an equivalent circuit model. The transmitted electromagnetic wave from the focused horn antenna is divided by  $100 \times 100$  and applied to the equivalent circuit model considering the curvature and incident angle proposed above. Electromagnetic waves that do not reflect to the antenna are generated by the curvature, and electromagnetic wave performance is predicted by excluding these electromagnetic waves.

The electromagnetic wave generated from the focused horn antenna has a size of 60mm as shown in Figure 3.14, and has the same magnitude distribution as the Gaussian distribution. Therefore, when dividing an electromagnetic wave, it must be calculated by considering the magnitude distribution of the electromagnetic wave. Weight ratio was applied in consideration of the magnitude of the electromagnetic wave, and the magnitude of the reflected electromagnetic wave to the antenna was calculated using the ray tracing method and the equivalent circuit model of the divided electromagnetic wave.

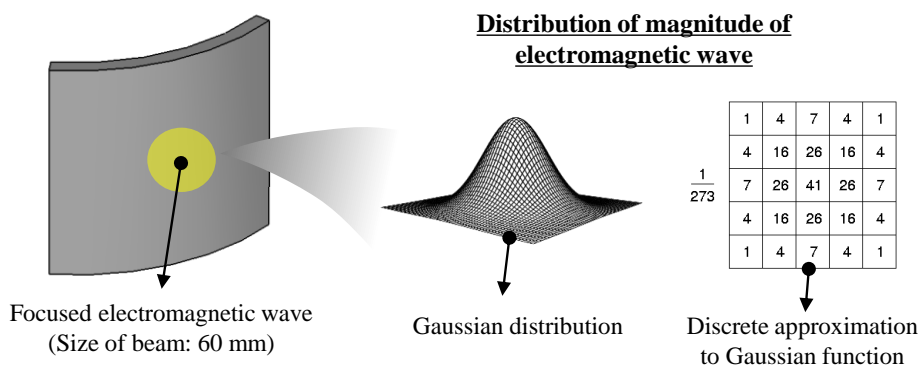


Figure 3.14: Magnitude distribution of electromagnetic waves generated from a focused horn antenna

Then, the reflection coefficient according to the curvature was calculated by summing the electromagnetic performance of the divided electromagnetic waves using Equation 3.17. Here,  $W_k$  is the weight ratio of the magnitude of the electromagnetic wave, and the sum of the weight ratio is 1. For the weight ratio, a matrix obtained by discrete approximation of the Gaussian function was used.

$$|\Gamma|^2 = \sum_{k=1}^N W_k \frac{\langle P_r \rangle}{\langle P_i \rangle} = \sum_{k=1}^N W_k |\Gamma_k|^2 \quad (3.17)$$

Before measuring the electromagnetic performance of the curved structure, since the active frequency selective surface is not completely symmetric, the electromagnetic performance varies depending on the direction of curvature. Therefore, it is necessary to predict the electromagnetic performance according to the mode of the electromagnetic wave and the direction of the curvature as shown in Figure 3.15.

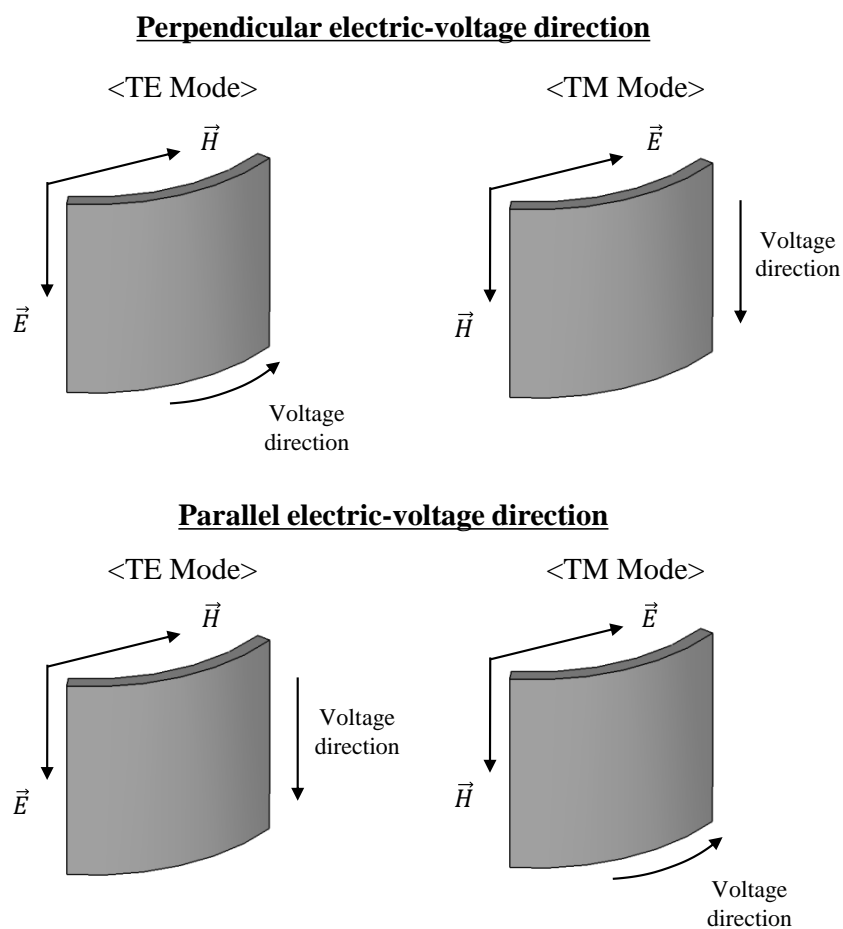


Figure 3.15: Cases of measuring the electromagnetic performance of the curved structure

In each case, electromagnetic performance was predicted when the radius of curvature was 150 mm and 100 mm, the electromagnetic performance is predicted using the equivalent circuit model and ray tracing method as shown in Figures 3.16 and 3.17. Table 3.1 shows the transmission frequencies of the predicted variable frequency stealth radome according to the curvature and voltage. As the prediction results, the transmission frequency tends to increase as the curvature increases. The transmission frequency shifts to an average of 0.55 GHz for a flat plate, an average of 0.48 GHz for a 150 mm radius of curvature, and an average of 0.38 GHz for a 100 mm radius of curvature. As the curvature increases, the transmission frequency shifts less. In addition, it can be confirmed that the reflection loss significantly changes according to the curvature compared to the transmission loss, and this result is considered to have appeared because the ray tracing method was used.

Table 3.1: Transmission frequency prediction results according to curvature and voltage of variable frequency stealth radome

Transmission frequency [GHz]		Perpendicular electric-voltage direction					
		TE mode			TM mode		
		Flat	R = 150 mm	R = 100 mm	Flat	R = 150 mm	R = 100 mm
Applied voltage	0V	9.64	10.12	10.68	9.64	9.94	10.1
	30V	10.03	10.66	11.24	10.03	10.61	10.67
Transmission frequency [GHz]		Parallel electric-voltage direction					
		TE mode			TM mode		
		Flat	R = 150 mm	R = 100 mm	Flat	R = 150 mm	R = 100 mm
Applied voltage	0V	11.57	12	12.37	11.57	12.1	12.06
	30V	12.28	12.4	12.4	12.28	12.4	12.4

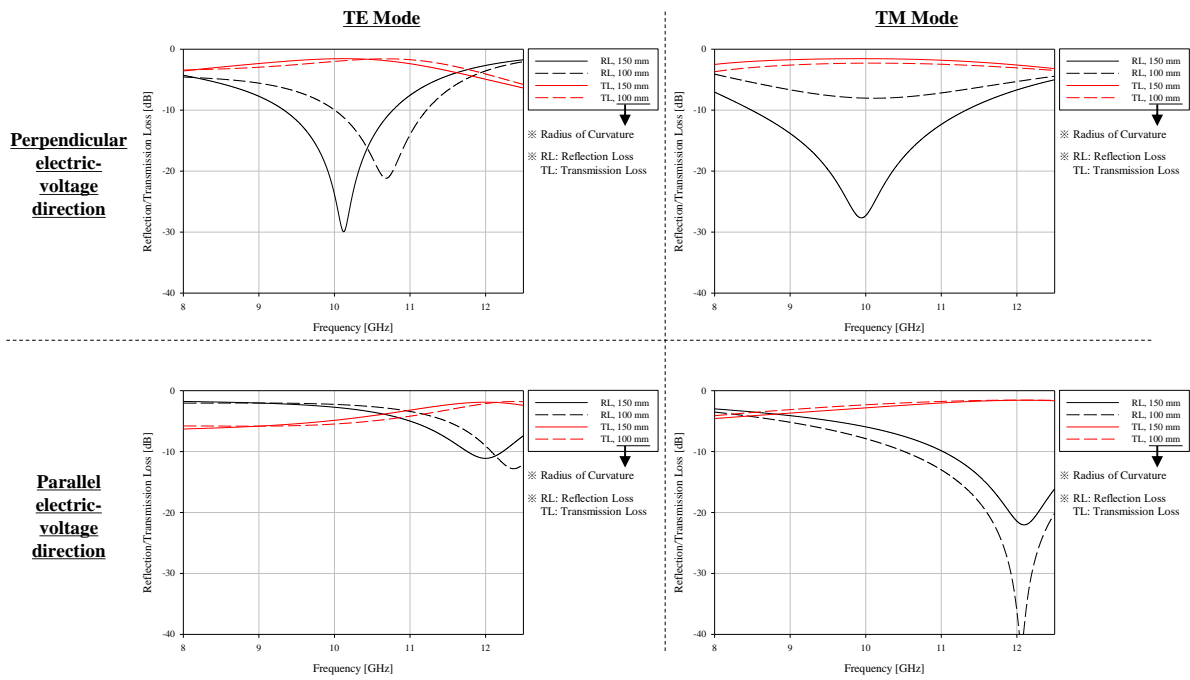


Figure 3.16: Prediction results of electromagnetic performance of variable frequency stealth radome according to curvature when there is no voltage

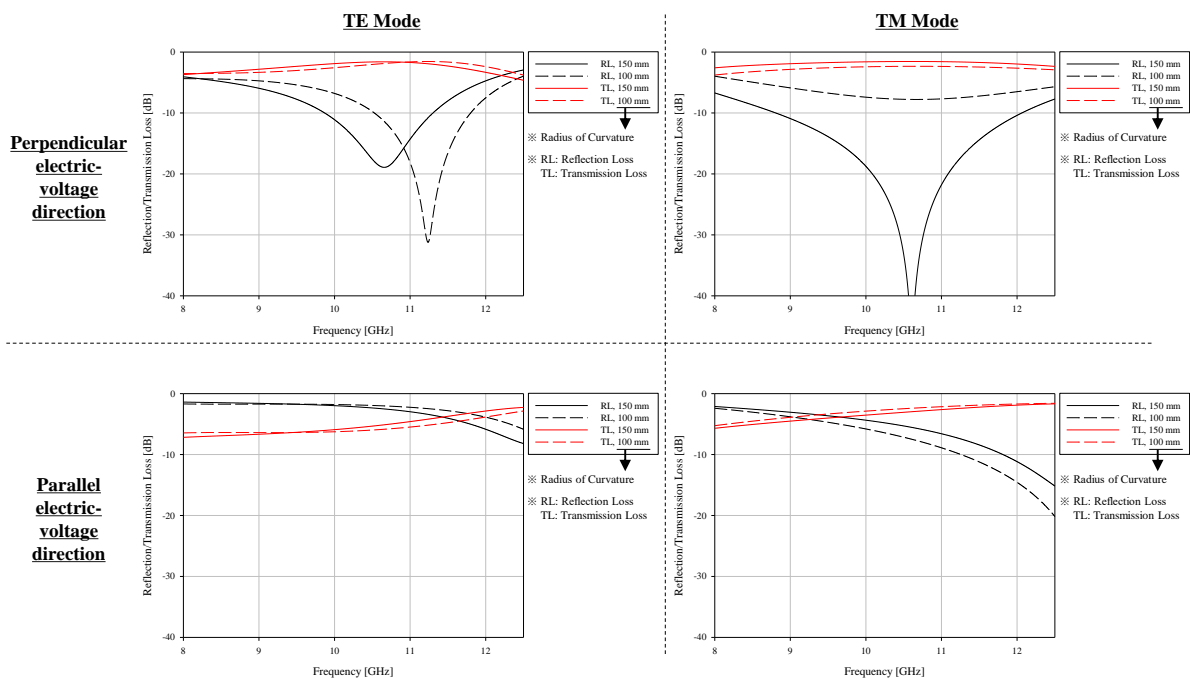


Figure 3.17: Prediction results of electromagnetic performance of variable frequency stealth radome according to curvature when the voltage is 30 V

To verify the electromagnetic performance prediction process of curved structure applied with frequency selective surface, a specimen was fabricated as shown in Figure 3.18. The specimen was manufactured with the same geometry as the variable frequency stealth radome designed above, and only the curvature was different. As shown in Figure 3.19, the fabricated variable frequency stealth radome with curvature was measured using a free space measurement with a focused horn antenna.

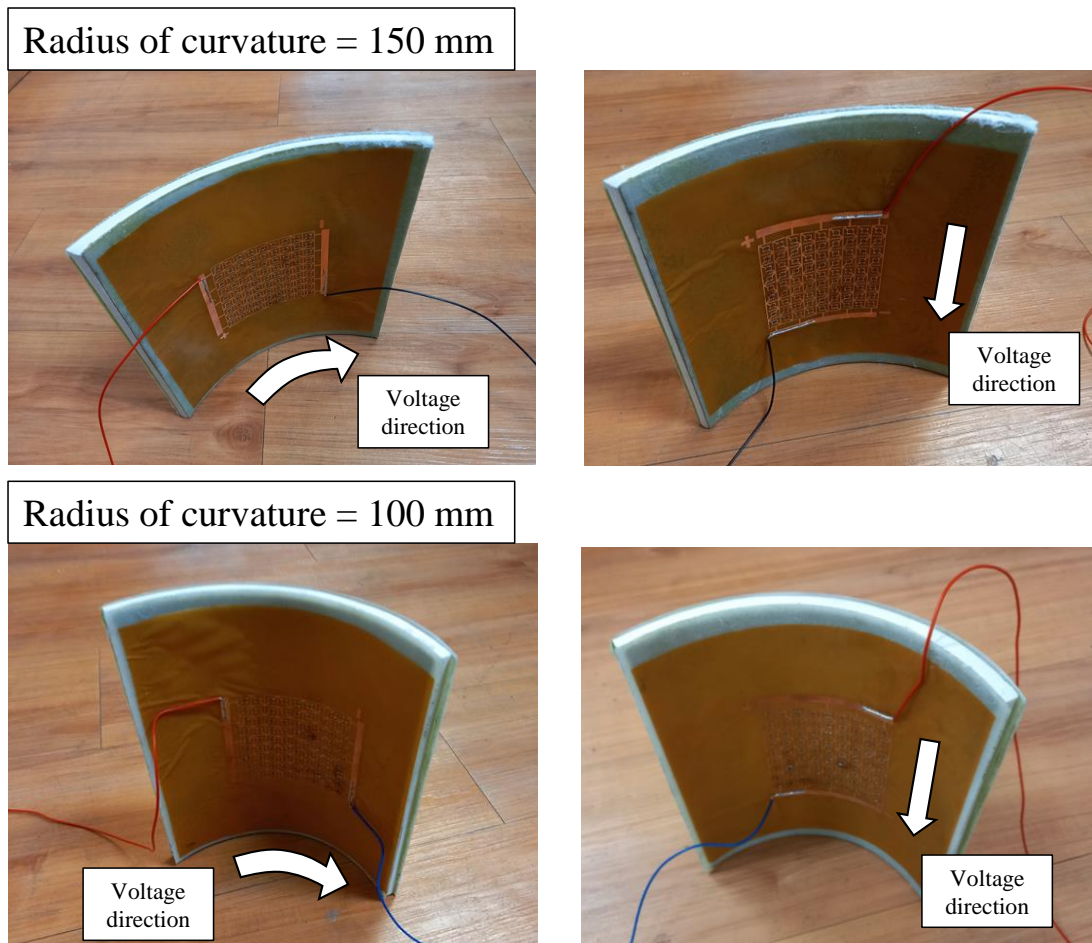


Figure 3.18: Variable frequency stealth radome specimen with different curvatures

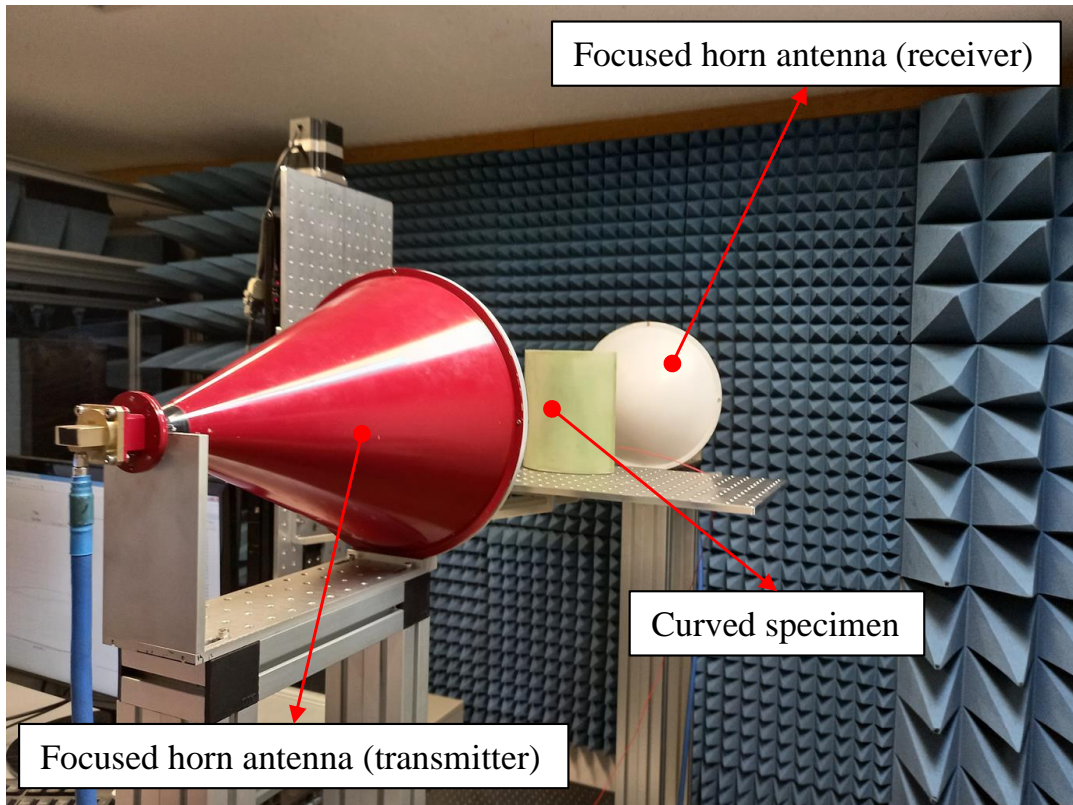


Figure 3.19: Measurement of electromagnetic performance of variable frequency stealth radome specimen with curvature

The measured results are shown in Figures 3.20 and 3.21. As the measurement results, it was confirmed that the transmission frequency tends to increase as the curvature increases, as in the predicted results, in most cases. However, it can be confirmed that the reflection loss is significantly different from the predicted results. Most of the electromagnetic waves transmitting through the specimen reach the receiving antenna by the curved structure, but all electromagnetic waves reflected by the curved structure do not return to the antenna. Therefore, when using the ray tracing method, this difference is expected to occur because the electromagnetic wave returned to the antenna was not accurately predicted. Therefore, in order to accurately predict the reflection loss, it is necessary to consider the electromagnetic propagation characteristics when the electromagnetic wave generated from the focused horn antenna reaches the specimen. To understand the electromagnetic characteristics of a focused horn antenna, a near-field analysis is required. However, since transmission loss is more important than reflection loss in variable frequency stealth radome, accurate prediction of reflection loss through near-field analysis was not performed.

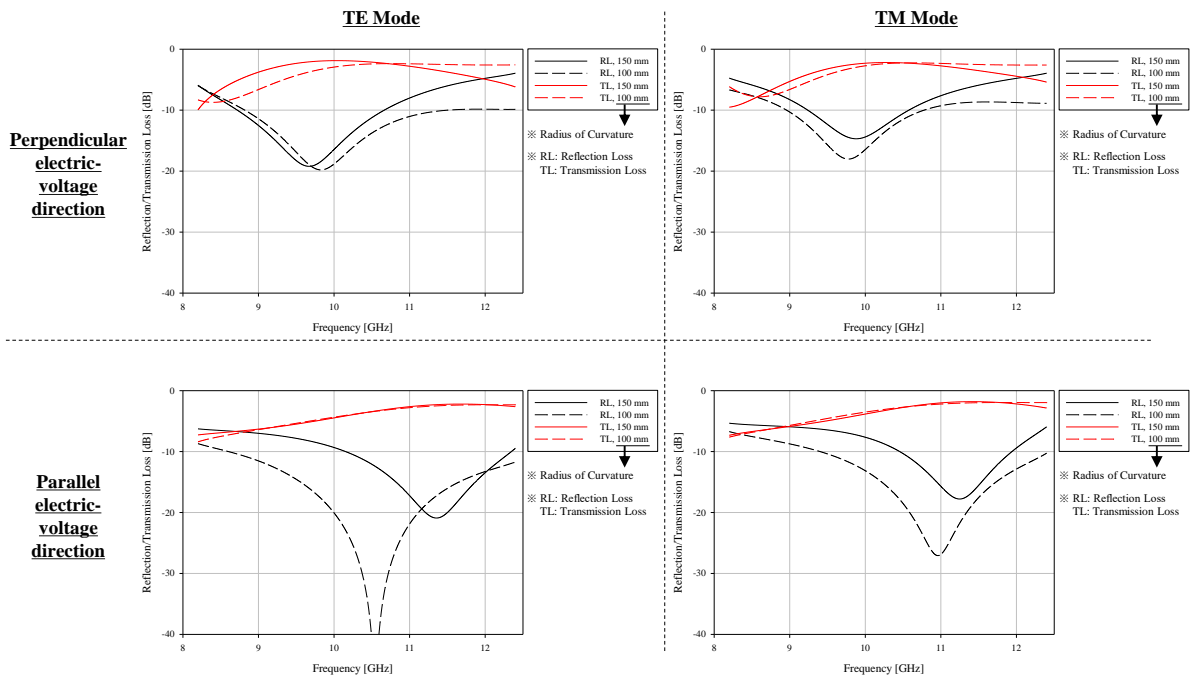


Figure 3.20: Measurement results of electromagnetic performance of variable frequency stealth radome according to curvature when there is no voltage

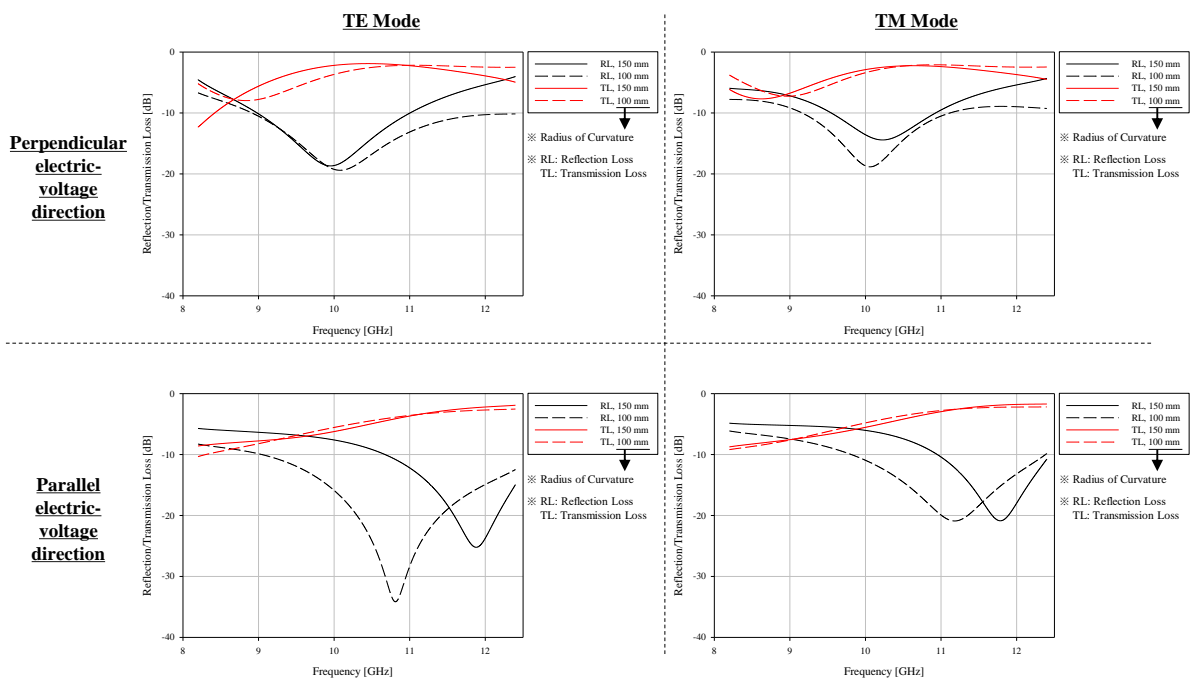


Figure 3.21: Measurement results of electromagnetic performance of variable frequency stealth radome according to curvature when the voltage is 30 V

Table 3.2 shows the transmission frequency measurement results according to the curvature and voltage of the variable frequency stealth radome. As the prediction results, the transmission frequency tends to increase as the curvature increases. The transmission frequency shifts to an average of 0.57 GHz for a flat plate, an average of 0.62 GHz for a 150 mm radius of curvature, and an average of 0.3 GHz for a 100 mm radius of curvature. When comparing the error rate of the transmission frequency obtained through the process of predicting the electromagnetic performance of the curvature structure and the transmission frequency obtained by the measurement, it can be confirmed that the transmission frequency was predicted relatively accurately with an average of 1.8 %. Therefore, the process of predicting the electromagnetic performance of the curvature structure proposed in this study could be verified through experiments.

Table 3.2: Transmission frequency measurement results according to curvature and voltage of variable frequency stealth radome

Transmission frequency [GHz]		Perpendicular electric-voltage direction					
		TE mode			TM mode		
		Flat	R = 150 mm	R = 100 mm	Flat	R = 150 mm	R = 100 mm
Applied voltage	0V	9.4	10.04	10.75	9.4	10.28	10.61
	30V	9.72	10.45	11.06	9.72	10.64	10.64
Transmission frequency [GHz]		Parallel electric-voltage direction					
		TE mode			TM mode		
		Flat	R = 150 mm	R = 100 mm	Flat	R = 150 mm	R = 100 mm
Applied voltage	0V	11.35	11.68	12.07	11.35	11.41	11.85
	30V	12.16	12.4	12.4	12.16	12.4	12.4

## 4 Mechanical Performance Prediction of Variable Frequency Stealth Radome

### 4.1 *Properties mapping technique of frequency selective surface*

The active frequency selective surface has a smaller unit cell than the mesh of the stealth radome, and the size of the mesh is not constant because the stealth radome has a dome shape. In addition, since the unit cell of the active frequency selective surface is generally square, it cannot be uniformly distributed in the stealth radome. Therefore, there is a need for a technique for mapping mechanical properties to a stealth radome analysis model in consideration of the active frequency selective surface pattern.

In order for mapping mechanical properties, it is necessary to calculate the equivalent properties for the mesh, and a method similar to this mapping technique is the homogenization technique. The homogenization technique is a technique that determines a representative area, calculates the equivalent mechanical properties, and performs a structural analysis using it. It is mainly applied to heterogeneous materials such as composite materials.

The most representative of the homogenization techniques is the method of using the Rule of mixture [49-51], which calculates the equivalent properties according to the volume ratio. In addition, there is a technique [51,52] that calculates equivalent material properties using a theoretical solution when a material with a predetermined shape is applied to an infinite plate. And there is a technique [53] capable of obtaining equivalent properties for arbitrary material shapes through asymptotic expansion, focusing on the periodic distribution of heterogeneous materials, and applying periodic boundary conditions to the governing equation.

In this study, a method of calculating the equivalent physical properties is proposed using material mechanics equations. Since the frequency selective surface is manufactured of a thin film, an example as shown in Figure 4.1 was made to define the equations for calculating the equivalent properties. Here, the thicknesses are all the same, and  $E_1$ ,  $E_2$ ,  $E_3$ , and  $E_4$  are determined by the pattern of the variable frequency selective surface.

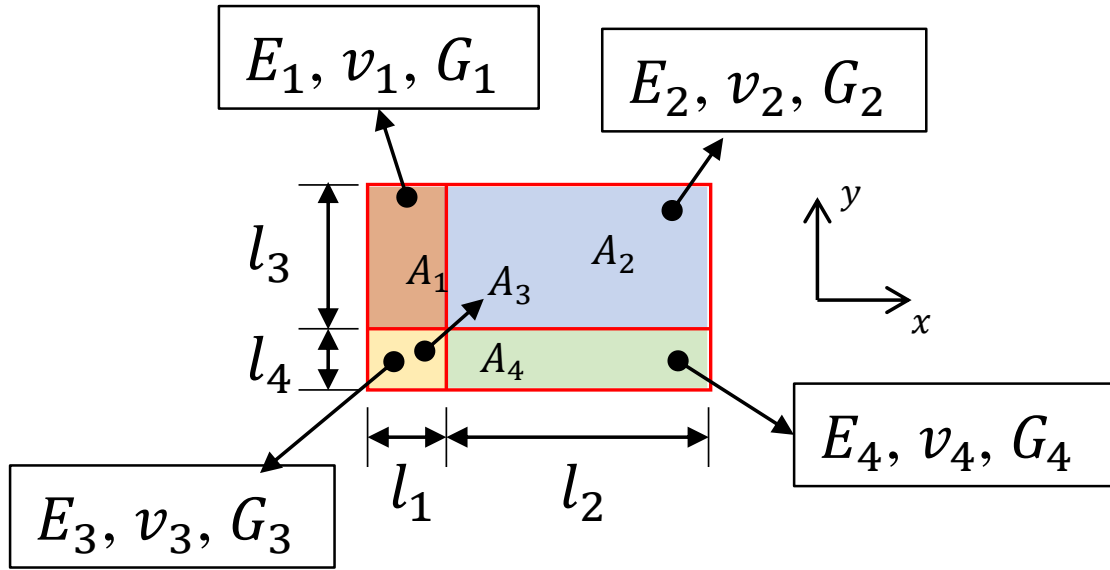


Figure 4.1: An example for calculation of equivalent mechanical properties

First of all, the equivalent mechanical properties of the  $x$  direction among the in-plane directions can be calculated using the following equations. To calculate the equivalent properties in the  $x$  direction, the equivalent property of the property perpendicular to the  $x$  direction must be firstly calculated. As in Equations 4.1 and 4.2, the equivalent properties of  $E_1$  and  $E_3$  and the equivalent properties of  $E_2$  and  $E_4$  are calculated, respectively. Using the equivalent properties perpendicular to the  $x$  direction, the equivalent properties in the  $x$  direction as shown in Equation 4.3 can be finally calculated. By using this method, it is possible to calculate the equivalent properties at once even more densely divided structure.

$$E'_1 = \frac{E_1 l_3 + E_3 l_4}{l_3 + l_4} \quad (4.1)$$

$$E'_2 = \frac{E_2 l_3 + E_4 l_4}{l_3 + l_4} \quad (4.2)$$

$$E_x = \frac{l_1 + l_2}{\frac{l_1}{E'_1} + \frac{l_2}{E'_2}} \quad (4.3)$$

Equivalent properties in the  $y$  direction use the same method as calculating the equivalent properties in the  $x$  direction, and the result is as follows.

$$E'_3 = \frac{E_1 l_1 + E_2 l_2}{l_1 + l_2} \quad (4.4)$$

$$E'_4 = \frac{E_3 l_1 + E_4 l_2}{l_1 + l_2} \quad (4.5)$$

$$E_y = \frac{l_3 + l_4}{\frac{l_3}{E'_3} + \frac{l_4}{E'_4}} \quad (4.6)$$

Since all four properties are perpendicular to the thickness direction, the equivalent property in the thickness direction can be calculated directly with the following equation.

$$E_z = \frac{E_1 A_1 + E_2 A_2 + E_3 A_3 + E_4 A_4}{A_1 + A_2 + A_3 + A_4} \quad (4.7)$$

To calculate the equivalent properties of the shear modulus, the calculation for each direction in a similar manner to the previous method is as follows. In general, the  $xy$  and  $yx$  directions of the shear modulus are the same. However, since non-uniform properties are calculated as equivalent properties, the shear modulus values in the  $xy$  and  $yx$  directions are different.

$$G'_1 = \frac{G_1 l_3 + G_3 l_4}{l_3 + l_4}, G'_2 = \frac{G_2 l_3 + G_4 l_4}{l_3 + l_4}, G'_3 = \frac{G_1 l_1 + G_2 l_2}{l_1 + l_2}, G'_4 = \frac{G_3 l_1 + G_4 l_2}{l_1 + l_2} \quad (4.8)$$

$$G'_{xy} = \frac{l_1 + l_2}{\frac{l_1}{G'_1} + \frac{l_2}{G'_2}}, G'_{yx} = \frac{l_3 + l_4}{\frac{l_3}{G'_3} + \frac{l_4}{G'_4}} \quad (4.9)$$

$$G'_{xz} = \frac{l_1 + l_2}{\frac{l_1}{G'_1} + \frac{l_2}{G'_2}}, G'_{zx} = \frac{G'_1 l_1 + G'_2 l_2}{l_1 + l_2} \quad (4.10)$$

$$G'_{zy} = \frac{G'_3 l_3 + G'_4 l_4}{l_3 + l_4}, G'_{yz} = \frac{l_3 + l_4}{\frac{l_3}{G'_3} + \frac{l_4}{G'_4}} \quad (4.11)$$

To make the different shear modulus the same as in Equations 4.9 to 4.11, the method shown in Figure 4.2 can be used. Figure 4.2a is a typical shear behavior, and Figure 4.2b is a case where two different properties undergo shearing behavior at the same time. If the two behaviors are expressed by equations at the same time, it is as shown in Equation 4.12, and the shear modulus in the  $xy$  and  $yx$  directions can be equalized.

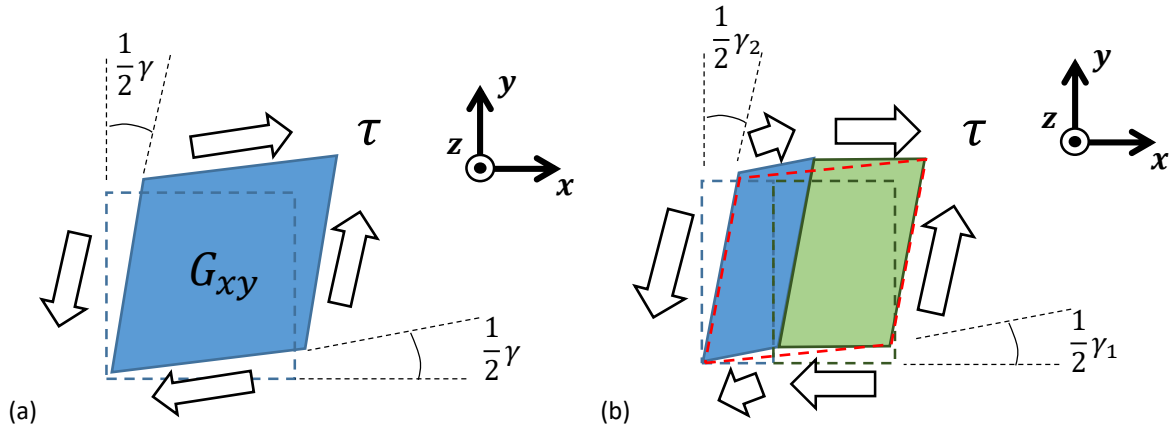


Figure 4.2: Schematic diagram of shear behavior (a) isotropic material (b) heterogeneous material

$$\tau = G_{xy}\gamma = G_{xy}\left(\frac{1}{2}\gamma_1 + \frac{1}{2}\gamma_2\right) = G_{xy}\left(\frac{1}{2}\frac{\tau}{G'_{xy}} + \frac{1}{2}\frac{\tau}{G'_{yx}}\right) \quad (4.12)$$

Using Equation 4.12, the final equivalent shear modulus can be expressed as the following equations.

$$G_{xy} = \frac{2}{\frac{1}{G'_{xy}} + \frac{1}{G'_{yx}}}, G_{xz} = \frac{2}{\frac{1}{G'_{xz}} + \frac{1}{G'_{zx}}}, G_{yz} = \frac{2}{\frac{1}{G'_{yz}} + \frac{1}{G'_{zy}}} \quad (4.13)$$

Unlike the previous elastic modulus and shear modulus, the equivalent poisson ratio goes through a more complicated process. This is because the displacement that decreases in the thickness direction when an in-plane load is applied depends on the poisson ratio and elastic modulus. Before calculating the equivalent poisson ratio of the four materials, it is necessary to calculate the equivalent poisson ratio of the two materials.

As shown in Figure 4.3, the equivalent poisson ratio was calculated assuming that two different properties were subjected to in-plane loads. Under the in-plane load, it transforms from the cross section of the red dotted line to the cross section of the black dotted line, but the displacement in the thickness direction varies due to different properties.

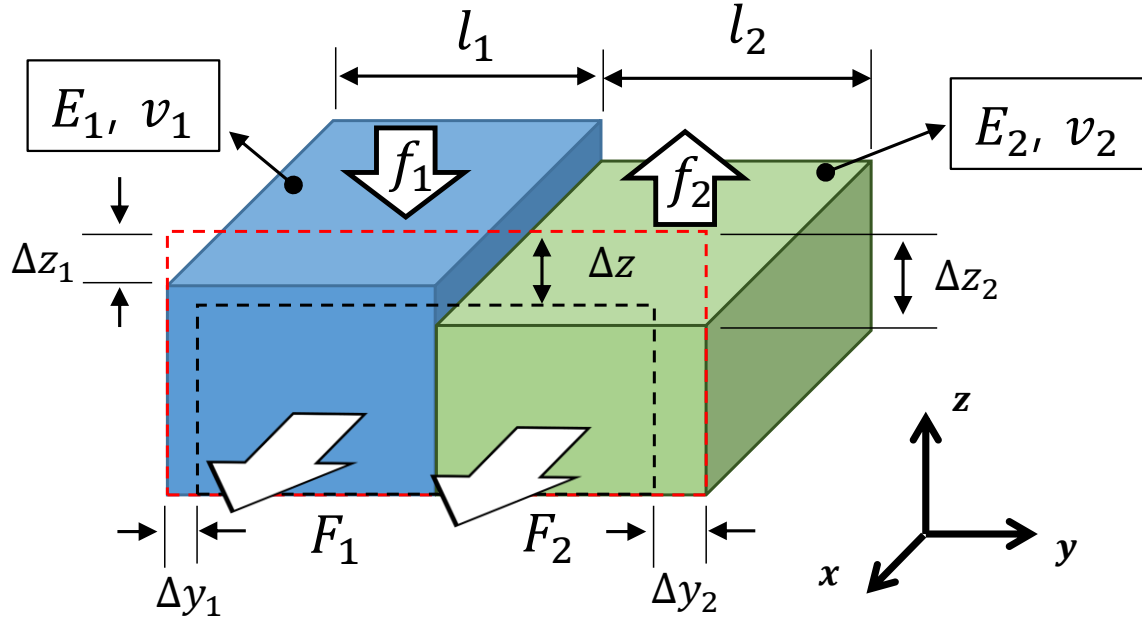


Figure 4.3: Schematic diagram of the behavior that occurs when a load is applied to a heterogeneous material in one axis

To calculate the equivalent poisson ratio, the displacement in the thickness direction is made equal by applying virtual forces  $f_1$  and  $f_2$ , and the displacement value is calculated as Equation 4.14. Using this equation, the equivalent poisson ratio of  $v_{xz}$  is calculated as Equation 4.15.

$$\Delta Z = \frac{E_1 l_1 \Delta z_1 + E_2 l_2 \Delta z_2}{E_1 l_1 + E_2 l_2} \quad (4.14)$$

$$v_{yz} = \frac{E_1 l_1 v_1 + E_2 l_2 v_2}{E_1 l_1 + E_2 l_2} \quad (4.15)$$

Using Equation 4.15, the equivalent poisson ratio in Figure 4.1 can be calculated in the same way as the previously calculated elastic modulus and shear modulus, as shown in the following equations.

$$E'_{1x} = \frac{E_1 l_3 + E_3 l_4}{l_3 + l_4}, E'_{2x} = \frac{E_2 l_3 + E_4 l_4}{l_3 + l_4}, E'_{1y} = \frac{l_3 + l_4}{\frac{l_3}{E_1} + \frac{l_4}{E_3}}, E'_{2y} = \frac{l_3 + l_4}{\frac{l_3}{E_2} + \frac{l_4}{E_4}} \quad (4.16)$$

$$v'_{1xy} = \frac{v_1 l_3 + v_3 l_4}{l_3 + l_4}, v'_{2xy} = \frac{v_2 l_3 + v_4 l_4}{l_3 + l_4}, v_{yx} = \frac{v'_{1xy} \frac{E'_{1y}}{E'_{1x}} l_1 + v'_{2xy} \frac{E'_{2y}}{E'_{2x}} l_2}{l_1 + l_2}, v_{xy} = \frac{E_x}{E_y} v_{yx} \quad (4.17)$$

$$v'_{1xz} = \frac{E_1 v_1 l_3 + E_3 v_3 l_4}{E_1 l_3 + E_3 l_4}, v'_{2xz} = \frac{E_2 v_2 l_3 + E_4 v_4 l_4}{E_2 l_3 + E_4 l_4}, v_{zx} = \frac{v'_{1xz} l_1 + v'_{2xz} l_2}{l_1 + l_2}, v_{xz} = \frac{E_x}{E_z} v_{zx} \quad (4.18)$$

$$v'_{1yz} = \frac{E_1 v_1 l_1 + E_2 v_2 l_2}{E_1 l_1 + E_2 l_2}, v'_{2yz} = \frac{E_3 v_3 l_1 + E_4 v_4 l_2}{E_3 l_1 + E_4 l_2}, v_{zy} = \frac{v'_{1yz} l_3 + v'_{2yz} l_4}{l_3 + l_4}, v_{yz} = \frac{E_y}{E_z} v_{zy} \quad (4.19)$$

If the properties mapping technique proposed in this study is used, it is possible to calculate equivalent properties with only simple pattern information. Previously, only the equivalent elastic modulus could be calculated, and in the case of poisson ratio or shear modulus, the equivalent properties could not be calculated. Therefore, Finite element analysis was performed by modeling the unit cell to calculate the equivalent poisson ratio or the equivalent shear modulus. If the properties mapping technique is used, the finite element analysis of such a unit cell is not required, so there is an advantage in that the structure analysis can be performed more quickly. This properties mapping technique is suitable when small patterns such as frequency selective surface are applied to large structures. Therefore, if the properties mapping technique is used to perform the structural analysis of the variable frequency stealth radome, it is possible to perform a faster structure analysis.

## 4.2 Structure analysis of Variable frequency stealth radome

The frequency selective surface applied to the stealth radome is manufactured and designed in a pattern having a unit cell, but the stealth radome is mainly manufactured and used in the shape of a dome. Therefore, the performance of the stealth radome greatly varies depending on how the unit cell of the frequency selective surface is arranged in the dome shape. To apply the active frequency selective surface to the dome shape, a planar figure in the shape of a dome is required. Planar figure basically has a structure in which polygons are connected. To make a planar figure without the most restrictive shape, planar figure is constructed on the basis of triangles. There is a geodesic dome, which is used in various buildings as shown in Figure 4.4, as a method of making a dome shape with a triangle as a basic shape.



Figure 4.4: Geodesic dome

In this study, a stealth radome was modeled using such a geodesic dome to perform structural analysis, and the planar figure and information of the designed geodesic dome are shown in Figure 4.5. It is designed without adding curvature because it is for the purpose of confirming the structural analysis results of the variable frequency stealth radome by applying the properties mapping technique proposed above. To supply voltage to the active frequency selective surface, a voltage supply line is arranged as shown in Figure 4.5, and an active frequency selective surface is arranged between them.

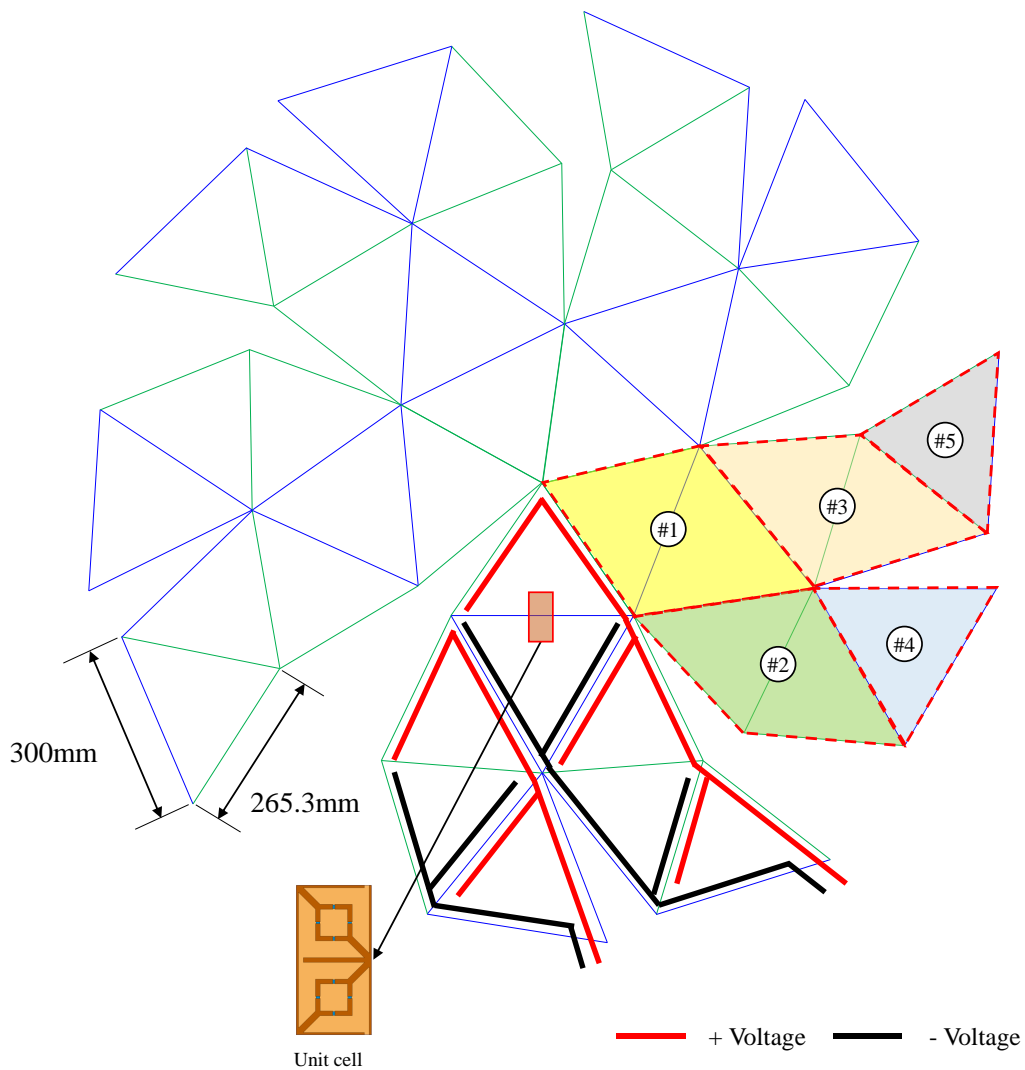


Figure 4.5: Planar figure and information of the designed variable frequency stealth radome

When arranging the active frequency selective surface, the direction of the unit cell must be considered. This is because the electromagnetic performance varies depending on the direction of the unit cell of the active frequency selective surface. The direction of the unit cell of the active frequency selective surface arranged to

face the center of the dome in order to have a structure symmetrical with the entire dome. In order for mapping the variable frequency selective surface to the dome shape, properties mapping technique was performed by dividing into five regions as shown in Figure 4.5. When dividing the regions, it was divided into regions taking into account the voltage supply line.

The active frequency selective surface applied to the stealth radome is arranged so that the direction of the unit cell faces the center of the dome, as shown in Figure 4.6. In the calculation of equivalent properties for mapping, only the active frequency selective surface was used, excluding the sandwich structure. This is because most of the load is supported by GFRP in the sandwich structure, so if the equivalent properties of the sandwich structure are calculated as well, the bending stiffness varies greatly. Therefore, the mapping technique was applied to the copper layer having a pattern on the PI film to calculate the equivalent properties.

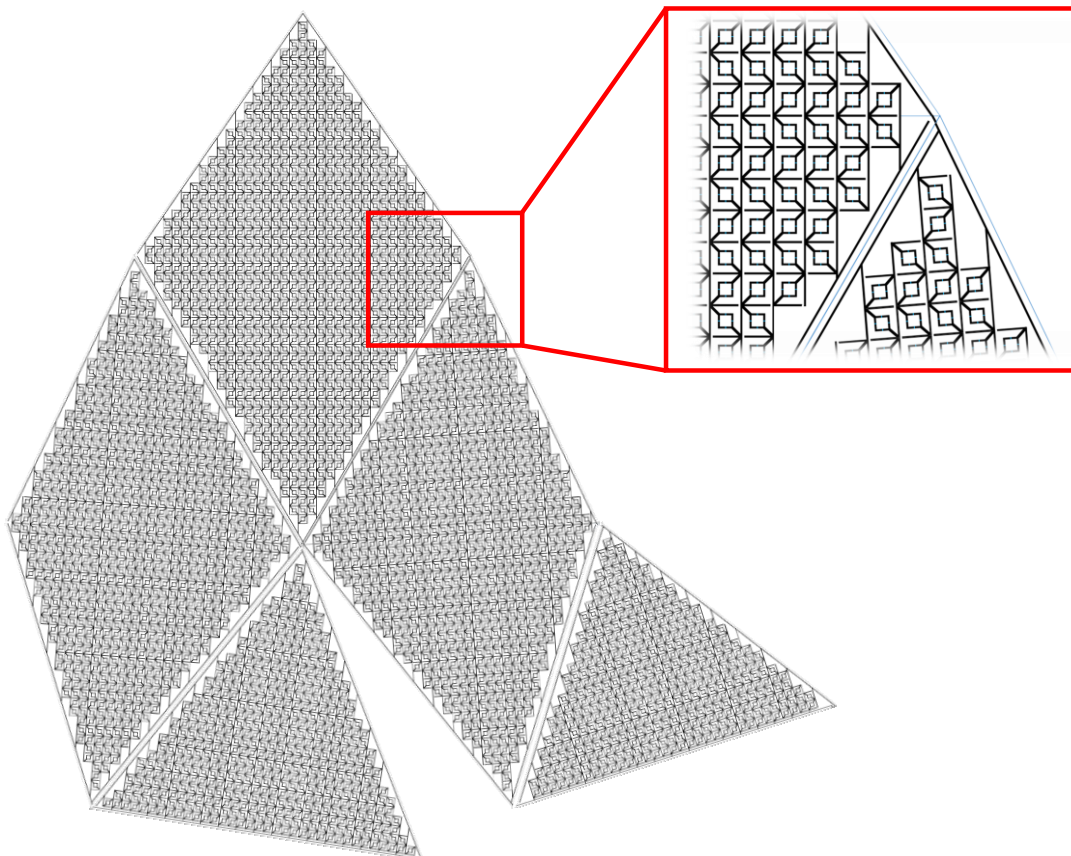


Figure 4.6: Active frequency selective surface pattern distribution of stealth radome

The used copper had an elastic modulus of 110 GPa, a poisson ratio of 0.34, a PI film had an elastic modulus of 2.34 GPa, and a poisson ratio of 0.3. When calculating the equivalent properties, 0.1 GPa was applied to the regions where copper was not present. As for the diode, 17.3 GPa, which is an elastic modulus of EMC (Epoxy Molding Compound), which is mainly used for IC chip package, was used. The size of the element to be used in

the analysis was 5mm, and the active frequency selective surface pattern and the properties mapping results arranged in the regions divided by five regions are shown in Figures 4.7 to 4.11.

Equivalent property calculation and mapping were performed using Matlab. In the mapping results, copper does not exist because it is difficult to apply the unit cell of active frequency selective surface to the location of the voltage supply line. Therefore, it has a low elastic modulus because only the elastic modulus of the PI film exists. In addition, by using the properties mapping technique, it is possible to calculate all the property necessary for analysis as shown in Figure 4.7.

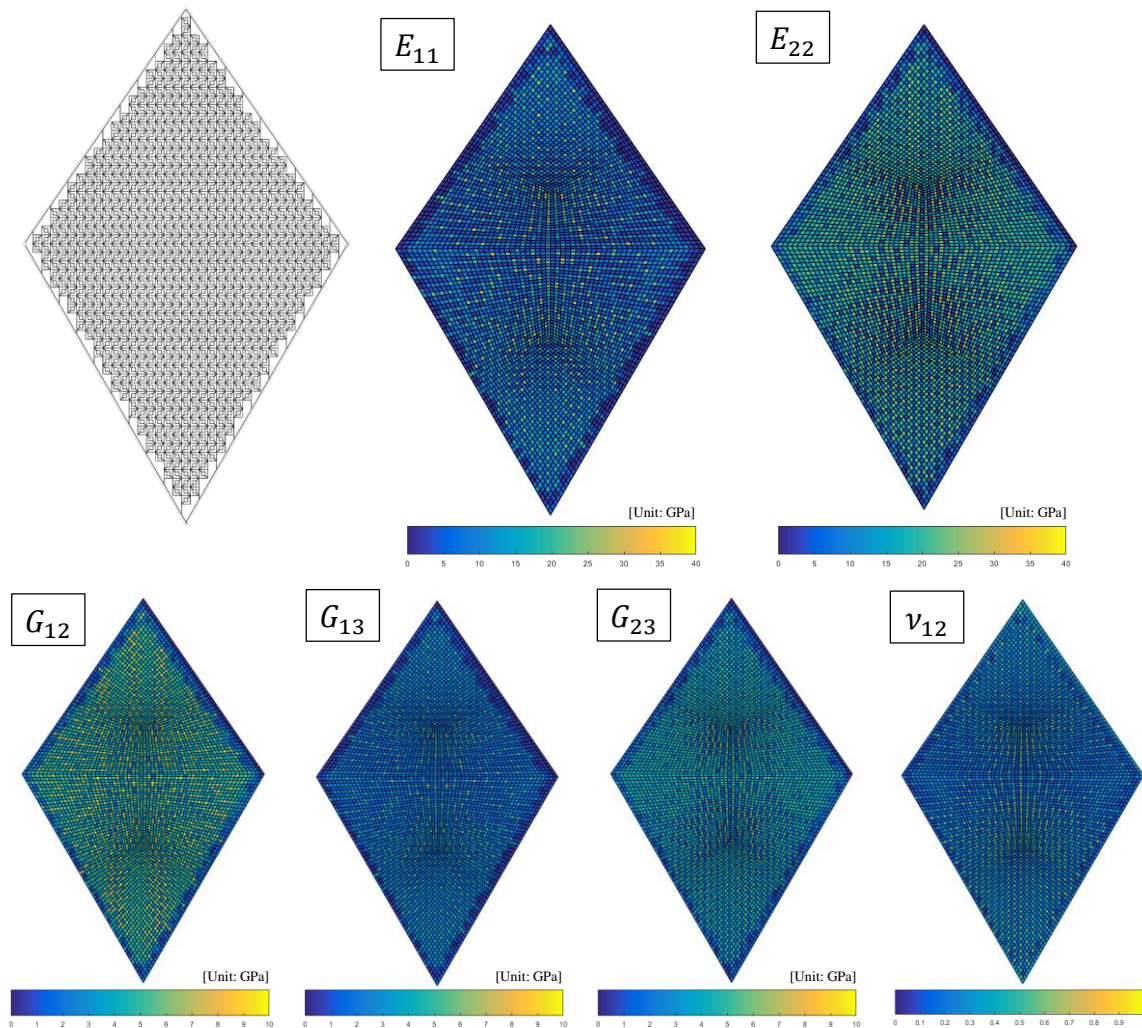


Figure 4.7: Properties mapping results of active frequency selective surface in #1

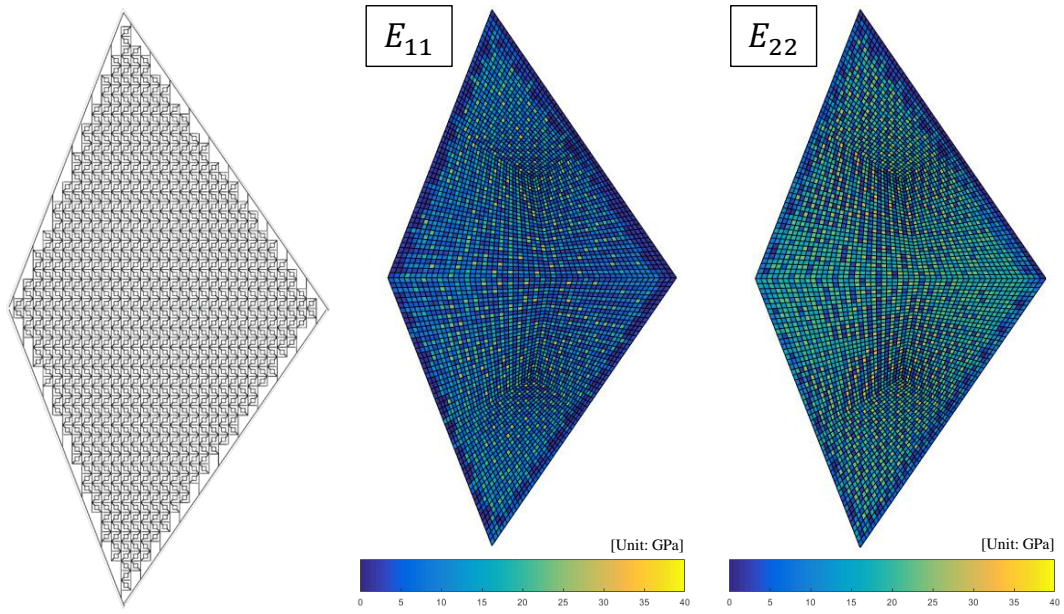


Figure 4.8: Properties mapping results of active frequency selective surface in #2

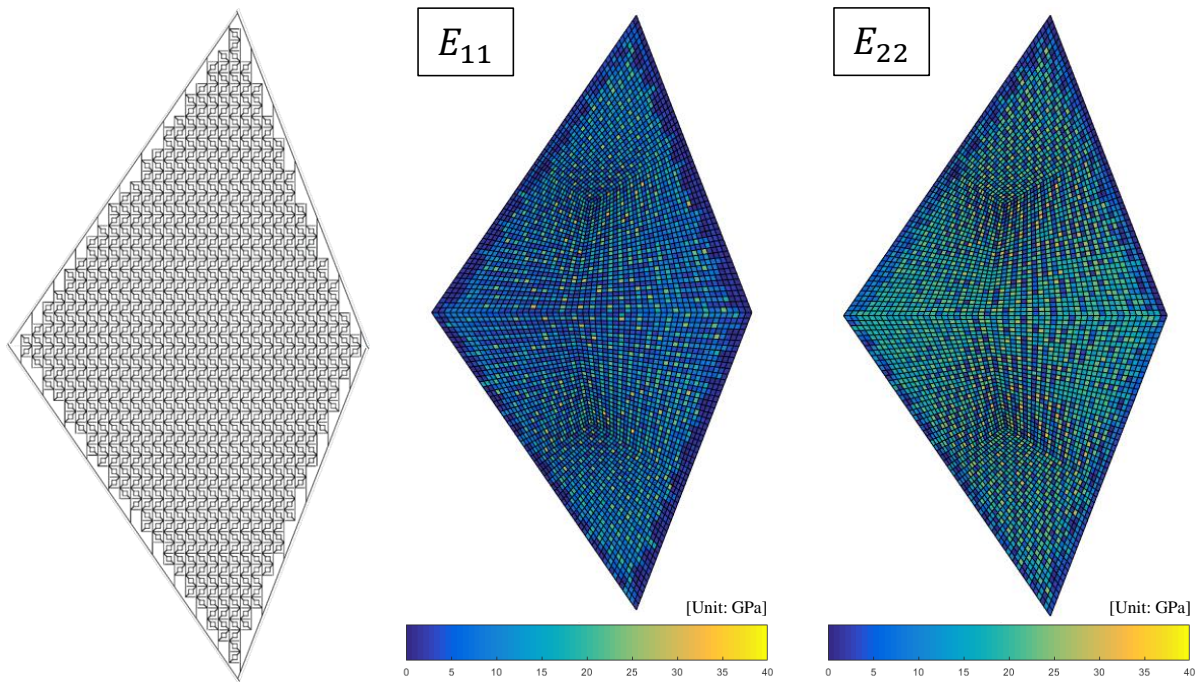


Figure 4.9: Properties mapping results of active frequency selective surface in #3

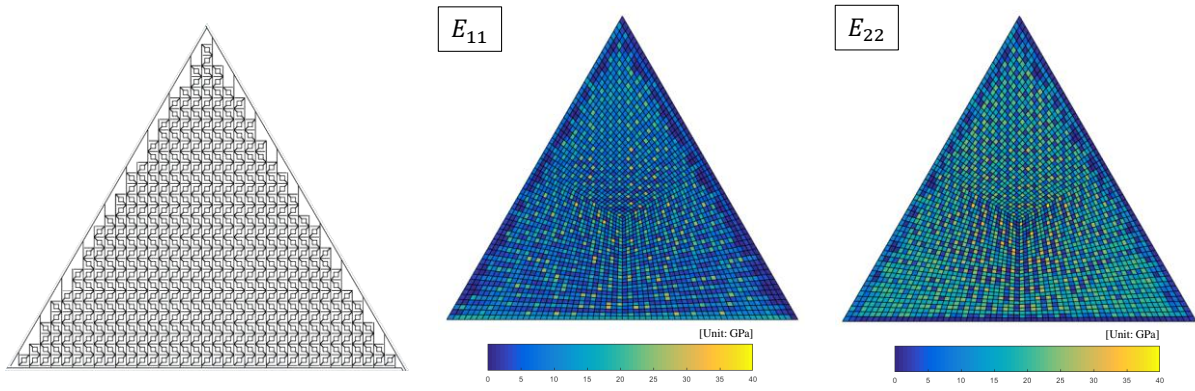


Figure 4.10: Properties mapping results of active frequency selective surface in #4

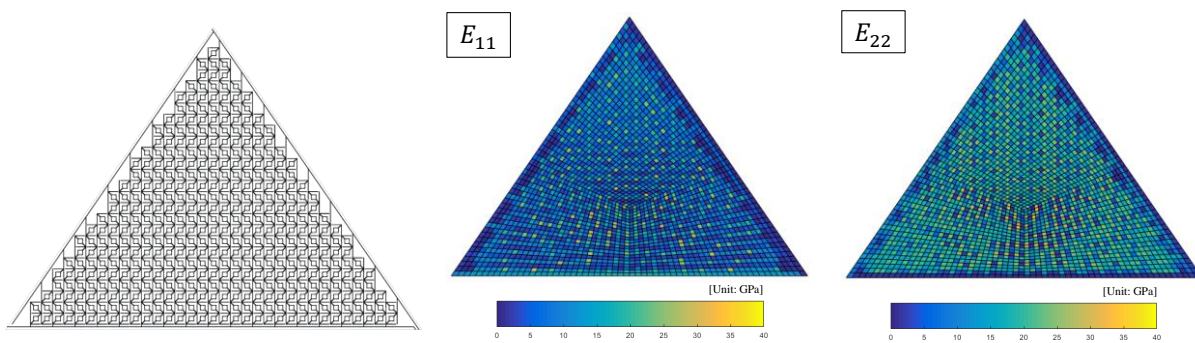


Figure 4.11: Properties mapping results of active frequency selective surface in #5

A variable frequency stealth radome was modeled using the elements mapped with equivalent properties, and the analysis model and boundary conditions are shown in Figure 4.12. A dome shape was created from the elements of the five regions that were mapped and used for analysis. Structure analysis was performed by fixing the lower part of the dome and applying a uniform pressure of 0.1 MPa to the entire dome. The properties used are as shown in Table 4.1, and the structure analysis was performed using Abacus 6.13-4, a commercial structure analysis software. A shell element capable of modeling composite materials was used, and a sandwich structure composed of GFRP and PVC foam was applied as previously designed. That is, frequency selective surface with equivalent properties mapped and sandwich structure were applied to the shell element. The thickness of the upper GFRP and the lower GFRP is 1mm, and the thickness of the PVC foam is 6mm. The analysis result of the variable frequency stealth radome to which the properties mapping technique is applied is shown in Figure 4.13. The analysis result is the distribution of the maximum principal strain in active frequency selective surface. It was confirmed that the maximum value appears in the center of the triangular region because it is applying a uniform pressure. In the next section, this results are compared with the analysis results of the commonly used multi-scale technique to confirm whether the properties mapping method is appropriate.

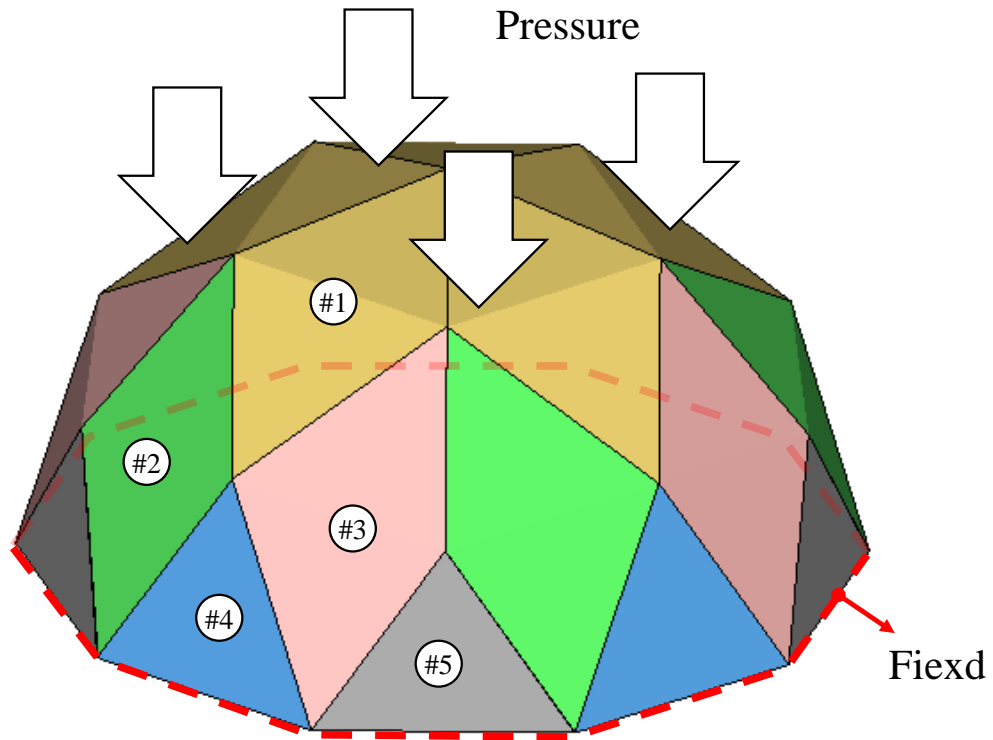


Figure 4.12: Structure analysis model of variable frequency stealth radome

Table 4.1: Properties used for structure analysis of variable frequency stealth radomes

	Elastic modulus	Poisson's ratio
<b>Copper</b>	110 GPa	0.34
<b>PI</b>	2.34 GPa	0.3
<b>PVC foam</b>	1.26 GPa	0.33
<b>GFRP</b>	$E_{11} = 21$ GPa $E_{22} = 21$ GPa $G_{12} = 1.52$ GPa $G_{13} = 2.65$ GPa $G_{23} = 2.65$ GPa	$\nu_{12} = 0.26$

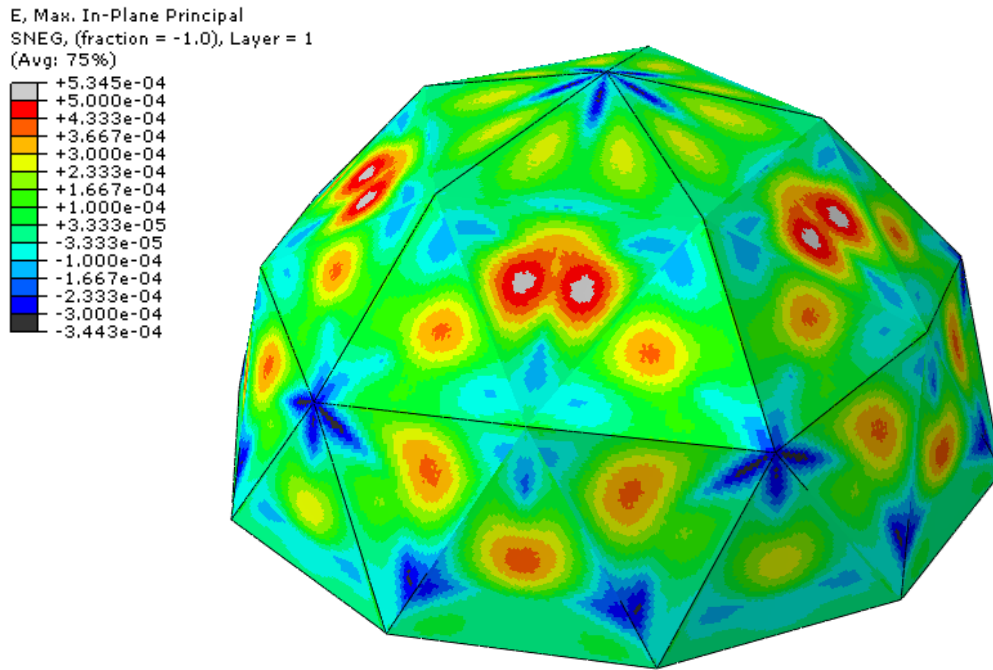


Figure 4.13: Analysis results of variable frequency stealth radome using properties mapping technique

### 4.3 Verification of the structure analysis using properties mapping technique

To verify structure analysis of the variable frequency stealth radome using the previously proposed properties mapping technique, it was compared with the multi-scale technique. The multi-scale technique is a technique that increases the scale from small unit cells to gradually larger structures as shown in Figure 4.14. After performing the unit cell analysis, the equivalent properties are calculated from the analysis results and applied to the scale structure in the next step to perform the analysis.

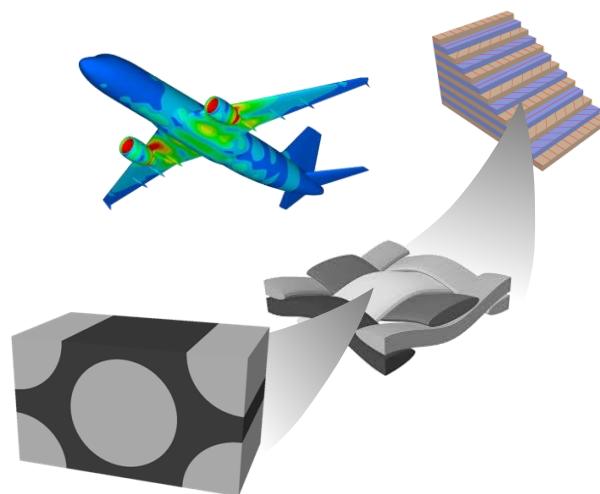


Figure 4.14: Structural analysis applying multi-scale technique

To apply multi-scale technique to a variable frequency stealth radome, the unit cell of the active frequency selective surface must be analyzed. From the unit cell analysis, the equivalent properties to be used for the stealth radome analysis must be calculated. The equivalent properties of the active frequency selective surface required for the structural analysis of the stealth radome are  $E_{11}$ ,  $E_{22}$ ,  $\nu_{12}$ ,  $G_{12}$ ,  $G_{13}$ ,  $G_{23}$ . There are five analysis models required to calculate each property, and the analysis models are shown in Figure 4.15.

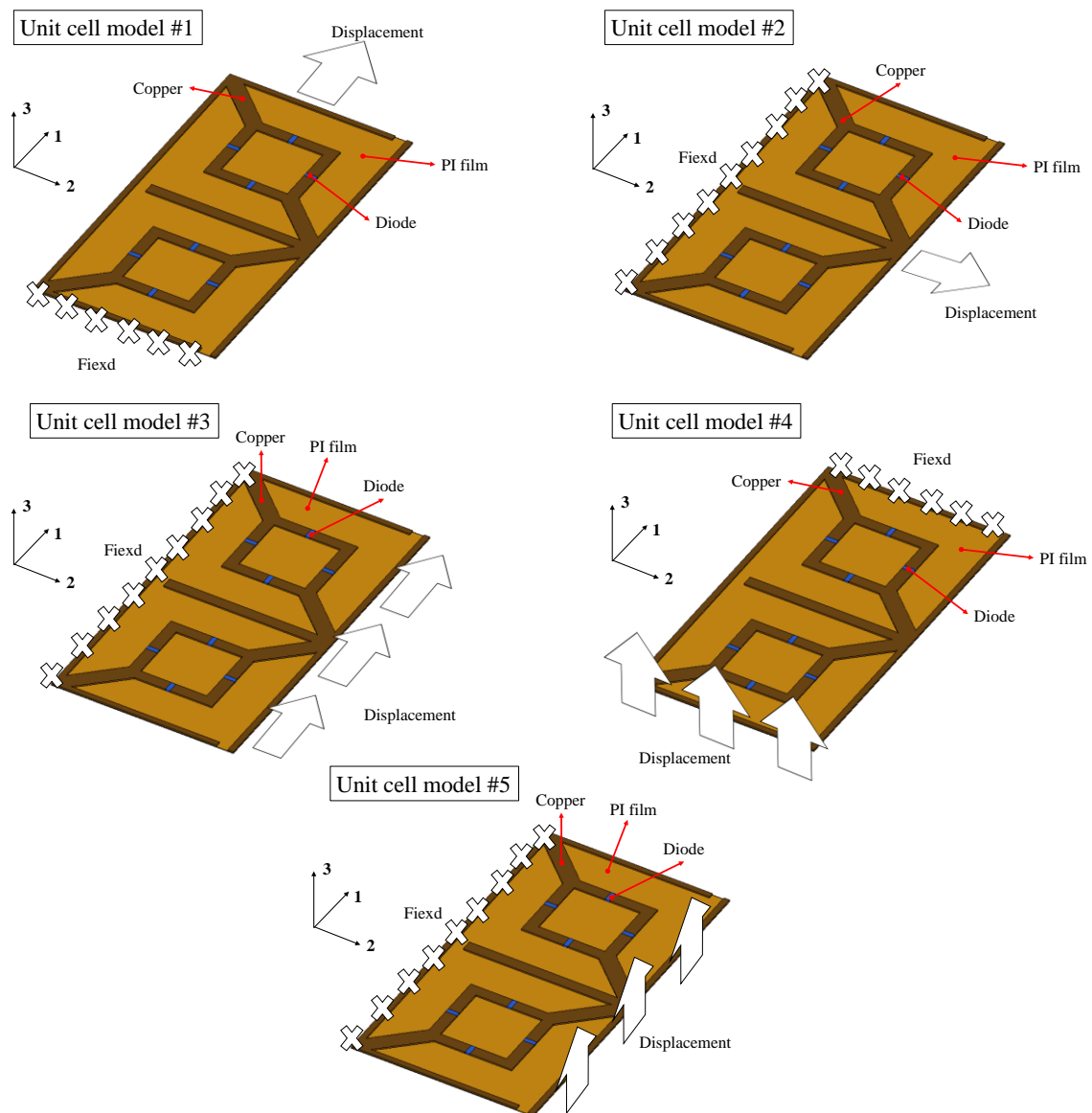


Figure 4.15: Unit cell structure analysis models of active frequency selective surface

$E_{11}$  and  $\nu_{12}$  can be obtained as the first unit cell analysis model, and  $E_{22}$  and  $\nu_{21}$  can be obtained as the second unit cell analysis model. The third unit cell analysis model can obtain  $G_{12}$ , and the fourth unit cell analysis

model can obtain  $G_{13}$ . As the fifth unit cell analysis model can obtain  $G_{23}$ . Since the element used in the structural analysis of the variable frequency stealth radome is the shell element, five unit cell analysis models are required. However, if a solid element is used, one more unit cell analysis model is required because the equivalent properties in the thickness direction are also required.

The element used in the five unit structure models was C3D20R, and a quadratic solid element was used. Since the thickness of the active frequency selective surface is thin, only one solid element was used to consider the aspect ratio. However, when only one element is used, the analysis for the thickness direction is not performed properly. Therefore, the unit cell analysis was performed using the quadratic element. Equivalent properties were calculated using the analysis results. As a result,  $E_{11}$  was 6568.5 MPa,  $E_{22}$  was 2188.5 MPa,  $\nu_{21}$  was 0.323,  $G_{12}$  was 650.3 MPa,  $G_{13}$  was 0.055 MPa, and  $G_{23}$  was 0.156 MPa.

A variable frequency stealth radome was modeled by applying the equivalent properties obtained by the unit cell analysis, and the structure analysis was performed by giving the same boundary and load conditions as the analysis using the previous properties mapping technique. The result is shown in Figure 4.16. It was confirmed that the strain distribution similar to the analysis results applying the previous mapping technique appeared.

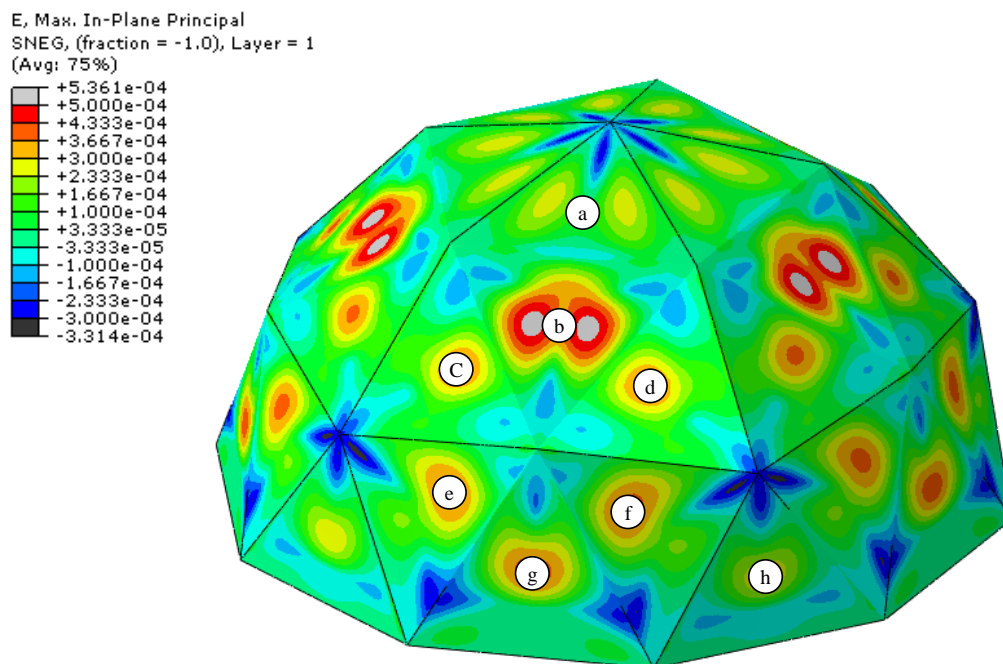


Figure 4.16: Analysis results of variable frequency stealth radome using multi-scale technique

To compare the results analyzed by the multi-scale technique and the properties mapping technique, eight points from a to h were selected. The maximum principal strain obtained by the properties mapping technique and the multi-scale technique was compared at selected points, and the results are shown in Table 4.2.

Table 4.2: Comparison of multi-scale technique and properties mapping technique at 8 points

<b>Max. principal strain</b>	<b>a</b>	<b>b</b>	<b>c</b>	<b>d</b>
<b>Properties mapping technique</b>	7.95E-05	3.72E-04	3.69E-04	3.76E-04
<b>Multi-scale technique</b>	6.77E-05	3.74E-04	3.79E-04	3.78E-04
<b>Difference rate</b>	17.4 %	0.5 %	2.65 %	0.7 %
<b>Max. principal strain</b>	<b>e</b>	<b>f</b>	<b>g</b>	<b>h</b>
<b>Properties mapping technique</b>	2.82E-04	2.79E-04	3.28E-04	1.30E-04
<b>Multi-scale technique</b>	2.86E-04	2.87E-04	3.38E-04	1.35E-04
<b>Difference rate</b>	1.13 %	2.91 %	2.8 %	4.04 %

The element used in the five unit structure models was C3D20R, and a quadratic solid element was used. Since the thickness As a result, it was confirmed that the properties mapping technique and the multi-scale technique were almost similar, and an average difference rate of 4.02 % occurred based on the multi-scale technique. The results of the two techniques are actually considered more similar because the difference rate is larger when the maximum principal strain is small, such as a and h. Therefore, it was verified that there was no difference between the analysis results using the multi-scale technique and the analysis results using the properties mapping technique. When the properties mapping technique is used, analysis of the unit cell is not required, and analysis can be performed immediately with just the pattern information of the frequency selective surface, so analysis cost can be reduced. In addition, even if the frequency selective surface has a complex pattern, it is possible to easily analyze and model through a properties mapping technique. Therefore, it was verified that it is more suitable to use the properties mapping technique to perform the structure analysis of the variable frequency stealth radome.

## 5 Conclusion

The stealth radome has an electromagnetic characteristic that transmits only the communication frequency of the internal antenna and absorbs or reflects other frequencies. Because of this electromagnetic performance requirement, if the stealth radome blocks all electromagnetic waves, the antenna cannot function properly. However, using this feature, if a fighter is detected with the transmission frequency of the stealth radome, the antenna inside the stealth radome is exposed as it is. Therefore, RCS of the fighter increases, which increases the likelihood of being detected by radar. For this reason, the transmission frequency of the stealth radome is managed so that it is not exposed to the enemy as a confidential matter. Since the transmission frequency of the stealth radome is determined by the pattern of the frequency selective surface inserted inside, the stealth radome itself must be changed to change the transmission frequency. Therefore, a study was conducted on a variable frequency stealth radome that can change the transmission frequency as a stealth technology to cope with the anti-stealth technology.

In this study, a variable frequency stealth radome was designed, and its electromagnetic and mechanical performances was predicted and verified through experiments. In general, stealth radomes have a sandwich structure to which a composite material is applied, and a frequency selective surface is inserted inside. However, since active elements are mounted on the surface of the active frequency selective surface, it is difficult to satisfy mechanical performance with conventional methods. This is because if the active frequency selective surface is placed inside the sandwich structure to which the composite material is applied, the small diodes is surrounded by the composite material, which increases the risk of damage. If the active frequency selective surface is positioned outside, most of the load is supported by the sandwich structure, so it is possible to prevent the active frequency selective surface from being damaged. To apply this structure, the active frequency selective surface should be designed to use only one-side surface so that it can be attached inside the stealth radome. In addition, when the size of a small unit cell is applied to a large stealth radome, many unit cells are applied. If the active element supplies voltage in series, a high operating voltage is required. Therefore, active elements must be connected in parallel to be designed to operate at low voltages. In conclusion, the active frequency selective surface applicable to the stealth radome uses only one-side surface, and there is a design limitation that must be able to supply voltage to the active element in parallel. In this study, an active frequency selective surface that satisfies these conditions was designed and the possibility of application to stealth radomes was verified.

First, the electromagnetic characteristics of the frequency selective surface were analyzed. After determining the basic array elements, it was classified how the electromagnetic characteristics changed according to the combination. In addition, it was predicted how the electromagnetic characteristics change when an active element is added to the basic array elements. Based on the classified information, an active frequency selective surface was designed that can be applied to a stealth radome by arranging active elements and adding a voltage feed line for parallel connection. A specimen of the designed active frequency selective surface was fabricated

to measure the electromagnetic performance, and it was confirmed that the electromagnetic characteristic changed according to voltage.

Since the structure of the stealth radome is manufactured in a curved structure for the construction of the aerodynamic surface of an aircraft, a technique for predicting the electromagnetic performance of the curved structure is required. In this study, the theoretical approach, equivalent circuit model, and ray tracing method were used to predict the electromagnetic characteristics of the curved structure. First, the electromagnetic characteristics of the curved structure were predicted using the theoretical approach to the curved structure and the equivalent circuit model of the frequency selective surface according to the incident angle. Only theoretical equations and equivalent circuit models can predict electromagnetic performance for only one point. Therefore, the electromagnetic performance of the entire curved structure was predicted using ray tracing method. The predicted results were verified using a focused horn antenna, and it was confirmed that the proposed technique for predicting electromagnetic performance was effective.

Stealth radome must satisfy these electromagnetic characteristics as well as mechanical performance because it must withstand the loads it receive in the flight environment. Therefore, when designing a stealth radome, it must be designed in consideration of not only electromagnetic characteristics but also mechanical performance. To predict the mechanical performance of stealth radome, properties mapping technology is needed. The active frequency selective surface has a smaller unit cell size than the mesh of the stealth radome, and the size of the mesh is not constant because the stealth radome has a dome shape. Also, since the unit cells of the active frequency selective surface are generally square, they cannot be uniformly distributed in the stealth radome. Therefore, there is a need for a technique for mapping properties to a stealth radome analysis model in consideration of the active frequency selective surface pattern. In this study, a method for calculating the equivalent properties of shear modulus and poisson ratio as well as the elastic modulus was proposed.

To verify the effectiveness of the proposed properties mapping technique, a variable frequency stealth radome with a geodesic dome shape was designed. After arranging the pattern of the active frequency selective surface applicable to the dome shape, the equivalent properties of the active frequency selective surface were calculated using a properties mapping technique. When calculating the equivalent property, a properties mapping technique was used, so that it was possible to calculate the equivalent property considering not only the equivalent property of the unit cell but also the arrangement of the voltage supply line. Structure analysis of a variable frequency stealth radome to which the properties mapping technique was applied was performed by applying an arbitrary load. To verify the analysis results, it was compared with the multi-scale technique widely used in the past. To apply the multi-scale technique to a variable frequency stealth radome, an analysis of the unit cell was performed. Since the unit structure has asymmetry, five unit structure analyzes were performed to obtain the equivalent elastic modulus, poisson ratio, and shear modulus in each direction. Structure analysis was performed by applying the equivalent properties calculated as a unit cell to a variable frequency stealth radome. To compare the results of the structure analysis with the multi-scale technique applied and the structure analysis with the properties mapping technique applied, eight random locations were selected and the maximum principal strain of the active frequency selective surface was compared. As a result, it was confirmed that the

difference between the structure analysis applied with the multi-scale technique and the structure analysis applied with the properties mapping technique was not significant. Therefore, it could be verified that the properties mapping technique is suitable for structural analysis of variable frequency stealth radome.

If the properties mapping technique proposed in this study is used, the unit cell analysis performed by the multi-scale technique becomes unnecessary. Therefore, there is an advantage of reducing the analysis cost. In addition, the multi-scale technique has the disadvantage of having to perform many unit cell analysis for all patterns in the case of structures to which various patterns are applied. However, if the properties mapping technique is used, there is an advantage that it is possible to perform structural analysis applied with complex pattern by calculating equivalent properties immediately without performing unit cell analysis. In other words, even a structure having a complex pattern can easily perform a structure analysis in which information on all patterns is reflected. It was confirmed that this advantage can be maximized when an active frequency selective surface having a small pattern is applied to a stealth radome which is a large structure.

Through this study, a new concept of variable frequency stealth radome that can apply active frequency selective surface to stealth radome was developed. In addition, a process for predicting the electromagnetic performance of curved variable frequency stealth radome was developed. To verify the developed process, a variable frequency stealth radome was designed that can shift the transmission frequency up to an average of 0.57 GHz in the X-band. The transmission frequency shifts to an average of 0.62 GHz for 150 mm radius of curvature, and an average of 0.3 GHz for 100 mm radius of curvature. When comparing the electromagnetic performance prediction results according to the curvature and the experimental results, it was confirmed that the average error was 1.8%. Therefore, the developed process was able to verify the process of predicting the electromagnetic performance of a variable frequency selective surface with curvature. In addition, a properties mapping technique was developed to evaluate the mechanical performance of a variable frequency stealth radome. The effectiveness of the developed technique was verified by comparing it with the commonly used multiscale technique. It is expected that the survivability of fighter can be improved by using the variable frequency stealth radome applied with the active frequency surface.

## 6 Bibliography

- [1] F. Costa, S. Genovesi and A. Monorchio, "A frequency selective absorbing ground plane for low-rcs microstrip antenna arrays," *Progress In Electromagnetics Research*, vol. 126, pp. 317-332, 2012.
- [2] S. E. Lee, W. J. Lee, K. S. O and C. G. Kim, "Broadband all fiber-reinforced composite radar absorbing structure integrated by inductive frequency selective carbon fiber fabric and carbon-nanotube-loaded glass fabrics," *Carbon*, vol. 107, pp. 564-572, 2016.
- [3] C. Wang, M. Chen, H. Lei, K. Yao, H. Li, W. Wen and D. Fang, "Radar stealth and mechanical properties of a broadband radar absorbing structure," *Composites Part B: Engineering*, vol. 123, pp. 19-27, 2017.
- [4] B. Zohuri, "Radar Energy Warfare and the Challenges of Stealth Technology," Springer International Publishing: Berlin, Germany, 2020.
- [5] H. Singh, E. D. D. J, H. S. Rawat and R. George, "Fundamentals of EM Design of Radar Absorbing Structures (RAS)," Springer, 2018.
- [6] D. S. Son, J. M. Hyun, J. R. Lee and W. J. Lee, "Optimization of the design of radar-absorbing composite structures using response surface model with verification using scanning free space measurement," *Composite Structures*, vol. 186, pp. 106-113, 2018.
- [7] P. C. Kim, D. G. Lee, I. S. Seo and G. H. Kim, "Low-observable radomes composed of composite sandwich constructions and frequency selective surfaces," *Composites Science and Technology*, vol. 68, pp. 2163-2170, 2008.
- [8] V. S. Chernyak, "Fundamentals of Multisite Radar Systems," New York: Gordon and Breach, 1998.
- [9] D. S. Son, J. M. Hyun and J. R. Lee, "Reflection loss field visualization of curved RAS based on scanning free-space measurement and curvature compensation using perfect electric conductor," *Measurement*, vol. 153, 107408, 2020.
- [10] R. S. Anwar, L. Mao and H. Ning, "Frequency Selective Surfaces: A Review," *Applied Sciences*, vol. 8, no. 9, pp. 1689, 2018.
- [11] B. A. Munk, *Frequency Selective Surfaces: Theory and Design*, Wiley Online Library: Hoboken, 2000.
- [12] E. A. Parker, "Convolute array elements and reduced size unit cells for frequency-selective surfaces," In *IEE Proceedings H (Microwaves, Antennas and Propagation)*, Stevenage, UK, pp. 19–22, 1991.
- [13] M. Nauman, R. Saleem, A. K. Rashid, M. F. Shafique, "A miniaturized flexible frequency selective surface for X-band applications," *IEEE Trans. Electromagn. Compat.*, vol. 58, pp. 419–428, 2016.
- [14] M. Yan, S. Qu, J. Wang, J. Zhang, A. Zhang, S. Xia and W. Wang, "A novel miniaturized frequency selective surface with stable resonance," *IEEE Antennas Wirel. Propag. Lett.*, vol. 13, pp. 639–641, 2014.
- [15] J. P. Gianvittorio, J. Romeu, S. Blanch and Y. Rahmat-Samii, "Self-similar prefractal frequency selective surfaces for multiband and dual-polarized applications," *IEEE Trans. Antennas Propag.*, vol. 51, pp. 3088–3096, 2003.
- [16] M. Gao, S. M. A. M. H. Abadi and N. Behdad, "A dual-band, inductively coupled miniaturized-element frequency selective surface with higher order bandpass response," *IEEE Trans. Antennas Propag.*, vol. 64, pp. 3729–3734, 2016.
- [17] A. Abbaspour, K. Sarabandi, and G. M. Rebeiz, "Antenna-filter-antenna arrays as a class of bandpass frequency selective surfaces," *IEEE Trans. Microw. Theory Tech.*, vol. 52, no. 8, pp. 1781–1789, 2004.
- [18] I.G. Lee and I.P. Hong, "3D frequency selective surface for stable angle of incidence," *Electronics Letters*, vol. 50, no. 6, pp. 423-424, 2014.
- [19] B. Li and Z. Shen, "Three-dimensional bandpass frequency-selective structures with multiple

- transmission zeros," *IEEE Trans. Microw. Theory Tech.*, vol. 61, no. 10, pp. 3578-3589, 2013.
- [20] X. Xu, Y. Zhao, F. Yu, L. Zhang and Q. Liu, "A novel horizontal polarization sensitive active frequency selective surface without biasing network at 2.4 GHz WiFi band," in *Proc. IEEE 3rd Asia-Pacific Conf. Antennas Propag.*, Harbin, China, pp. 277-279, 2014.
- [21] C. Mias, "Varactor-tunable frequency selective surface with resistivelumped-element biasing grids," *IEEE Microw. Wireless Compon. Lett.*, vol. 15, no. 9, pp. 570-572, 2005.
- [22] P. S. Taylor, E. A. Parker, and J. C. Batchelor, "An active annular ring frequency selective surface," *IEEE Trans. Antennas Propag.*, vol. 59, no. 9, pp. 3265-3271, 2011.
- [23] X. Wu, C. Hu, Y. Wang, M. Pu, C. Huang, C. Wang and X. Luo, "Active microwave absorber with the dual-ability of dividable modulation in absorbing intensity and frequency," *AIP Adv.*, vol. 3, no. 2, pp. 022114, 2013
- [24] H. Li, Q. Cao and Y. Wang, "A novel 2-B multifunctional active frequency selective surface for LTE-2.1 GHz," *IEEE Trans. Antennas Propag.*, vol. 65, no. 6, pp. 3084-3092, 2017.
- [25] H. Li, Q. Cao, L. Liu and Y. Wang, "An improved multifunctional active frequency selective surface," *IEEE Trans. Antennas Propag.*, vol. 66, no. 4, pp. 1854-1862, 2018.
- [26] M. Oliveira, M. Melo, I. Llamas-Garro and A. G. Neto, "Reconfigurable cross dipole-hash frequency selective surface," *IET Microw. Antennas Propag.*, vol. 12, pp. 224-229, 2017.
- [27] G. I. Kiani, K. L. Ford, L. G. Olsson, K. P. Esselle and C.J. Panagamuwa, "Switchable frequency selective surface for reconfigurable electromagnetic architecture of buildings," *IEEE Trans. Antennas Propag.*, vol. 58, pp. 581-584, 2010.
- [28] S. Ghosh and K. V. Srivastava, "Polarization-insensitive single-and broadband switchable absorber/reflector and its realization using a novel biasing technique," *IEEE Trans. Antennas Propag.*, vol. 64, pp. 3665-3670, 2016.
- [29] H. Li, C. Yang, Q. Cao and Y. Wang, "A novel active frequency selective surface with switching performance for 2.45 GHz WLAN band," *Microw. Opt. Technol. Lett.*, vol. 58, pp. 1586-1590, 2016.
- [30] Q. Zhang, Z. Shen, J. Wang and K. S. Lee, "Design of a switchable microwave absorber," *IEEE Antennas Wirel. Propag. Lett.*, vol. 11, pp. 1158-1161, 2012.
- [31] G. I. Kiani, K. L. Ford, K. P. Esselle, A. R. Weily, C. Panagamuwa and J. C. Batchelor, "Single-layer bandpass active frequency selective surface," *Microw. Opt. Technol. Lett.*, vol. 50, pp. 2149-2151, 2008.
- [32] W. Withayachumnankul, C. Fumeaux and D. Abbott, "Planar array of electric- LC resonators with broadband tenability," *IEEE Antennas Wirel. Propag. Lett.*, vol. 10, pp. 577-580, 2011.
- [33] H. Yuan, B. Zhu and Y. Feng, "A frequency and bandwidth tunable metamaterial absorber in x-band," *J. Appl. Phys.*, vol. 117, pp. 173103, 2015.
- [34] B. Sanz-Izquierdo, E. A. Parker, J. B. Robertson, J. C. Batchelor, "Tuning patch-form FSS," *Electron. Lett.*, vol. 46, pp. 329-330, 2010.
- [35] S. Ghosh, K. V. Srivastava, "Broadband polarization-insensitive tunable frequency selective surface for wideband shielding," *IEEE Trans. Electromagn. Compat.*, vol. 60, pp. 166-172, 2018.
- [36] H. Wang, P. Kong, W. Cheng, W. Bao, X. Yu, L. Miao and J. Jiang, "Broadband tunability of polarization-insensitive absorber based on frequency selective surface," *Sci. Rep.*, vol. 6, pp. 23081, 2016.
- [37] P. Kong, X. Yu, Z. Liu, K. Zhou, Y. He, L. Miao and J. Jiang, "A novel tunable frequency selective surface absorber with dual-DOF for broadband applications," *Opt. Express*, vol. 22, pp. 30217-30224, 2014.
- [38] L. Bao-Qin, Q. Shao-Bo, T. Chuang-Ming, Z. Hang, Z. Heng-Yang and L. Wei, "Varactor-tunable frequency selective surface with an embedded bias network," *Chin. Phys. B*, vol. 22, pp. 094103, 2013.
- [39] B. Philips, E. A. Parker and R. J. Langley, "Ray tracing analysis of the transmission performance of curved

- FSS," IEE Proc.-Microw. Antennas Propag., vol. 142, no. 3, pp. 193-200, 1995.
- [40] Z. Sipus, M. Bosiljevac and S. Skokic, "Analysis of curved frequency selective surfaces," in Proc. 2nd European Conf. Antennas Propag., Edinburgh, UK, pp. 1–5, 2007.
- [41] D. Ding, S. Tao and R. Chen, "Fast analysis of finite and curved frequency-selective surfaces using the VSIE with MLFMA," *Int. J. Numer. Model.*, vol. 24, pp. 425–436, 2011.
- [42] C. Park, Y. Jeong, I. Hong, H. Chun, Y. B. Park, Y. Kim and J. Yook, "Analysis of curved frequency selective surface for radome using characteristic basis function method," in Proc. 10th European Conf. Antennas Propag., Davos, Switzerland, pp. 1-4, 2016.
- [43] N. Begam, P. Samaddar, S. Saha, S. Sarkar, D. Chanda(Sarkar) and P. Sarkar, "Design of curved frequency selective surface with high roll off," *Microw. Opt. Technol. Lett.*, vol. 59, pp. 2660–2664, 2017.
- [44] C. Yu, C. Lu, "Analysis of finite and curved frequency-selective surfaces using the hybrid volume-surface integral equation approach," *Microw. Opt. Technol. Lett.*, vol. 45, no. 2, pp. 107-112, 2005.
- [45] M. Han, M. He and H. J. Sun, "Modeling and analysis of doubly-curved frequency selective surface," in Proc. Asia-Pacific Microw. Conf.(APMC), Nanjing, China, pp. 1-3, 2015.
- [46] N. Begam, S. Saha, S. Sarkar D. Sarkar and P. Sarkar, "Design of compact patch type curved frequency selective surface," *Int. J. RF Microw. Comput.-aided Eng.*, vol. 29, no. 9, pp. e21803, 2019.
- [47] B. Stupfel and Y. Pion, "Impedance boundary conditions for finite planar and curved frequency selective surfaces," *IEEE Trans. Antennas Propag.*, vol. 53, no. 4, pp. 1415-1425, 2005.
- [48] B. Stupfel, "Impedance boundary conditions for finite planar or curved frequency selective surfaces embedded in dielectric Layers," *IEEE Trans. Antennas Propag.*, vol. 53, no. 11, pp. 3654-3663, 2005.
- [49] Z. Hashin, "Analysis of composite material," *J. Appl. Mech.*, vol. 50, pp. 481~505, 1983.
- [50] B. Hassani and E. Hinton, "A review of homogenization and topology optimization I, II," *Comput. & Struct.*, vol. 69, pp.707~738. 1998.
- [51] S. Nemat-Nasser and M. Hori, *Micromechanics: overall properties of heterogeneous materials*, North Holland Publication, Amsterdam, 1993.
- [52] R. Hill, "A self-consistent mechanics of composite material," *J. Mech., Phys. Solids*, vol. 13, pp. 213~222, 1965.
- [53] J. Fish, W. Chen and R. Li, "Generalized mathematical homogenization of atomistic media at finite temperature in three dimensions," *Comput. Methods Appl. Mech. Engrg.*, vol. 196, pp. 908~922, 2007.



## Abstract

Stealth radome have electromagnetic properties that transmit only the communication frequency of the internal antenna and absorb or reflect other frequencies. However, if a fighter is detected at the transmission frequency of the stealth radome, the antenna inside the stealth radome is exposed as it is, increasing the possibility of being detected by the radar. In this study, a study on a stealth radome capable of changing the transmission frequency was conducted to reduce the possibility of such detection.

The electromagnetic performance was evaluated by designing and fabricating an active frequency selective surface applicable to stealth radome. In addition, a method were develeped to predict the electromagnetic characteristics of the curved stealth radome. The predicted results were verified by experiment using a free space measurement, and it was confirmed that the proposed method for predicting electromagnetic performance was effective.

When performing structural analysis, the mesh of the stealth radome is larger than the unit cell size of the active frequency selective surface and is not uniform due to the dome shape. Therefore, properties mapping technology was developed. A method of calculating equivalent properties required for mapping technology was proposed and the method was used to perform the structural analysis of the stealth radome.

Through this study, a technique to predict the electromagnetic and mechanical performance of a variable frequency selective surface was proposed and verified through experiments.

## Résumé

Les radômes furtifs ont des propriétés électromagnétiques qui ne transmettent que la fréquence de communication de l'antenne interne et absorbent ou réfléchissent d'autres fréquences. Cependant, si un chasseur est détecté à la fréquence d'émission du radôme furtif, l'antenne à l'intérieur du radôme furtif est exposée telle quelle, augmentant la possibilité d'être détectée par le radar. Dans cette étude, une étude sur un radôme furtif capable de changer la fréquence de transmission a été menée pour réduire la possibilité d'une telle détection.

Les performances électromagnétiques ont été évaluées en concevant et en fabriquant une surface active sélective en fréquence applicable au radôme furtif. De plus, une méthode a été développée pour prédire les caractéristiques électromagnétiques du radôme furtif incurvé. Les résultats prévus ont été vérifiés par expérience en utilisant une mesure d'espace libre, et il a été confirmé que la méthode proposée pour prédire les performances électromagnétiques était efficace.

Lors de l'analyse structurelle, le maillage du radôme furtif est plus grand que la taille de cellule unitaire de la surface sélective de fréquence active et n'est pas uniforme en raison de la forme du dôme. Par conséquent, la technologie de cartographie des propriétés a été développée. Une méthode de calcul des propriétés équivalentes requises pour la technologie de cartographie a été proposée et la méthode a été utilisée pour effectuer l'analyse structurelle du radôme furtif.

Grâce à cette étude, une technique de prédiction des performances électromagnétiques et mécaniques d'une surface sélective à fréquence variable a été proposée et vérifiée par des expériences.